NTNU

Norwegian University of
Science and Technology

History Matching of Vertical Gas Injection Displacement Experiments

Anton Lindahl

Petroleum Geoscience and Engineering
Submission date: June 2018
Supervisor: Odd Steve Hustad, IGP

Norwegian University of Science and Technology
Department of Geoscience and Petroleum

Summary

This master thesis presents simulations of two core flooding experiments. The two experiments consisted of injecting gas in a gravity stable manner into a vertical core, after the core had been waterflooded. The main difference between the two experiments was the use of equilibrium gas in the first experiment, while dry separator gas was used in the second. Using these different injection gases would expose the difference in the oil production due to mass transfer effects.

The second experiment revealed that as oil was vaporized, water production from the core increased as well. Other investigators were unsuccessful of simulating this phenomenon and thus obtaining a proper history match of the water phase. The problem was identified as a problem with how the capillary pressure was managed throughout the simulations. Traditional three-phase models does not address the issue.

To properly simulate the two experiments, the ODD3P three-phase model is used. This model is utilizing saturation functions between all phases, also gas and water. The model combines hysteresis and miscibility to both capillary pressure and relative permeability in a continuous manner. The model also applies live scaling of capillary pressure with respect to changing interfacial tension. By using the ODD3P model, it was possible to obtain a history match of all three phases in both experiments. The increased water production due to vaporization of oil is accurately simulated by the use of a transition from water-oil capillary pressure into water-gas capillary pressure. By applying this transition at very low oil saturation, more water is allowed to flow.

The oil and gas phases are also accurately simulated to history match experimental data. A surface equation of state is made to perform the flash calculations from reservoir to standard conditions. Injection of gas created an oil bank in both experiments. After the oil bank was produced a rather small flow of oil was seen in the first experiment. In the second experiment oil was produced in fairly high rate after the oil bank was produced. Analysis of the oil flow mechanisms revealed that this was a results of vaporization of oil. The vaporization effect proved to be significant. Approximately twice as much oil were recovered by using a dry separator gas instead of an equilibrium gas.

Sammendrag

Denne hovedoppgaven presenterer simuleringene av to kjernefløming-eksperimenter. De to eksperimentene bestod av å fløme gass inn i vertikale kjerner på en gravitasjonstabil måte, etter at kjernen allerede hadde vært utsatt for vannfløming. Den største forskjellen på de to eksperimentene var at den første kjernen ble fløm med en gass som var i likevekt med oljen, mens i det andre eksperimentet ble brukt en tørr separatorgass. Formålet med å bruke to forskjellige typer gass, var å utforske effekten massetransport mellom fasene ville ha på oljeproduksjonen fra kjernen.

Det andre eksperimentet avslørte at fordamping av olje i kjernen også førte til økt vannproduksjon. Det er tidligere gjort forsøk på å simulere en historietilpasning av vannproduksjonen fra dette eksperimentet, men ingen har vært suksessfulle. Andre etterforskere har indikert at problemet har vært behandlingen av kapillærtrykk i simuleringene. Tradisjonelle trefase-modeller adresserer ikke dette problemet.

For å få presise simuleringer av disse to eksperimentene, er trefase-modellen ODD3P tatt i bruk. Denne modellen utnytter metningsfunksjoner mellom alle faser, også mellom gass og vann. Modellen kombinerer både hysterese og blandbarhet på både relativ permeabilitet og kapillærtrykk på en kontinuerlig måte. Den inkluderer også skalering av kapillærtrykk med hensyn til forandring i grenseflatespenning. Ved å bruke ODD3P-modellen var det mulig å simulere en historietilpasning som var tilpasset samtlige faser i begge eksperimenter. Den økte vannproduksjonen på grunn av oljefordampning ble korrekt simulert ved hjelp av en glatt overgang fra vann-olje kapillærtrykk til vann-gass kapillærtrykk. Ved å tillate en slik overgang ved veldig lave oljemetninger, vil mer vann strømme fra kjernen.

Olje og gass-produksjon er også blitt simulert, slik at de er historietilpasset til eksperimentelle data. En overflate-tilstandsligning er laget for å kalkulere endringene i fluidegenskaper fra reservoarforhold til overflateforhold. Injeksjon av gass i kjernen førte til at en oljebank ble dannet, noe som var observert i begge eksperimentene. Etter at denne oljebanken var produsert, var en lav produksjonsrate av olje observert i det første eksperimentet. I det andre eksperimentet ble en større produksjonsrate av olje observert, etter at oljebanken var produsert. En analyse av strømmingsmekanismene avslørte at den store oljeproduksjonsraten i eksperiment nummer to, var forårsaket

av fordampning av olje i kjernen. Fordampningseffekten viste seg å være signifikant. Omtrent dobbelt så mye olje ble utvinnet fra kjernen ved å bruke en tørr injeksjonsgass, istedenfor en likevektsgass.

Preface

This master thesis was carried out in the spring of 2018 at The Department of Geoscience and Petroleum, Norwegian University of Science and Technology. The thesis is a part of a Master of Science degree in Petroleum Engineering, with specialization in Reservoir Technology.

I would like to express my sincerest gratitude to my supervisor Odd Steve Hustad (Equinor, NTNU) for providing me with an interesting problem, for helpful discussions and for sharing his experience and knowledge on the topic.

Trondheim, 11. June 2018

Anton Lindahl

Table of Contents

List of Figures

List of Tables

Chapter 1

Introduction

When producing an oil reservoir there are several different methods and technologies one may use to obtain the highest production of hydrocarbons, in a cost effective manner. Normally, the recovery mechanisms behind hydrocarbon production is divided into three categories; primary recovery, secondary recovery and tertiary recovery.

Primary recovery includes hydrocarbon production due to natural lift of oil and the use of artificial pumps. This stage of oil recovery is typically recognized by the fact that the reservoir has substantially higher pressure than the wellbore and oil is flowing into to the wellbore due to the reservoirs energy, or pressure. This includes waterdrive, gasdrive and gravity drainage, among others.

Secondary recovery begins when the production of the reservoir moves into a phase where artificial pressure support is required. This includes water and gas injection, which provides pressure support in the reservoir, but also displaces more of the remaining hydrocarbons in the reservoir.

Normally, primary and secondary recovery techniques only recover about 50% of the initial oil in place in the reservoir. Hence, one would often take use of tertiary recovery techniques, also called enhanced oil recovery. This is unconventional methods to extract more oil by improving displacement efficiency in the reservoir. There are three main types of tertiary recovery; chemical flooding, miscible gas injection and thermal recovery.

This thesis presents experiments that explores one of these three methods, namely

tertiary gas injection. As the name suggests, tertiary gas injection is a process where gas is injected after a reservoir has been waterflooded. A successful tertiary gas flooding can typically improve the oil recovery by 5% to 30%, depending on the mechanisms seen in the reservoir. Miscible, and near-miscible, gas may have substantial mass transfer effects, which improves the oil recovery further than only increasing the displacement efficiency would. Hence, there are two main effects at work when injecting gas into a reservoir: Increased displacement efficiency and mass transfer between oil and gas. The increased displacement efficiency is normally seen on a porescale level, where the residual oil is reduced compared to only flooding with water. The mass transfer effect is typically a process where oil is vaporized into the gas phase, and then transported by the gas to the wellbore.

To explore the mechanisms in tertiary gas injection, Hustad et al. (1992) conducted two core flooding experiments in 1992. The aim of the experiments was to investigate the effect mass transfer had in a tertiary gas flooding. The first experiment included gas flooding after water flooding of a vertical core. The injection gas was in equilibrium with the oil, ensuring no mass transfer took place. The second experiment was very similar, but instead of equilibrium gas, a dry separator gas was injected. The overall goal was to reveal the the mass transfer effect the dry gas has on the oil production, compared to the equilibrium gas.

The experiments were successful of proving the effects of mass transfer on oil production, but revealed unknown phenomena. As the oil in the core was vaporized, the water production increased as well. The authors came up with different theories of the mechanisms behind the increased water flow, presented later in this thesis.

Furthermore, Hustad et al. (1992) includes simulation attempts of the two core flooding experiments. However, the simulations were not able to history match the water production properly, although a lot of effort was attributed into the simulations. It was speculated that the problem was with the modelling of the three-phase saturation functions.

As the two experiments had three phases flowing simultaneously, so-called three-phase models was applied to predict the flow properties in the three-phase space. Reservoir simulation of such problems require special treatment, due to the complex nature of three-phase flow. As the properties are cumbersome to measure in the three-phase

space, correlations are used to predict these properties.

There is a range of different three-phase models that predicts these properties. These methods are typically utilizing two-phase properties to predict the three-phase properties. This includes models widely used in the industry, such as Stones models and Bakers model. However, these models have proved to have limited performance, due to the fact that the models were designed with respect to simple reservoir conditions and conservative assumptions.

Hustad et al. (1992) experienced that neither of Stones models were able to reproduce the experimental results. The lack of performance by these models were the inspiration of developing the ODD3P three-phase model (Hustad and Browning, 2010). This model was developed to utilize measured data between all phases in a three-phase system. It includes flexibility to model the more complex three-phase problems, such as tertiary gas injection and water alternating gas injection.

Using the ODD3P three-phase model, an entirely new attempt to history match the experiments in Hustad et al. (1992) is presented in this thesis. The simulations are emphasizing on obtaining an improved history match of the water phase, and reproducing the increased water production due to vaporization of oil. However, the oil and gas phases are also simulated and history matched. A surface equation of state is made to fit the hydrocarbon phases fluid properties. The thesis is divided into chapters, with the following content:

- Chapter 1: Introduction
- Chapter 2: Literature Study

  The literature study provides an introduction the some of the basic theory that is required for understanding the following content, such as basic reservoir properties, tertiary gas injection and three-phase flow. It also includes an overview of the most common three-phase models that are historically used in the industry. An understanding of these older models gives a background to understand the ODD3P model, and its features. Lastly, a series of field studies of tertiary gas injection are presented.
- Chapter 3: Theory

  This chapter presents theory that is directly applied in the simulations of the two

experiments. This includes the E300 reservoir simulator, ODD3P three-phase model and equation of state. Of these three subchapters, the ODD3P model is by far the most important to understand with respect to the following content.

- Chapter 4: Background

  A thorough introduction to the two experiments, that were conducted by Hustad et al. (1992) is given. This includes both experimental measurements and procedures, but also the results of the experiments and associated simulations. Theories that may explain the cause of the inaccurate simulations are also presented.

- Chapter 5: Method and Procedure

  This chapter explain the simulation procedure and method used for the two experiments. It also includes a PVT modelling chapter. Most emphasis are on the implementation of ODD3P model specific inputs.

- Chapter 6: Results

  Results of the simulations of the two experiments are presented. This includes the history match with production curves, saturation profiles and the results of a sensitivity study.

- Chapter 7: Discussion

  This chapter provides discussion around the presented results. Including analysis of the ODD3P models features, water production, oil recovery mechanisms and potential sources of error.

- Chapter 8: Conclusion

  Summarizes the most important findings of the simulations.

- Chapter 9: Further Work

  A recommendation of further work on the topic.

Chapter 2

Literature Study

This thesis describes and discuss several phenomena and methods seen in the production of oil reservoirs. Some of these methods are considered advanced, and are based on more established concepts in reservoir technology.

Before introducing the more advanced methods, a literature study is presented. This literature study presents models and concepts found in the literature regarding tertiary gas injection, and models used to model three-phase flow. A short introduction to basic reservoir properties, reservoir simulation, and special core analysis is also given.

2.1 Basic Reservoir Properties

Fluid flow in porous media can be described by Darcys law, given in equation 2.1 (Simmons, 2008).

$$q = -\frac{kA\nabla p}{\mu} \tag{2.1}$$

q is the flow rate, A is the cross-sectional area, k is permeability, μ is viscosity of the flowing fluid and ∇p is pressure gradient. This is one of the most basic forms of describing flow in a reservoir, and the basis of more advanced models of flow.

Permeability

The permeability, k, is a parameter that describes the ability of a fluid to flow through a porous medium. This parameter is not a description of one physical parameter, but rather the result of a series of different parameters. The most important may be the porosity and the geometry of the pores. One can differentiate the permeability into two subcomponents, the absolute permeability, k_a, and the relative permeability, k_r. The absolute permeability is a property of the rock, while the relative permeability is a fluid-rock property. This parameter depends on how the fluids in the rock interact with each other and the rock. The relationship between relative permeability and absolute permeability can be seen in equation 2.2 (Skjæveland and Kleppe, 1992).

$$k_r = \frac{k_e}{k_a} \tag{2.2}$$

The relative permeability is found by measuring the effective permeability of a given fluid at a series of different saturations, and then dividing it on the absolute permeability. The absolute permeability is found by measuring the permeability when only one fluid is present in the porous medium. Due the relation with the present fluids, the relative permeability is heavily dependent on the phase saturations. As the phase saturation decreases, the relative permeability of the given phase is also decreasing. When the saturation reaches the residual saturation, the relative permeability is zero.

Interfacial Tension

Interfacial tension is the tension found at the boundary between two immiscible fluids. This tension originates from the difference in energy for molecules at a fluids interphase and those in the bulk of the fluid (Skjæveland and Kleppe, 1992). The interfacial tension between two fluids provides a pressure difference in the fluids described by the Laplace equation, seen in equation 2.3.

$$\Delta p = \sigma \left(\frac{1}{r_1} + \frac{1}{r_2} \right) \tag{2.3}$$

r_1 and r_r are the radii of the curvature between the two phases. Δp is the pressure difference and σ is the interfacial tension between the two phases. This phenomenon

affects a large range of fluid properties in the porous medium, and relates to capillary pressure. The interfacial tension may change with changing fluid compositions.

Wettability

Wettability is a measure of the tendency a solid surface has to adhere with one fluid over another (Skjæveland and Kleppe, 1992). The adhesive forces are resulting in a spreading effect, where one fluid will have a tendency to spread along the solid surface. The phase that has more spreading on the solid is the so-called wetting phase, while the other phase is the non-wetting phase. Contact angle is the most common measure of wettability. A schematic of how contact angle is defining wettability can be seen in figure 2.1.

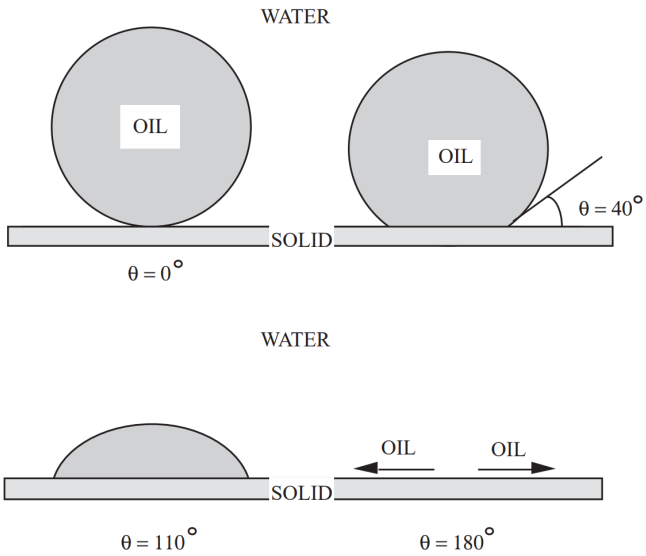

Figure 2.1: Wettability and contact angle. (Skjæveland and Kleppe, 1992)

The contact angle is the angle between the solid surface and the wetting phase.

Capillary pressure

A direct consequence of the wettability and interfacial tension properties between the fluids and the rock is capillary pressure. Capillary pressure is defined as the pressure difference between two phases. This can be expressed through the interfacial tension,

contact angle and radius of the pore, as seen in equation 2.4, (Skjæveland and Kleppe, 1992).

$$P_c = p_2 - p_1 = \frac{2\sigma cos(\theta)}{R} \tag{2.4}$$

The capillary pressure is also directly linked to the saturations of the respective fluids in the pore system.

Hysteresis

Both capillary pressure and relative permeability are functions of saturation history, which results in hysteresis curves. The fluids distribution in the pores depends not only on the wettability, but also on how and when the respective fluids were introduced to the pore. A process where the non-wetting fluid is flowing into a porous system and displacing the wetting fluid is called drainage. When the opposite process occurs, when the non-wetting fluid flows out of the porous system, it is called imbibition (Skjæveland and Kleppe, 1992). Due to pore-geometry and capillary forces, the relative permeability and capillary pressure curves do not follow the same mechanisms during imbibition and drainage. This is exemplified in figure 2.2 (a) and (b).

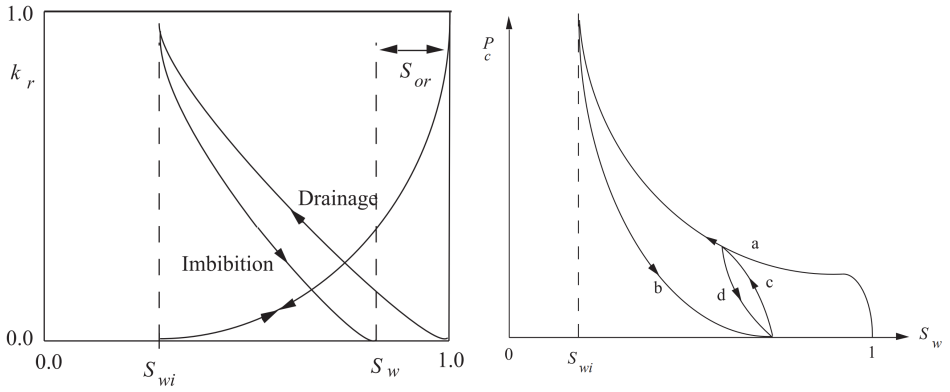

(a) Relative permeability.

(b) Capillary pressure.

Figure 2.2: Schematic showing the principle of hysteresis.(Skjæveland and Kleppe, 1992)

The difference in the relative permeability and capillary pressure due to different hysteresis curves might have large impact on the resulting flow in the reservoir.

Recovery Efficiency

When measuring quantities of oil production from an oil reservoir a normal measure is the Recovery Efficiency, defined in equation 2.5 (Lake, 1989).

$$E_r = E_d E_v \tag{2.5}$$

E_r is the recovery efficiency, which is indicating the percentage of oil from the reservoir that has been produced. When looking at displacement processes with an injected fluid displacing oil, the recovery efficiency may be differentiated into two parts, the displacement efficiency, E_d, and the volumetric sweep efficiency, E_v. The volumetric sweep efficiency defines what percentage of the reservoir that has been reached by the displacing fluid. The displacement efficiency is a measurement of how much of the oil that is displaced in the parts reached by the displacement fluid. Thus, indicating how much of the oil that is displaced on a porescale level.

2.2 Reservoir Simulation and SCAL

To predict future performance of an oil reservoir, a reservoir simulator tool is normally used. A reservoir simulator is a tool that combines a series of models for numerical calculations of fluid flow in the reservoir, with the aim to reproduce the fluid flow seen in the actual reservoir and to predict future performance (Chen, 2007). The core function of this type of tool is to discretize the reservoir into a series of smaller blocks. Every block are provided with geological data from a geological model. This data may be found from a range of geological and geophysical surveys. This static geological model is combined with a dynamic fluid model, which describes the flow properties of the respective fluids in given rock. A numerical solver can then calculate flow, and change in saturation and pressure from block to block. The ability to acquire flow data from block to block instead of for the whole reservoir as one makes it possible to model more advanced phenomena. These calculations are often based on conservation of mass, combined with some fluid flow model, such as Darcys law (Simmons, 2008).

There is a large range of different options and methods that can be applied with a reservoir simulator. Different fluid models, gridblock systems, numerical solvers, flow

equations and reservoir types exists. Thus, the options and configurations depends largely on the problem at hand and the possibilities with the chosen reservoir simulator.

Even though reservoir simulators mainly are used to simulate the performance of massive reservoirs, they can also be applied in the study of special core analysis, long for SCAL. SCAL is a process where a rock core taken from a hydrocarbon reservoir is analyzed in the lab. The core is subjected to a range of measurements to find the properties of the rock and fluid interactions with the rock. This includes a study of how different fluids flow in the rock. It can also be used to study phenomena related to different fluid flooding methods, and find the effect it has on recovery of oil.

As the variations of many parameters are far smaller in a core than in a reservoir, it is possible to isolate and study certain phenomena more easily in a core than in a full field model. This is a helpful tool for calibrating a reservoir model to a certain process before applying it on a full field scale model. In the full field model a range of different processes could occur at different places, beclouding the phenomena of interest.

2.3 Three-phase Flow

A typical hydrocarbon reservoir often consists of some sort of impregnable structure that traps the hydrocarbon in place. Beneath this trap, the reservoir fluids are found in porous reservoir media. The reservoir fluids are segregated and distributed due to gravity and capillary forces. Normally, gas is found in the upper part, followed by an oil section with water beneath. Capillary forces provides transition zones between oil-gas and water-oil. When producing the oil in such a reservoir, water encroaches from beneath and gas from the top. This produces two-phase flow between water and oil in lower part of the reservoir and two-phase flow between oil and gas in the upper part. Water is found in the upper part as well, but only in irreducible saturation, which will not produce any flow. During primary and secondary recovery, this is the main flow pattern, and three-phase flow is of no concern. This production scheme and thought process is the logic behind most of the reservoir flow models. Thus, many models are based on such assumptions and models are formed accordingly.

However, with more advanced recovery techniques three-phase flow is very likely to occur in the reservoir. For three phases to flow simultaneously, all the respective phases

must have higher saturation than the residual saturation. This is shown in figure 2.3.

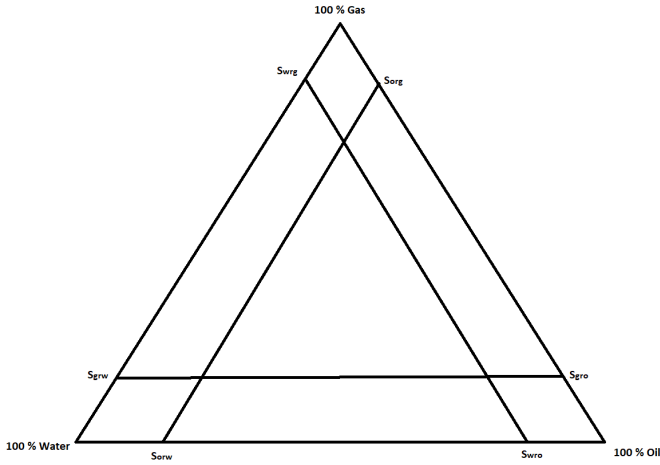

Figure 2.3: Ternary diagram showing the three-phase space.

The three-phase space is found in the middle triangle in the schematic. Conditions for three-phase flow may be found in several production methods. This includes tertiary gas injection and water alternating gas injection.

When moving into the three-phase space the two-phase properties are unlikely to represents the fluid flow precisely. Special considerations needs to be taken to find how relative permeability and capillary pressure behaves during these conditions. There are many methods to model this behavior, which are shown in the next section.

2.4 Three-Phase Models

If three phases are flowing simultaneously, the flow properties must be known at all combinations of the respective phases. As it is cumbersome to measure three-phase flow properties in an experiment, the use of prediction models are the most common method to obtain this data in the industry. The literature proposes a range of different models to predict relative permeability for three-phase flow. These methods can be divided into three subcategories (Skjæveland and Kleppe, 1992):

- Network theory models
- Models based on two-phase properties

- Interpolation methods

2.4.1 Network theory models

Network theory models are based on porescale network flow. Many of the correlations originates from thought experiments with bundles of capillary tubes. The main problem with these types of models are the lack of flexibility to fit the models to experimental data (Skjæveland and Kleppe, 1992).

Burdine (1953) proposed such a model for three-phase relative permeability of the drainage process of oil. The model is based on a bundle of tubes to represent a porescale network. Burdine (1953) suggested that the relative permeability is proportional to the hydraulic area of the respective phases. A tortuosity factor is also included that would ensure better fit the experimental data. The relationship can be seen in equation 2.6.

$$k_{ro,dr} = \left(S_o^*\right)^2 \frac{\int_{S_w^*}^{S_l^*} \frac{1}{P_c^2} dS_l^*}{\int_0^1 \frac{1}{P_c^2} dS_w^*} \tag{2.6}$$

S_o^*, S_w^* and S_l^* are oil, water and liquid saturation. The star indicates that the saturations are normalized, and can be described by the Corey drainage capillary pressure, seen in equation 2.7 (Skjæveland and Kleppe, 1992).

$$S_w^* = \left(\frac{P_c}{P_e}\right)^{\lambda} \tag{2.7}$$

λ is an index that describes pore size distribution. By combining equation 2.6 and 2.7, one obtains Burdines three-phase prediction of oil relative permeability.

$$k_{ro} = \left(\frac{S_o}{1-S_{lr}}\right)\left[\left(\frac{S_o + S_w - S_{lr}}{1-S_{lr}}\right)^{\frac{2+\lambda}{\lambda}} - \left(\frac{S_w - S_{lr}}{1-S_{lr}}\right)^{\frac{2+\lambda}{\lambda}}\right] \tag{2.8}$$

Equation 2.8 provides a relationship that describes the relative permeability of oil as a function of liquid saturations and the pore size distribution. S_{lr} is the residual of liquid, at maximum gas saturation. This parameter can be tuned to make the model a better fit to experimental data. The relationship only applies for drainage processes where oil is the intermediate phase, and water is the wetting phase. Water and gas relative permeability are assumed functions of their respective saturations only.

Naar and Wygal (1961) suggested a similar type of network model, only for imbibition processes. The model is based on a bundle of capillary tubes modified to include the effect of bypass and trapping of the non-wetting fluid. The correlation can be seen in equation 2.9.

$$k_{ro,im} = \left(S^*_{of}\right)^3 \left(S^*_{of} + 3S^*_{fw}\right) \tag{2.9}$$

S^*_{of} is the normalized oil flowing saturation and S^*_{wf} is the normalized water flowing saturation. A modification of equation 2.8 was proposed by Parker et al. (1987) which defines the Corey relationship in a different manner, seen in equation 2.10.

$$S^* = \left[1 + (\nu P_c)^n\right]^{-m}, \quad m = \frac{1}{m} \tag{2.10}$$

Where m is an user-defined value and ν is the shape factor. Equation 2.10 can be used to derive Parker et al. (1987) prediction of oil three-phase relative permeability, seen in equation 2.11.

$$k_{ro,im} = \left(S^*_t - S^*_w\right)^{0.5} \left[\left(1 - \left(S^*_w\right)^{\frac{1}{m}}\right)^m - \left(1 - \left(S^*_t\right)^{\frac{1}{m}}\right)^m\right]^2 \tag{2.11}$$

This correlation does only apply to imbibition of oil. The water and gas relative permeability are functions of their respective saturations. S^*_t is defined in equation 2.12.

$$S^*_t = \frac{S_t - S_{wi}}{1 - S_{wi}}, \quad S_t = S_w + S_o \tag{2.12}$$

2.4.2 Models based on two-phase properties

The two-phase based models are three-phase models that are based on measured two-phase properties. These models are very common in the industry, due to the fit with experimental data and that these models often resemble the two-phase properties at the two-phase limit (Skjæveland and Kleppe, 1992).

It is normal procedure to measure the properties between oil and gas, and oil and water. This is due to the assumption that oil are separating the gas and water in the pores. This implies that the oil flow may be obstructed by the other phases and thus is a

function of all three saturations. These measurements yields one water relative permeability curve and one gas relative permeability curve, but two oil relative permeability curves. Most models based on two-phase properties are combining these two oil curves to provide distinct values at any given oil saturation.

Stone et al. (1970) proposed a model based on the so-called “channel flow theory”. This theory states that only one phase will flow in a given pore channel at any given time. This also implies that the smallest pores are water filled and the larger pores are mostly filled with gas. This resembles a water wet reservoir system. The model assumes that water and gas blocks the flow of water independently of each other. The model is shown in equation 2.13.

$$k_{ro} = S_o^* \beta_w \beta_g = S_o^* \left(\frac{k_{row}}{1 - S_w^*} \right) \left(\frac{k_{rog}}{1 - S_g^*} \right) \tag{2.13}$$

k_{row} is the relative permeability of oil from the water-oil measurement and k_{rog} is the relative permeability of oil from the oil-gas measurement. β_g and β_w are factors that describe the blockage of oil by the gas and water phase respectively. S_i^* is the normalized saturations with respect to phase i. The normalization can be seen in equation 2.14.

$$S_i^* = \frac{S_i - S_{ir}}{1 - S_{wir} - S_{om} - S_{gc}} \tag{2.14}$$

i is the phase that is normalized, S_{wir} is the water irreducible saturation, S_{gc} is the connate gas saturation and S_{om} is the oil residual. As the saturations are approaching the two-phase boundary, the oil relative permeability approaches the two-phase measurements. Thus, when only two phases are flowing, the model will provide the exact measured relative permeability data.

Stone also suggested another model, called Stones second model (Stone, 1973). This model is based on a probability of either gas or water blocking the oil. The blockage of oil by either phase is assumed to be independent of each other. The model are shown in equation 2.15.

$$k_{ro} = (k_{row} + k_{rw}) \left(k_{rog} + k_{rg} \right) - \left(k_{rw} + k_{rg} \right) \tag{2.15}$$

Aziz (1979) suggested alterations to both of Stones models. This consisted of adding a normalization term, which can be seen in equation 2.16 and 2.17

$$k_{ro} = \frac{S_o^*}{k_{rocw}} \beta_g \beta_w = \frac{S_o^*}{k_{rocw}} \frac{k_{row}}{1 - S_w^*} \frac{k_{row}}{1 - S_w^*} \tag{2.16}$$

$$k_{ro} = \frac{(k_{row} + k_{rw})\left(k_{rog} + k_{rg}\right)}{k_{rowc}} - \left(k_{rw} + k_{rg}\right) \tag{2.17}$$

k_{rocw} is the permeability of oil at connate water saturation. This alteration ensures that the relative permeability of oil with respect to water is unity at connate water saturation.

Fayers (1989) suggested to alter the residual oil saturation term to provide more modelling flexibility to Stones first model. The oil residual saturation is given in equation 2.18 and is a part of the normalization of the phases. This term is often used to fit the Stone model to experimental data (Skjæveland and Kleppe, 1992). The alteration can be seen in equation 2.18.

$$S_{om} = S_{orw} - \left[\frac{S_{orw} - S_{org}}{1 - S_{wc} - S_{org}}\right] S_g - \epsilon \left[\left(1 - S_w - S_{org}\right) S_g - S_g^2\right] \tag{2.18}$$

ϵ is a user defined parameter used to fit the model to experimental data. Equation 2.18 provides more advanced residual saturation features. As water saturation approaches zero the oil residual will move towards the endpoint of oil with respect to water, S_{org}. Likewise, when gas saturation is zero, the oil residual will be equal to the oil residual with respect to water, S_{orw}. This is an important feature, since the oil residual may vary a lot when drained by different fluids (Hustad et al., 1992).

Hustad et al. (1992) presented an alterations to Stones first model to provide more user flexibility. The so-called Extended Stones model is given in equation 2.19.

$$k_{ro} = \frac{k_{rog} k_{row}}{k_{rowc}} \left(\frac{S_o^*}{\left(1 - S_w^*\right)\left(1 - S_w^*\right)}\right)^n \tag{2.19}$$

As seen in equation 2.19, the alteration was to add an user-defined exponent, n. This exponent allows to the user change the shape of the oil isoperms seen in a ternary diagram.

All the presented two-phase models resembles the two-phase relative permeabil-

ity at the two-phase boundaries. Henceforth, the main difference of the models is the ability to predict three-phase relative permeability in the three-phase space. There is no consensus of which model is better, as some models fit given situations better than others. However, Stones first and second model are widely used in the industry due to their simplicity.

2.4.3 Interpolation methods

Baker et al. (1988) investigated different three-phase models. It was found that an effective model to predict the three-phase relative permeability of oil was a linear interpolation between k_{row} and k_{rog} in the three-phase space. This provides straight lines in a ternary diagram. As the experimental oil relative permeability often yields straight lines when plotted in a ternary diagram, this interpolation method is often precise. The method can also be used to obtain the water and gas relative permeability as a function of the interpolated two-phase properties. The drawback of this method is the computational complexity required to calculate the linear interpolation (Skjæveland and Kleppe, 1992).

Baker et al. (1988) also suggested a simpler interpolation method. This method calculates the oil relative permeability by weighting the two-phase properties by the saturations. This can be seen in equation 2.20.

$$k_{ro} = \frac{(S_w - S_{wc})\, k_{row} + \left(S_g - S_{gr}\right) k_{rog}}{(S_w - S_{wc}) + \left(S_g - S_{gr}\right)} \tag{2.20}$$

This model is both simple and honors the two-phase properties at the two-phase boundaries. However, if the residual endpoints of oil are very different, the isoperms in a ternary diagram will be either very concave or convex. Thus, the model may not be very accurate at all times.

2.4.4 Three-phase models comparison

Baker et al. (1988) explored the performance of different three-phase models. Most of the models performed very well when at high oil relative permeability. However, as many three-phase situation occurs at low oil saturations, performance at low relative

permeability is often more important. Baker et al. (1988) found that the interpolation methods performed very well with respect to the experimental data. The pore network methods performed overall poorly.

The pore network and two-phase based methods are mainly based on a water-wet system. It is also often assumed that water and gas never are in contact or affect each other. This might not be true, and may affect the validity of the models. Furthermore, many of the models presented does not differentiate between the residual saturations. A phase may have very different residual saturation when drained by different fluids.

2.5 Tertiary Gas Injection

When producing an oil reservoir using only the reservoirs natural pressure and waterflooding, the recovery factor of oil is normally found at around 50%. The main reason for such low recovery of oil is how the water displaces oil on a porescale level. Due to bypass of oil in smaller pores or snap-off making the oil phase discontinuous in the pores are physically stopping the water from displacing the oil. The residual oil saturation with respect to water, S_{orw}, is typically found at around 20% to 40%.

To increase the oil recovery from the reservoir an option is to inject gas after the reservoir has been subjected to waterflooding. This process is called tertiary gasflooding. Investigators Hustad et al. (1992) has observed that introducing gas to a reservoir system reduces the residual saturations of the present liquid phases. Oil residual saturation decreases down to far smaller residual saturations. Thus, when oil is displaced by gas, far more can be recovered, than if it was only displaced by water. This feature and other mechanisms are discussed further, along with saturation functions and field studies of tertiary gas injection.

2.5.1 Gas Flooding Mechanisms

When injecting a gas in the reservoir after waterflooding there are several mechanisms at work to increase the microscopic sweep efficiency. The injection gas provide a lower residual saturation for oil, but it may also reach areas of the reservoir where to water cannot. The gas may also involve some mass transfer effect, which could yield more oil.

After a reservoir has been subjected to a waterflood, the remaining oil is often trapped in the water phase in the pores. As the oil is discontinuous, it will not flow. A schematic of how gas invades a pore in such a situation is given in figure 2.4.

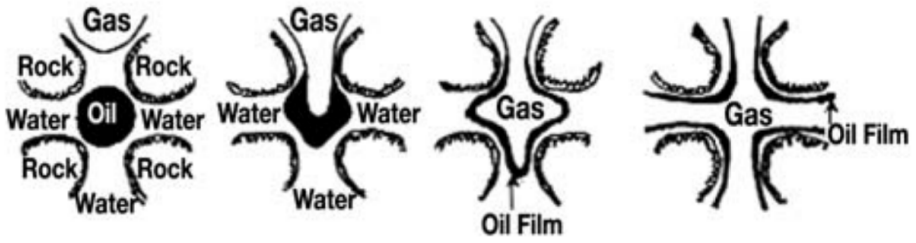

Figure 2.4: Porescale gas displacement schematic (Ren et al., 2004)

The gas will flow into the residual oil phase and oil will typically form a film around the injected gas, and flow in the film. As gas often is injected from the top of the reservoir, a mechanism of oil flow in the oil film may be gravity force downwards in the film. The introduction of gas will mobilize the oil, making it flow in the pores (Ren et al., 2004). Another mechanism that may occur is vaporization of oil. The magnitude of the vaporization process depends on the injection gas. A range of different injection gases may be used for injection. The most common gases includes CO2, N2, lean hydrocarbon gas and rich gas. These injection gases may be either immiscible or miscible with the reservoir oil depending on compositions and conditions. However, exchange of components between the gas and oil takes place for almost all cases. The magnitude of the mass transfer is larger for miscible processes than immiscible. The mass transfer normally takes place at the gas injection front, where typically intermediate components moves from the oil phase into the gas phase, creating a vaporization effect of the oil (Skjæveland and Kleppe, 1992). A schematic of a typical tertiary gas flooding process is shown in figure 2.5.

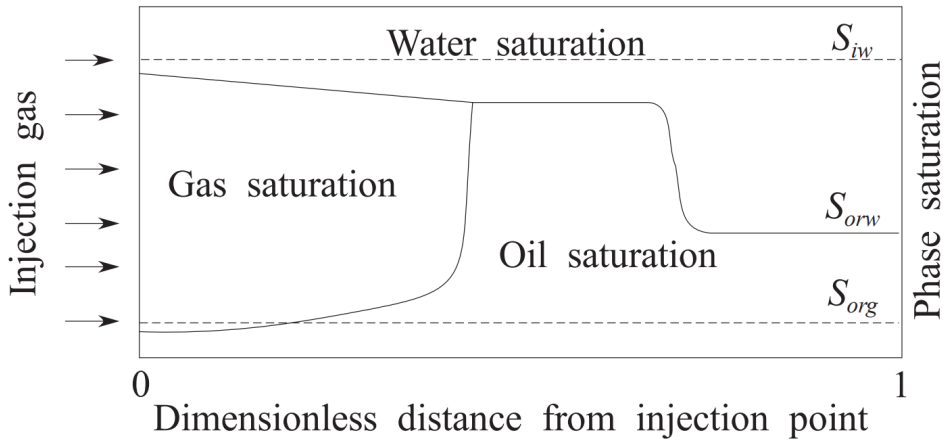

Figure 2.5: Schemtic of a tertiary gas flooding process (Skjæveland and Kleppe, 1992)

As seen from the schematic, the gas mobilizes oil that produces an oil bank in front of the gas displacement front. The microscopic sweep efficiency makes the oil residual to gas, S_{org}, smaller than the residual to water S_{orw}. The difference in these two values are the driving force in the oil bank formation. As seen from the schematic, the oil saturation may also decrease below S_{org}, due to vaporization.

The drawback with tertiary gas injection, and gas injection in general, is the volumetric sweep efficiency. As the injection gas has lower density than the fluids in the reservoir, gravity drives the injection gas upwards in the reservoir. Thus, the oil in the lower part of the reservoir may not be swept properly. This problem is normally addressed with some form of water alternating gas method, or so-called WAG. As the name suggest WAG-methods combine water and gas injection, and the two phases are injected in some sort of pattern. This ensures a larger volumetric sweep efficiency. Furthermore, if the reservoir has a dip angle, it is possible to inject gas from the top of the reservoir in a gravity stable manner. This may also provide a high volumetric sweep efficiency.

2.5.2 Saturation Functions

During a tertiary gas injection process, there is a large probability that three phases will flow simultaneously. Especially around the formation of an oil bank will both gas, water

and oil have a tendency to flow at the same time. Three-phase flow may induce complex flow behavior, thus requiring advanced treatment. To model the three phase properties some sort of three-phase model is used to model the saturations functions.

A large range of the more traditional three-phase models was presented in the previous section. These models emphasized on predicting the three-phase relative permeability of oil only. Some of the models addressed the three-phase relative permeability of water and gas as well. No models were found in the literature that explored the impact three-phase flow has on capillary pressure, except the ODD3P (Hustad and Browning, 2010), that will be presented in depth later in this thesis.

Ren et al. (2003) performed numerical simulations of tertiary gas injection processes. The study involved the use of different three-phase models to model the three-phase relative permeability of oil. Even though the author wanted to apply the most advanced models, only Stones two models and Bakers two interpolation models were available in the respective reservoir simulator. Ren et al. (2003) concluded that different three-phase models had significant effect on the simulated oil production. It was found that proper modelling of the oil relative permeability was especially important at low oil saturations.

Treatment of capillary pressure is also addressed by Ren et al. (2003). A normal two phase-capillary pressure formulation was used in the simulations. Simulations with and without capillary pressure were explored. As expected, ignoring capillary pressure yielded very optimistic oil recovery. It was acknowledged that measured two-phase capillary pressure might not have been representative for a three-phase flow situation. This phenomena was investigated by Kantzas et al. (1998). The study makes a clear distinction between two-phase capillary pressure and three-phase capillary pressure. The three-phase capillary pressure is depend on saturation history, pore geometry and spreading coefficients, among other parameters. It also implies that three-phase capillary pressure can be represented by combing two-phase capillary pressure data.

Shahverdi and Sohrabi (2013) investigated how to model three-phase relative permeability during a WAG injection. It was seen that using different hysteresis curves were of high importance when modelling three-phase relative permeability. Stones first model performed poorly to predict the oil relative permeability due to the cyclic hysteresis effects. The investigators also proposed a model that measured three-phase

relative permeability of the first WAG cycles. The measurements were used to predict the relative permeability of the forthcoming WAG cycles.

2.5.3 Tertiary Gas Flooding Field Studies

Investigation of tertiary gas injection in laboratory scale often reports recovery factors of oil as large as 100%. However, such high recoveries of oil are rarely seen in the field. To get an understanding of the significance tertiary gas injection may have on a field scale, a series of field studies are presented.

Bonnin et al. (2002) presents a field study of a full field tertiary gas injection program. The reservoir in question was a mature carbonate reservoir, located offshore Abu Dhabi. Before gas injection the field had already been produced for 20 years, mainly due to a strong aquifer. To enhance oil production in this mature field, a program to inject hydrocarbon gas was initiated. The pressure in the reservoir was not adequate to ensure miscible conditions between oil and injected gas. However, lab tests had indicated positive effects of a potential gas injection program. The tertiary gas injection was expected to increase recovery with 2% STOIIP with an injection rate of 70 MMSCFD in a span of 10 years. Bonnin et al. (2002) found that after 5 years, significant effects were seen, and 30% of the total oil rate was caused by the gas injection. By numerical reservoir modelling a predication was made using the historical production. The excellent simulation results were motivation for a more extensive injection program, where more injection wells were supposed to be drilled. Bonnin et al. (2002) concluded that the injection of immiscible hydrocarbon gas had significant effect on the oil production and recovery of oil.

Lawrence et al. (2002) presents a field study of miscible tertiary gas injection in the Jay field found in the US. This field is a carbonate reservoir located at a depth of 4600 meters with light oil. Nitrogen was used as injection gas, in combination with water in a WAG-program. The injection rate of gas was 2.2E10 $\frac{stm^3}{day}$ and water rate of 27 000 $\frac{stm^3}{day}$. By applying tertiary gas injection of nitrogen, the field is expected to reach a recovery of 60%. Out of this recovery, approximately 10% is estimated to be caused by the miscible gas injection. Extensive reservoir simulation was used to optimize the injection of gas and water. Unfortunately, Lawrence et al. (2002) does not include any mention of which

three-phase model that was used in the simulations. With the use of history matching of early stages of injection, the reservoir model proved to predict the increased oil production precisely. An evaluation of the tertiary gas injection project indicated that 10% more of the OOIP was produced, compared to only injecting water.

Graue and Blevins (1978) is a field study of a tertiary gas injection pilot of CO2. The reservoir used for this pilot was an area in the Sacroc field in Texas. The pilot consisted of injecting 2.3 BSCF slugs in six wells over a period of nine months to explore the effects of CO2 injection. A waterflooding process was applied to the reservoir before the gas injection pilot. The gas injection increased the recovery with 3% to 5.75% of OOIP. Analysis of the process revealed that the volumetric sweep efficiency was approximately 33%. Investigations proved that the injection process was stopped too early, and that it was possible to increase the recovery further. Furthermore, compositional analysis of the produced fluids in the six different wells proved that miscibility took place some places, while the reservoir fluids and the CO2 was not miscible in other parts of the reservoir. The miscibility was indicated by the increase in intermediate components in the produced gas, due to vaporization of oil.

A field study of the Alwyn North reservoir is presented by Burns et al. (2002). The field is a North Sea reservoir, found in the UK sector. The reservoir is located in the Middle Jurassic Brent group. The field has been produced with pressure support from water injection from 1988. To enhance oil production in later stages of the field development, a tertiary gas injection pilot was initiated in 1997. Due to the success of this pilot, full field injection began in 1999 with an injection rate of 1.68 $\frac{Gsm^3}{day}$. The injection gas was recycled gas from production, hence a lean hydrocarbon gas. The conditions in the reservoir facilitated miscibility between the injected gas and the reservoir oil. At the time of publishing of Burns et al. (2002), in 2002, it was estimated that 1.5 million bbl of incremental oil was produced. An estimation predicted a potential of approximately 33 Mboe incremental oil from the gas injection program. To obtain such insights reservoir simulation models were made, and extensive simulations were conducted. The measurements of relative permeability of oil-water and gas-oil proved that the residual oil saturation with respect to water, S_{orw}, ranged from 18% to 35%. The oil residual with respect to gas, S_{org}, was found to be significantly smaller, ranging from 7% to 15%. Even though Burns et al. (2002) mentions measurements of saturation functions for use in

reservoir simulations, there is no mention of any specific three-phase modelling. However, the simulation of the tertiary gas injection was vital to predict performance of the program.

As seen from the presented field studies, the tertiary gas injection often increases the oil recovery significantly, but never as much as seen in laboratory experiments. Many of the field studies also reports that reservoir simulation of the tertiary gas injection was used to predict the EOR advantage. Thus, implementation of such projects in the industry seems to be very dependent on accurate forecasts by precise reservoir simulation of the phenomena seen during tertiary gas injection.

Chapter 3

Theory

This chapter presents theory necessary to understand the simulations of the core flooding experiments. Theory presented in this section is directly applied to simulate the core flooding experiments. Especially the ODD3P three-phase model is different from traditional models, and a deeper explanation of its functionalities is of high importance. Furthermore, the following topics will be presented in this chapter:

- E300 and Reservoir Simulations
- ODD3P Three-Phase Model
- PVT and Equation of State

3.1 E300 and Reservoir Simulations

To simulate the core flooding experiments Schlumbergers Eclipse E300 is used. This is an industrial compositional reservoir simulator. Different from a black oil simulator, a compositional simulator requires tracking of all the components or pseudocomponents concentration throughout the simulation. Using this type of simulator is of high importance for these experiments, as it is expected that significant mass transfer effects will play an important role. A black oil type reservoir simulator would not be able to include this type of mass transfer phenomena, since it does not include changes in compositions. A compositional simulator relies one a PVT model that calculates the

phase equilibriums and the distribution of compositions in the fluid phases. Such a model is also able to handle changes in fluid densities, interfacial tension and viscosity.

The E300 includes all these features. This simulator allows the user to use a wide range of models and inputs. In addition, it includes the option to use equation of state to model the fluid PVT behavior. This is utilized in the simulations of the experiments, as correct PVT modelling is of high importance.

Furthermore, one of the most important features of the E300 simulator in this case, is the fact that the ODD3P three-phase model is implemented. This allows for painless implementation of the model. E300 includes a range of keywords specific to the ODD3P model, where the most important data can be supplemented.

3.2 ODD3P Three-Phase Model

The ODD3P model is a fully coupled three-phase model (Hustad and Browning, 2010). The model is utilizing data between all phases to model the saturation functions; relative permeability and capillary pressure. Inspired by the lack of flexibility in the more traditional models, such as Stones first and second model and Bakers model, the ODD3P model is not restricted to any specific wettability or such assumptions. Many of the problems related to these models, discussed in chapter 2, should be possible to model properly with the ODD3P model, due to its flexible nature.

The ODD3P model makes a connection between the capillary pressure and the relative permeability. Furthermore, the model incorporates both primary and hysteresis to both capillary pressure and relative permeability, while maintaining the two-phase properties at the two-phase boundaries. The model accounts for miscibility between the oil and gas phase. There is also high flexibility regarding residual saturations, as all residual saturations with respect to every phase are required as input. This includes both residual saturation for primary and hysteresis processes. Residual saturation, relative permeability and capillary pressure are all scaled throughout the simulation with respect to changing interfacial tension.

All these properties of the ODD3P model are presented in this chapter. The model is categorized with the other three-phase models that are based on measured two phase properties to calculate the three-phase properties.

Firstly, the models two-phase formulation is presented. This includes all input data and processing of this data. The model uses the two-phase properties to make up a three-phase formulation. The three-phase properties are being calculated from the two-phase properties, with different approaches. Hustad and Browning (2010) presents a weighting scheme for the relative permeability and two different approaches to calculate the three-phase capillary pressure.

3.2.1 Input data

The ODD3P three-phase model requires more input data than the more traditional models. Two-phase relative permeability and capillary pressure data between all phases are required. This includes oil-water, gas-oil and gas-water data, and both primary and hysteresis curves. None of the models presented in the literature study, chapter 2, take use of the saturation functions between water and gas, as it is assumed that these phases are not in contact. This is not the case in the ODD3P model, which takes use of all data. All the saturation functions are stated in form of tables in the E300 simulator, as a function of one of the phase-pairs saturations. Furthermore, all phase pair also has an associated interfacial tension reference as an input. This reference must be higher than the threshold interfacial tension between the phases, which is an input as well. The significance of the interfacial tension and how it is used for scaling, will be elucidated further later in this chapter. The gas-water properties may be represented by the oil-water data. If the oil and gas are miscible, this representation is recommended to avoid to unnecessary data management complexity. As the hydrocarbon phases approach each other in a miscible run, the properties of water-hydrocarbons also have to approach each other. This may be complex if the data is not represented by the same curves.

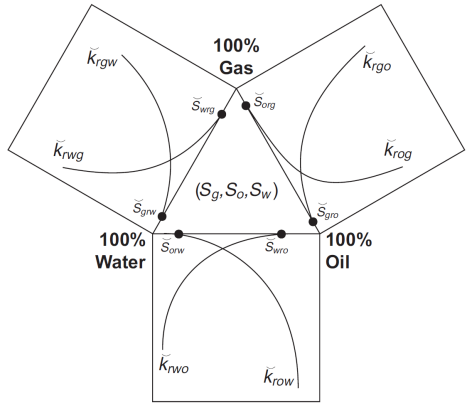

Figure 3.1: Required input data for the ODD3P-model (Hustad and Browning, 2010)

There is no limits on the number of saturation function data sets in the ODD3P model. If the reservoir model require different types of saturation functions for different regions, one may input as many sets of saturation functions as necessary and delegate the sets to the specific regions. The model accounts for wettability through the input rock curves. The wettability properties are reflected in the two-phase measurements, especially if both primary and hysteresis data are included. Hustad and Browning (2010) exemplifies this with the natural saturation process seen in reservoirs. A reservoir is always initially filled with only formation water. As oil imbibes the reservoir with time the primary oil-water properties are used. This data describes the primary saturation functions between oil and water in a water-wet system. Initially, the system must be water-wet, due to the lack of any other phase. At later times, when the reservoir is depleted, the nature of the system may have obtained wetting properties different from water-wet. This will be seen in the hysteresis data between oil and water. Hence, the ODD3P model incorporates the wettability properties by utilizing the data found in the two-phase saturation functions.

The ODD3P model requires all endpoint saturations of every phase, with respect to every other phase. A phase may have very different end-points when displaced by different fluids. Many investigators (Hustad et al., 1992) have seen a trend where endpoints saturations of liquids are significantly lower when gas entered the system. Hence, all the end-points are input data for the model, and both primary and hysteresis endpoints are required, as they may differ. The required endpoint data may be seen in

equation 3.1. $\bar{S}_{irj}$ refers to the input saturation end-point of phase i with respect to phase j. The superscript pr indicates primary endpoints, while hr indicates hysteresis.

$$\begin{array}{llllll} \bar{S}^{pr}_{gro}, & \bar{S}^{pr}_{grw}, & \bar{S}^{pr}_{org}, & \bar{S}^{pr}_{orw}, & \bar{S}^{pr}_{wrg}, & \bar{S}^{pr}_{wro} \\ \bar{S}^{hr}_{gro}, & \bar{S}^{hr}_{grw}, & \bar{S}^{hr}_{org}, & \bar{S}^{hr}_{orw}, & \bar{S}^{hr}_{wrg}, & \bar{S}^{hr}_{wro} \end{array} \tag{3.1}$$

3.2.2 Two-Phase Formulation

The model uses a two-phase saturation formulation to handle the input data in an appropriate process before calculating the three-phase properties. This process includes scaling with respect to interfacial tension due to miscibility, hysteresis, and so-called Land scaling.

The model performs a normalization of the input saturation curves with respect to the input endpoint saturations, as seen in equation 3.2.

$$S_i = \frac{\check{S}_i - \check{S}_{irj}}{1 - \check{S}_{irj} - \check{S}_{jri}} \tag{3.2}$$

S_i is the normalized saturation, while $\check{S}_i$ is the input saturation. This normalization ensures that when a gridblock saturation is used to look up values in a saturation function, the table is normalized from zero to unity. As will be seen later, the gridblock endpoints may vary due to several factors. Hence, the gridblock saturations will be normalized with respect to the gridblocks endpoints, and obtain a scale from zero to unity. When this normalized gridblock saturation is used to look up values, the table with the saturation function must also be normalized. This ensures a one-to-one relationship between the gridblock saturations and the input saturations.

The end-point saturations should always be in-line with the proposed reference interfacial tension. If the interfacial tension should decrease to values smaller than the threshold value, an IFT-scaling is invoked on the gridblock end-points. Hence, no IFT-scaling is applied as long as the interfacial tension remains above the threshold value. When the interfacial tension falls beneath the threshold value, the following scaling factor is calculated, seen in equation 3.3.

$$f^{IFT}_{ij} = \left(\frac{\sigma_{ij}}{\sigma^{th}_{ij}} \right)^{n_{ij}} \tag{3.3}$$

In equation 3.3 f_{ij}^{IFT} is the scaling factor between phase i and j. σ_{ij} is the interfacial tension and th marks that this is the input threshold value. Furthermore, n_{ij} denotes an user defined exponent, which may be applied to alter the relationship. This provides the user more flexibility. The constant has a default value of one.

One may also use capillary number as a scaling factor instead of interfacial tension. The capillary number is defined in equation 3.4.

$$N_{cij} = \frac{u_i \mu_i}{\sigma_{ij}} \tag{3.4}$$

N_{cij} denotes the capillary number between phase i and j. u_i is the darcy velocity, μ_i is viscosity and σ_{ij} is the interfacial tension. A similar scaling factor is defined for the capillary number scaling, which may be seen in equation 3.5.

$$f_{ij}^{N_c} = \left(\frac{N_{cij}}{N_{cij}^{th}} \right)^{m_{ij}} \tag{3.5}$$

Hence, a similar type as equation 3.3. N_{cij}^{th} is the threshold capillary number, which works in the same way as the threshold IFT with respect to scaling, except that it is inverse with respect to IFT. Scaling occurs when the capillary number is higher than the threshold capilalry number. m_{ij} is a user defined exponent, used if the user would like to alter the relationship. The scaling factors are applied to the grid block end-point saturation as seen in the following equation.

$$\hat{S}_{irj}^{m,\kappa} = \bar{S}_{irj}^{\kappa} f_{ij}^{\eta} \tag{3.6}$$

$\hat{S}_{irj}^{m,\kappa}$ is the scaled gridblock residual saturation of phase i with respect to phase j. κ shows if the given endpoint saturation is the primary or hysteresis endpoint. The superscript m is indicating that this is the scaled saturation value. $\bar{S}_{irj}^{\kappa}$ is the input gridblock endpoint saturation, and f_{ij}^{η} is again the scaling factor, where η is indicating whether scaling occurs due to IFT or capillary number.

As discussed in chapter 2, the endpoint saturations is often a function of the saturation history. To model this behavior the ODD3P model uses so-called Land scaling (Land et al., 1968). Hence, the gridblock endpoint saturations are subject to Land scaling, which may be seen in equation 3.7.

$$\hat{S}^{\kappa}_{irj} = \frac{\bar{S}^{max}_{i}}{1 + \frac{\bar{S}^{max}_{i}}{\hat{S}^{m,\kappa}_{irj}} - \frac{\bar{S}^{max}_{i}}{1-\hat{S}^{m,\kappa}_{irj}}} \tag{3.7}$$

$\bar{S}^{max}_{i}$ is the highest saturation of phase i seen in the gridblock and $\hat{S}^{\kappa}_{irj}$ is the scaled grid block value.

When switching from the primary endpoint to the hysteresis endpoint, the model takes special considerations, which ensures a smooth transition. There are several criteria the must be fulfilled for the transition to begin. The first criteria is that the saturation direction must have changed direction. Hence, the saturation must go from increasing to decreasing. Furthermore, the saturation must also be in the range of the hysteresis curves; if not, the switch from primary endpoints to hysteresis endpoints is not allowed to happen. The last criteria is that the relative permeability must be in the range of the hysteresis range as well. When all these criteria are fulfilled, the switching starts. To ensure that this transition goes smoothly a used defined rate of change is introduced, namely $\dot{S}$. The relationship is controlled as seen in equation 3.8.

$$|\bar{S}^{t}_{irj} - \bar{S}^{t+\Delta t}_{irj}| \leq \dot{S}\Delta t \tag{3.8}$$

Δt is the simualtion time-step and $\dot{S}$ is the rate of cahnge. The user may chose a value of $\dot{S}$, but it should be so that the endpoints change in a smooth manner.

After scaling the endpoints with respect to either capillary number or interfacial tension, process dependency (Land-scaling) and switching mechanisms, the endpoint values for each gridblock are used to calculate the normalized gridblock saturations.

The normalized saturation is used to find the value of relative permeability and capillary pressure for the given gridblock. However, switching saturation direction invokes switching from one hysteresis curve to another. This requires special treatment.

As both capillary pressure and relative permeability must be continuous functions, a sudden jump from one curve to another would not work very well. Hence, the two-phase formulation in the ODD3P model includes a method that ensures continuous curves when switching between the increasing and decreasing hysteresis curves.

This method involves using scanning lines to identify the saturations at the turning point when switching from one curve to another. This is shown in figure 3.3, which

includes the dotted scanning lines.

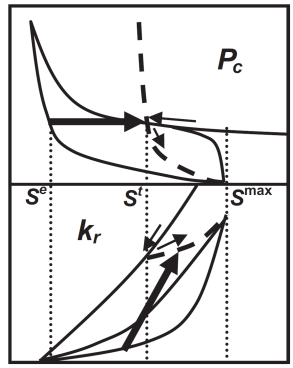

Figure 3.2: Hysteresis switching schematic (Hustad and Browning, 2010)

Figure 3.3 is a schematic showing the principle behind the hysteresis switching method. The upper part is devoted to capillary pressure and includes primary, increasing and decreasing functions, seen in thick hard lines. In the bottom half the relative permeability is shown, with primary, increasing and decreasing curves as well. The x-axis shows saturation for both capillary pressure and relative permeability.

The principle behind the method is shown in figure 3.3, which shows an example were saturation is decreasing and following the primary curve. At a given point the saturation direction turns into increasing, and the increasing hysteresis curve should be followed. This point is the turning saturation, S^t , seen in figure 3.3. The shape of the increasing hysteresis curve is the one to be followed, while the values must be continuous. To obtain this for the capillary pressure curve, the so-called equivalent saturation is used, S^e. This value is found by locating where the capillary pressure of the increasing curve has the same value as the primary curve. The associated saturation is the equivalent saturation. The increasing curve between the equivalent saturation and the maximum saturation is compressed into the new interval, from turning point saturation to maximum saturation. One may call it a normalization of the former interval into a new interval, illustrated by the striped line in figure 3.3. The model uses a mathematical expression to find the hysteresis saturation based on said principle, seen in equation 3.9.

$$S_i^h = S_i + \left(S_i^e - S_i^t\right)\left(\frac{1 - S_i^e}{1 - S_i^t}\right) \tag{3.9}$$

Equation 3.9 is only valid for switching to increasing saturation. S_i is the normalized input saturation found in equation 3.2. As long as the saturation is increasing after switching, equation 3.9 is used to find the hysteresis saturation, and S^e and S^t are treated as constants found at the moment of change in saturation direction.

When switching back to decreasing saturation, the model applies another mathematical expression, seen in equation 3.10.

$$S_i^h = S_i\left(\frac{S_i^e}{S_i^t}\right) \tag{3.10}$$

The model records the equivalent and turning point saturation in the same manner as for the expression for increasing saturation.

Using the S_i^h saturation to look up capillary pressures ensures that the right curve is used, the endpoints are correct and the capillary pressure is a continuous function. This method is applied to each gridblock, ensuring that each gridblock is assigned the proper hysteresis capillary pressure at all times. This formulation requires that the change in saturation direction between all phases in all gridblocks are recorded for every time step.

Furthermore, the model applies a similar mathematical model to the relative permeability hysteresis formulation. The aim is to follow the shape of the new curve, but maintain start and endpoints. The curves are also continuous at all times. For switching from the primary curve into the increasing saturation curve the model is using the following equation.

$$\tilde{k}_{rij}(S_i) = k^d_{rij}\left(S_i^t\right) + [k^i_{rij}(1) - k^d_{rij}\left(S_i^t\right)]\left[\frac{k^i_{rij}\left(S_i^h\right) - k^i_{rij}\left(S_i^e\right)}{k^i_{rij}(1) - k^i_{rij}\left(S_i^e\right)}\right] \tag{3.11}$$

$\tilde{k}_{rij}(S_i)$ is the representative relative permeability for the phase i, found from the hysteresis formulation. S^t and S^e are the equivalent and turning point saturation, found at the moment of switching. k^d_{rij} is the decreasing relative permeability curve, while k^i_{rij} is the decreasing relative permeability curve, both between phase i and j. As the input saturation is normalized, as seen in equation 3.2, the new range is from the equiv-

alent saturation to unity, hence, the new relative permeability is normalized into this range. Equation 3.11 is a mathematical expression of the schematic seen in figure 3.3. The expression may be simplified by dividing it into three terms on the right hand side. The first term, $k^d_{krij}\left(S^t_i\right)$, is the the relative permeability value at the turning point. As S^h_i must be equal to S^e initially, the two lasts terms is cancelled, and the start value of the hysteresis formulation begins in the turning point. The second term, seen in the first brackets, is the ultimate increase in relative permeability. The third term is moving from zero to unity when the saturation increases in the saturation range. Notice that when S^h_i is equal to unity the whole last bracket is equal to unity, and the whole expression ends up being equal to $k^i_{rij}(1)$ which is the end point of the increasing relative permeability curve. Hence, the representative permeability is always continuous and has the appropriate ending point that represent the input curves. As with the capillary pressure formulation, equation 3.11 only applies to switching from decreasing to increasing saturations. For switching from increasing to decreasing, the following equation is applied.

$$\tilde{k}_{rij}\left(S_i\right) = k^d_{rij}\left(S^h_i\right)\left[\frac{k^i_{rij}\left(S^t_i\right)}{k^d_{rij}\left(S^e_i\right)}\right] \tag{3.12}$$

Equation 3.12 works in a similar manner as equation 3.11. However, while equation 3.11 ensures that the representative permeability, $\tilde{k}_{rij}$, approaches the increasing relative permeability end-point value at the highest normalized saturation, equation 3.12 ensures that the representative relative permeability is zero when the normalized saturation is zero.

The hysteresis formulation for capillary pressure and relative permeability may seem complicated. However, the representative values for capillary pressure and relative permeability are always values found either on, or in the span of the input rock curves. The reader should also study figure 3.3, which gives a clear picture of the hysteresis process. Furthermore, a minimum limit to when the switching process between hysteresis curves occurs must be provided as an input. This ensures that switching between the given curves will not begin until the saturation change is larger than said limit. This prevents excessive switching between curves, and reduces CPU time.

If there are miscible processes involved in the simulation, the capillary pressure and

relative permeability must be scaled accordingly before used in the three-phase formulation. The capillary pressure is scaled using a scaling factor, given in equation 3.13.

$$f_{ij}^{P_c} = \left(\frac{\sigma_{ij}}{\sigma_{ij}^{r}} \right)^{l_{ij}} \tag{3.13}$$

σ_{ij} is the interfacial tension between the phases i and j, r indicates the reference value and $f_{ij}^{P_c}$ is the scaling factor. l_{ij} is a user-defined value, used if special consideration is necessary. The scaling of capillary pressure is not limited to any threshold value, and is applied for all interfacial tensions. The scaling factor is applied to the capillary pressure as seen in equation 3.14.

$$\hat{P}_{cij} = f_{ij}^{P_c} \tilde{P}_{cij} \tag{3.14}$$

The relative permeability is scaled with the scaling factor found in equation 3.3 and 3.5, as seen in equation 3.15 and 3.16.

$$\hat{k}_{rij} = \tilde{k}_{rij} \tag{3.15}$$

$$\hat{k}_{rij} = f_{ij}^{\eta} \tilde{k}_{rij} + \left(1 - f_{ij}^{\eta}\right) S_i \tag{3.16}$$

Note that scaling does only apply to the relative permeability, when the scaling factor, f_{ij}^{η}, is below unity. Thus, if the scaling factor is above unity, equation 3.15 is used. If not, equation 3.16 is used for scaling. The relative permeability scaling model is presented in Coats et al. (1980), but also applied in the ODD3P model.

If the phases are miscible special considerations have to be taken. The hydrocarbon phases must have the same endpoint at equal IFT with water. This is ensured with the use of equation 3.17 and 3.18. This is only applied in a miscible process, to ensure consistency when the oil and gas label is unclear. The ± sign is positive or negative depending on which endpoint is larger, and is chosen such that the last term in 3.17 and 3.18 are positive.

$$\bar{S}_{irw} = \bar{S}_{irw}^{\kappa} \pm \frac{1}{2} \left(1 - f_{go}^{\eta}\right) |\bar{S}_{grw}^{\kappa} - \bar{S}_{orw}^{\kappa}| \tag{3.17}$$

$$\bar{S}_{wri} = \bar{S}^{\kappa}_{wri} \pm \frac{1}{2}\left(1 - f^{\eta}_{go}\right)|\bar{S}^{\kappa}_{grw} - \bar{S}^{\kappa}_{orw}| \tag{3.18}$$

Before moving onto the three-phase formulation of the ODD3P model, the steps of obtaining the two-phase saturation functions are repeated in a bullet-style list:

- Input: Hysteresis and primary curves for capillary pressure and relative permeability between all three phases.
- Input: Primary and hysteresis endpoint saturation values.
- Input: Reference and threshold IFT, or Nc.
- The gridblock endpoint saturations are scaled with respect to IFT/Nc, saturation history (Land scaling) and switching formulation from primary to hysteresis endpoints.
- The new gridblock endpoint saturations are used to find the normalized gridblock saturation .
- This normalized gridblock saturation is used to find the representative relative permeability and capillary pressure with respect to hysteresis and primary curves.
- If there is miscibility the representative capillary pressure and representative relative permeability must be scaled accordingly.

3.2.3 Three-Phase Formulation

The ODD3P model is using the representative two-phase functions, $\tilde{k}_{rij}$ and $\tilde{P}_{cij}$, to formulate the three-phase properties in the three phase space. If scaling is applied the scaled representative functions are used, namely $\hat{k}_{rij}$ and $\hat{P}_{cij}$. To ensure both consistency and that the relative permeability is zero below the endpoints, the saturation functions are dependent on its own saturation.

Furthermore, the input saturations are normalized, as in the two-phase formulation. This allows the gridblock endpoints to vary within the three-phase space. This normalization is slightly more complex than the two-phase normalization. It utilizes the six gridblock endpoint saturations and the three gridblock input saturations, of the

three different phases. Using these values one may calculate the minimum and maximum saturations where the phase, i, may be mobile. This may be seen in equation 3.19 and 3.20.

$$\bar{S}_{imn} = \frac{\bar{S}_j \bar{S}_{irj} + \bar{S}_k \bar{S}_{irk} + \bar{S}_{irj} \bar{S}_{irk} \left(\bar{S}_i - 1\right)}{\bar{S}_j \left(1 - \bar{S}_{irk}\right) + \bar{S}_k \left(1 - \bar{S}_{irj}\right)} \tag{3.19}$$

$$\bar{S}_{imx} = \frac{\bar{S}_j \bar{S}_{kri} + \bar{S}_k \bar{S}_{jri} + \bar{S}_{jri} \bar{S}_{kri} \left(\bar{S}_i - 1\right)}{\bar{S}_j \bar{S}_{kri} + \bar{S}_k \bar{S}_{jri}} \tag{3.20}$$

$\bar{S}_{imn}$ is minimum saturation, $\bar{S}_{imx}$ is the maximum saturation and $\bar{S}_{irj}$ is the input endpoint saturation of phase i to the phase j or k. i, j and k indicates the three phases and can not be equal to one another. The principle behind equation 3.19 and 3.20 may be seen in figure 3.3.

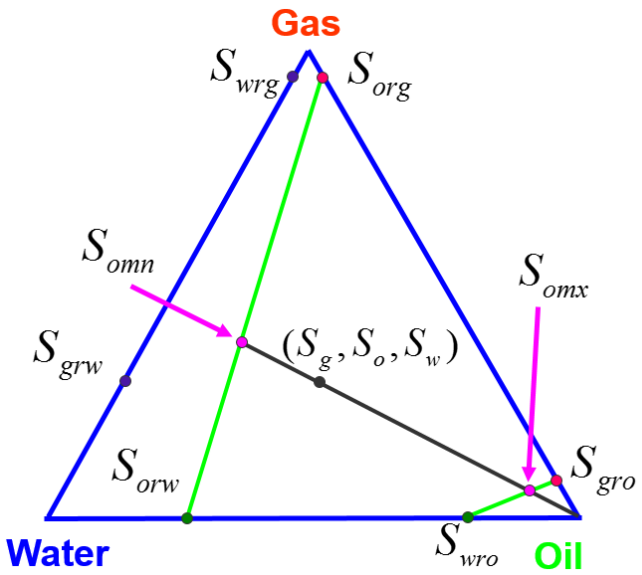

Figure 3.3: Schematic of three-phase normalization Hustad (2015)

The maximum and minimum saturation of each phase is then used in the normalization of the gridblock saturation, as seen in equation 3.21.

$$S_i = \frac{\bar{S}_i - \bar{S}_{imn}}{\bar{S}_{imx} - \bar{S}_{imn}} \tag{3.21}$$

One may notice that the three saturations may not sum to unity when normalized in the three-phase space. They do sum to unity at the two phase borders, which ensures consistency. Using the three-phase normalized saturation, the hysteresis saturation are calculated using equation 3.9 or 3.10, depending on whether the respective phase is increasing or decreasing. This is the same process that was seen in the two-phase formulation. Hence, the hysteresis saturations, S_o^h, S_g^h and S_w^h, are used to find the representative capillary pressure and relative permeability. This provides six different capillary pressures, as capillary pressure may be a function of one of the two phases in the phase pair. The six capillary pressures values can be seen in equation 3.22.

$$\begin{aligned} \tilde{P}_{cgo}(S_g^h), \quad \tilde{P}_{cgo}(S_o^h) \\ \tilde{P}_{cgw}(S_g^h), \quad \tilde{P}_{cgo}(S_w^h) \\ \tilde{P}_{cow}(S_o^h), \quad \tilde{P}_{cow}(S_w^h) \end{aligned} \tag{3.22}$$

From the six relative permeability input curves, two relative permeability values are found with the three normalized hysteresis saturations, listed in equation 3.23.

$$\begin{aligned} \tilde{k}_{rgo}(S_g^h), \quad \tilde{k}_{rgw}(S_g^h) \\ \tilde{k}_{rog}(S_o^h), \quad \tilde{k}_{row}(S_o^h) \\ \tilde{k}_{rwg}(S_w^h), \quad \tilde{k}_{rwo}(S_w^h) \end{aligned} \tag{3.23}$$

Notice the superscript on $\tilde{k}$ and $\tilde{P}_c$, which indicates that these are the representative values. These values may be subject to scaling. The capillary pressure is scaled with changing IFT, as seen in equation 3.14. If the interfacial tension falls below the threshold value, the relative permeability should be scaled accordingly as well, which gives the scaled representative values; $\hat{P}_{cij}$ and $\hat{k}_{rij}$.

Regarding relative permeability, each phase must only have one value of relative permeability at any given saturation. Hence, the relative permeability of a given phase is found from a saturation weighting scheme, using the two relative permeabilities with respect to that given phase. This can be seen in equation 3.24.

$$k_{ri} = \frac{\bar{S}_j}{\bar{S}_j + \bar{S}_k} \tilde{k}_{rij} + \frac{\bar{S}_k}{\bar{S}_j + \bar{S}_j} \tilde{k}_{rik} \tag{3.24}$$

$\bar{S}$ is the input saturation of the gridblock and i, j and k indicate oil, water and gas. This formulation ensures that the relative permeability is weighted against the saturation, and that the two-phase properties are ensured at the two-phase boundaries. The weighting scheme is also seen in earlier models, such as Baker (Baker et al., 1988), however, in a simpler form. Furthermore, in the ODD3P model, relative permeability between all phases are treated equally. Many traditional models does only address the relative permeability of oil, and ignores water and gas.

The same principle is seen regarding the capillary pressure, not all six values are used simultaneously. Hence, the ODD3P model includes two different approaches to determine which capillary pressure to use, and how to treat the given capillary pressure.

The first approach is the most flexible one, and involves choosing the capillary pressure most fit for the given situation. Each phase pair has two representative capillary pressures, hence six all together, seen in equation 3.22. One of the capillary pressures in each pair must be picked, and this may be done with respect to a range of different parameters, for example wettability of the system. To exemplify, one may choose between capillary pressure between oil and water that are either dependent on the hysteresis water saturation, S_w^h, or the hysteresis oil saturation, S_o^h. In water wet conditions the capillary pressure is typically a function of the water saturation, hence this dependency is chosen, as it fits the situation. This ensures full user flexibility. However, the capillary pressures must meet the following requirement, seen in equation 3.25.

$$P_{cgw} - P_{cgo} - P_{cow} = 0 \tag{3.25}$$

The three representative capillary pressures chosen, $\hat{P}_{cgw}$, $\hat{P}_{cgo}$ and $\hat{P}_{cow}$, may not summarize to zero, as required. Hence, a residual is introduced to fulfill the requirement in equation 3.25.

$$\hat{P}_{cgw} - \hat{P}_{cgo} - \hat{P}_{cow} = R \tag{3.26}$$

The residual, R, seen in equation 3.26, is distributed to each capillary pressure to obtain the capillary pressures used in the pressure equation. Hence, the residual is distributed with three distribution parameters, $F(S_w)$, $H(S_g)$ and $G(S_w, S_g)$.

$$F + G + H = 1 \tag{3.27}$$

As seen in equation 3.27, the distribution functions must sum to unity. The three functions are then used to distribute the residual, R, onto the three representative capillary pressures, to obtain the capillary pressure used directly in the flow equations.

$$P_{cgo} = \hat{P}_{cgo} + FR \tag{3.28}$$

$$P_{cgw} = \hat{P}_{cgw} - GR \tag{3.29}$$

$$P_{cow} = \hat{P}_{cow} + HR \tag{3.30}$$

These three equations ensures fulfillment of the capillary pressure criteria. Furthermore, the functions F, H and G, are dependent on several different mechanisms such as interfacial tension, wettability, rock characteristics and contact angels. Hence, no exact relationship is presented in the ODD3P model, however the functions are made dependent on several user-defined inputs, which makes them easily adjusted.

$$F = \frac{\delta_w \bar{S}_w^{\alpha_w}}{\bar{S}_w^{\alpha_w} + \left(1 - \bar{S}_w\right)^{\beta_w}} \tag{3.31}$$

$$H = \frac{\delta_g \bar{S}_g^{\alpha_g}}{\bar{S}_g^{\alpha_g} + \left(1 - \bar{S}_g\right)^{\beta_g}} \tag{3.32}$$

$$G = 1 - F - H \tag{3.33}$$

Equation 3.31, 3.32 and 3.33 describes a functional form of F, H and G. δ, α and β are user-defined, and may be tuned to make the distribution fit properly. Furthermore, dependency on the saturation of each phase is also included, to ensure consistency at the two-phase boundary.

The ODD3P model allows the F, H and G functions to be tabulated by the user, as a value versus saturation table. However, it must fulfill the boundary criteria, seen in

equation 3.34.

$$\begin{aligned} F(S_w = 0) = 0, \quad F(S_w = 1) = 1 \\ H(S_g = 0) = 0, \quad H(S_g = 1) = 1 \\ G(S_o = 0) = 0, \quad G(S_o = 1) = 1 \end{aligned} \tag{3.34}$$

ODD3P is included in Eclipse E300, where several combinations of choices of capillary pressure dependencies are given. In fact twelve different combinations. Each combinations represent different dependencies on saturation. For example does the sixth combination resemble a water-wet system, picking capillary pressure that resemble such conditions. These twelve options combined with the opportunity to control how the residual is distributed to the different capillary pressures at different saturations, gives the user full flexibility to model any given situation. The drawback is the requirement of measured data, and the complexity of the model, and the complexity of tuning the user-defined constants.

The second capillary pressure approach is somewhat simpler than the first approach. It includes a weighting scheme of the representative capillary pressures. Hence, one does not need to choose any specific dependency on any saturation. The capillary pressure are weighted with respect to the gridblock saturations, which may be seen in equation 3.35, 3.36 and 3.37.

$$PCG = \frac{\bar{S}_o}{\bar{S}_o + \bar{S}_w} \hat{P}_{cgo}\left(S_g^h\right) + \frac{\bar{S}_w}{\bar{S}_o + \bar{S}_w} \hat{P}_{cgw}\left(S_g^h\right) \tag{3.35}$$

$$PCO = \frac{\bar{S}_g}{\bar{S}_g + \bar{S}_w} \hat{P}_{cgo}\left(S_o^h\right) + \frac{\bar{S}_w}{\bar{S}_g + \bar{S}_w} \hat{P}_{cow}\left(S_o^h\right) \tag{3.36}$$

$$PCW = \frac{\bar{S}_g}{\bar{S}_g + \bar{S}_o} \hat{P}_{cgw}\left(S_w^h\right) + \frac{\bar{S}_o}{\bar{S}_g + \bar{S}_o} \hat{P}_{cow}\left(S_w^h\right) \tag{3.37}$$

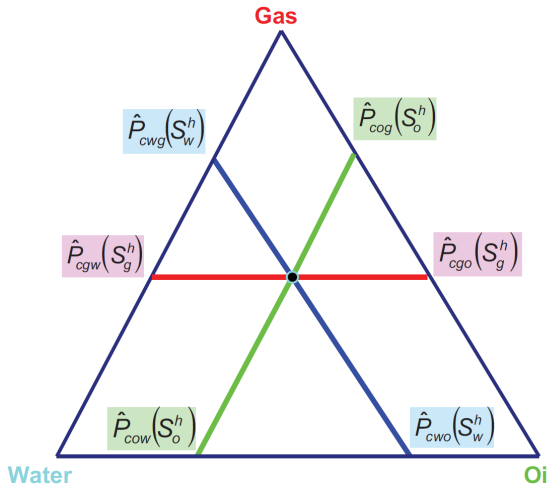

Figure 3.4: Capillary pressure weighting scheme. Hustad and Browning (2010)

$\bar{S}_i$ is the gridblock saturation. This formulation is based on the principle seen in figure 3.4, where gridblock saturations determines how much emphasis that should be put on each one of the two capillary pressure that represents each pair. Equations 3.35 to 3.37 may be written as a system of equations, seen in equation 3.38.

$$\begin{bmatrix} (\bar{S}_o + \bar{S}_w)\,PCG \\ (\bar{S}_g + \bar{S}_w)\,PCO \\ (\bar{S}_g + \bar{S}_o)\,PCW \end{bmatrix} = \begin{bmatrix} \bar{S}_o & \bar{S}_w & 0 \\ \bar{S}_g & 0 & \bar{S}_w \\ 0 & \bar{S}_g & \bar{S}_o \end{bmatrix} \begin{bmatrix} p_g - p_o \\ p_g - p_w \\ p_o - p_w \end{bmatrix} \tag{3.38}$$

Henceforth, by solving equation 3.38, the pressure of each phase is found explicitly.

Whether the first or second approach is used to find the true capillary pressure between the phases, the phase pressures are found from the capillary pressures. The phase pressures are calculated as seen in equation 3.39, 3.40 and 3.41.

$$p_o = p \tag{3.39}$$

$$p_g = p + P_{cgo} \tag{3.40}$$

$$p_w = p - P_{cow} \tag{3.41}$$

p_o, p_w and p_g are the phase pressure that is used in to solve the pressure equation

which governs the flow in the simulator.

To calculate the interfacial tension between water and either of the two hydrocarbon phases the following correlation is used.

$$\sigma_{iw} = A\left(\Delta\rho\right)^2 + B\Delta\rho + C \tag{3.42}$$

i is either gas or oil, σ is interfacial tension, ρ is density and A, B and C are user defined constants. $\Delta\rho$ is the difference between the water density and the hydrocarbon phase density. Notice how dependent IFT are on the density in this correlation.

The ODD3P model may seem overwhelmingly complex, both in theory and in practice. However, it is not too complex to use, as seen later in this thesis. All the normalizations and scalings are continuously handled by the reservoir simulator.

To summarize, the ODD3P model is a model that takes use of all data to predict the properties in the three-phase space. Miscibility, hysteresis and process dependency are all accounted for. The model does also apply the real endpoint saturation for every phase with respect to all phases, and not only one endpoint per phase. Furthermore, the ODD3P model makes the relative permeability depend on the capillary pressure, through the gridblock saturations.

3.3 PVT and Equation of State

As just presented, the ODD3P three-phase model is highly dependent on correct fluid properties, as they may change a lot through a simulation. Thus, predicting the correct fluid parameters such as density, interfacial tension and viscosity is vital. These properties largely depends on the phase behavior and the relationship between pressure, volumes and temperature, so-called PVT. Often this relationship is not measurable at all conditions, which entrusts this relationship to be predicted by some fluid model, or equation of state, long for EOS.

An equation of state is a model that relate the temperature, pressure and volumes to describe fluid and phase behavior properly. Often equation of states utilizes critical values of a series of different components to describe the resulting mix of all the components (Whitson et al., 2000). It is uncommon to use all components in a com-

positional simulator, rather than using a series of pseudocomponents. To get the fluid model right it is common to find, or tune, the critical parameters for the pseudocompents to represent the fluid behavior seen in experiments. Critical parameters include critical molar volume, critical pressure, critical temperature and acentric factor. These values are defined values for most known components, however, when applying pseudocomponents these critical parameters have to be found, or tuned to experimental data, for each pseudocomponent. The meaning of the critical parameters is the given components value when the component is at its critical point (Whitson et al., 2000).

There is a large range of different EOS in the literature, such as van der Waals, Redlich-Kwong, Peng-Robinson, Martin and Soave-Redlich-Kwong. As Soave-Redlich-Kwong, SRK, is applied in the simulations, a brief introduction is given to this particular EOS. The SRK-EOS are given in equation 3.43 (Whitson et al., 2000).

$$p = \frac{RT}{v-b} - \frac{a}{v(v+b)} \tag{3.43}$$

R is the ideal gas constant, p is pressure, T is temperature and V is volume. a and b are coefficients given by equation 3.44 and 3.45.

$$a = \Omega_a^o \frac{R^2 T_c^2}{p_c} \alpha(T_r) \tag{3.44}$$

$$b = \Omega_b^o \frac{RT_c}{p_c} \tag{3.45}$$

Ω_a^o is a constant with value 0.42747 and Ω_b^o is 0.08664. T_c is the critical temperature and p_c is the critical pressure. α is given by equation 3.46.

$$\alpha = \left[1 + m\left(1 - T_r^{0.5}\right)\right]^2 \tag{3.46}$$

T_r is the reduced temperature, given by equation 3.47, and m is defined in equation 3.48.

$$T_r = \frac{T}{T_c} \tag{3.47}$$

$$m = 0.480 + 1.574\omega - 0.176\omega^2 \tag{3.48}$$

ω is the acentric factor. Thus, by using the critical parameters of the pseduocomponents, the relationship between pressure, temperature and volume can be calculated. According to Whitson et al. (2000) the SRK EOS has a tendency to overestimate liquid volumes in a petroleum mix. Furthermore, the SRK EOS should also provide very good predictions of vapor properties.

Chapter 4

Background

As mentioned earlier, this master thesis revolves around two core flooding experiments conducted by Hustad et al. (1992) in 1992. This chapter presents an in depth description of the experiments, and the following experimental results. Understanding how the experiments were conducted is vital for understanding the recent simulations associated with this thesis. Furthermore, there have also been earlier attempts to simulate the experiments and obtain an accurate history match. However, none have been completely accurate with respect to all phases. Thus, a small section in this chapter is dedicated to discuss previous attempts and why it was not possible to obtain the desired results. Such a section gives the reader a background to why such advanced modelling is used, and needed, in the new simulations.

4.1 Core Flooding Experiments

Two core flooding experiments were conducted in 1992, in relations to the RUTH research program (Hinderaker et al., 1996). The objective of these experiments was to reveal the effects of mass transfer during tertiary gas injection. To explore these effects, two core flooding experiments were conducted on vertical cores. In the first experiment, hereby referred to as Experiment 1, the investigators used a gas that was in equilibrium to the oil. This would ensure that no, or to a small extent, mass transfer effect would happen throughout the experiment. The second experiment, hereby called Ex-

periment 2, was conducted at similar conditions; however, this time a dry separator gas was used instead. Hence, the only difference was supposedly the mass transfer effects.

Vertical cores were used for both experiments, and the floodings were done with a low injection rate to ensure a gravity stable sweeping process. Both cores was initially water filled. Firstly, oil was injected until reaching residual water saturation. This process ensured that the saturation direction and process of a real reservoir was maintained in both experiments. The saturation process may affect the residual saturations (Land et al., 1968) and the wetting of the system. This was followed by water flooding, and then by tertiary gas injection. All experiments were executed under reservoir conditions. Produced fluids were then directly brought to surface conditions, in a one-stage flash. The produced fluid volumes were measured at standard conditions.

4.1.1 Rocks and fluids

A Bentheimer sandstone was used in the experiments and rock curves measurements. Three different cores were used for measuring relative permeability and the displacement experiments, while smaller plugs were used for the measurements of parameters such as capillary pressure. The cores used in the displacement experiments had a length of approximately 1.2 meters, a porosity of approximately 23 percent and an absolute permeability of around 2600 mD. The cores used for Experiment 1 and 2 and the one used for relative permeability measurements had small differences in properties, and the exact data may be seen in table 4.1.

Table 4.1: Rock properties

Use	Diameter [cm]	Porosity [%]	Pore Volume [cm^3]	Permeability [D]
Rel. perm.	3.77	22.7	156.9	2.467
Experiment 1	3.78	22.7	312.8	2.566
Experiment 2	3.77	23.3	317.2	2.645

A North Sea oil was the hydrocarbon basis for fluids used in the displacement experiments. This live oil was obtained by recombination of oil and gas, with the ratio found from known separator rates. The systems equilibrium were found at 91.9° celcius and 313.5 bar. Furthermore, with the use of gas chromatography the compositions of the

fluids were found, along with other fluid properties. This may be seen in table A.2 in the appendix.

An artificial water composition was also made to represent formation water. The formation factor of this artificial water was measured to be 1.02187 sm3/Scm3 at 91.9° Celsius and 314 bar and 1.0255 sm3/Scm3 at 99° Celsius and 315 bar. A table of the ion compositions in the water may be seen in table A.3 in the appendix.

4.1.2 Measurements

Several properties were measured to obtain information around rock curves, rock properties and fluid properties. The interfacial tension between the fluids were measured using the pendant drop method. The authors observed a rather low interfacial tension between the oil and gas. The interfacial tensions may be seen in table A.2. By using plugs of the Bentheimer sandstone and centrifuge methods the capillary pressure was measured. In these measurements, decane was used for oil and air for gas. The wetting phase was always drained by the non-wetting phases. The resulting capillary curves may be seen in figure 4.1.

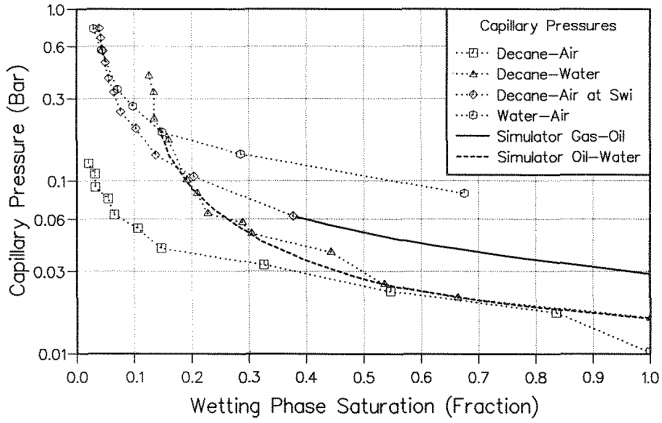

Figure 4.1: Capillary pressure measurements. (Hustad et al., 1992)

While making these measurements the authors noticed that when introducing gas into the system the liquid residual always went to lower values than if only liquids were present. The residual saturations and the interfacial tension between the fluids in the measurements can be seen in table 4.2. The interfacial tension was used for scaling the

capillary curve, making it representative for the actual fluids used in the displacement experiments.

Table 4.2: Residuals and IFT from draining processes with air, decane and water

Process	Residual Saturation	IFT
Decane drained by air	$S_{org} = 5.3\%$	$\sigma_{og} = 23.4 mN/m$
Water drained by decane	$S_{wro} = 13.2\%$	$\sigma_{wo} = 37.1 mN/m$
Water drained by decane, then by air	$S_{wrg} = 0.5\%$	-
Water drained by air	$S_{wrg} = 4.5\%$	$\sigma_{wg} = 72 mN/m$

Furthermore, relative permeability was measured using a smaller core than used in the coreflooding experiments. Here, decane was still used for oil, while nitrogen was used for gas. During these measurements, the core was always initially saturated with artificial formation water. This was followed by injection of fixed rates of different fluid combinations. The resulting curves may be seen in figure 4.2.

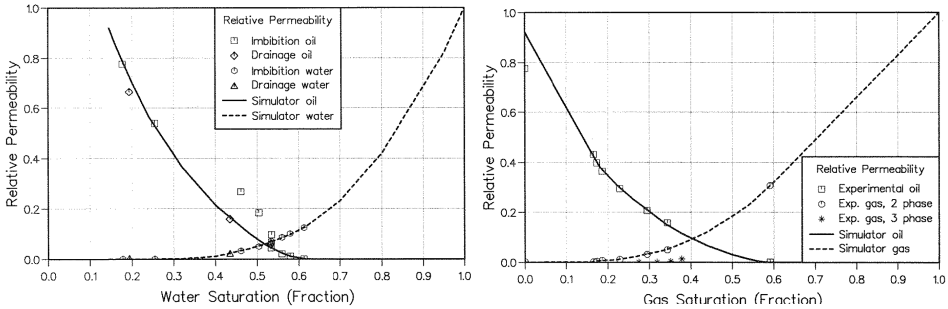

(a) Oil-water relative permeability.

(b) Gas-Oil relative permeability.

Figure 4.2: Relative permeability measurements. (Hustad et al., 1992)

Figure 4.2 a) shows the relative permeability between water and oil, while 4.2 b) shows relative permeability between oil and gas. These measurements also provided residual phase saturations. Irreducible water saturation was found to be 17.7%. However, when gas was introduced in the measurements of oil-gas relative permeability, the irreducible water saturation decreased to 13.2%. Residual oil saturation was found to be 38.4% when drained by water, and 27.7% when drained by gas. As may be seen in the gas-oil curves in figure 4.2 b), the gas residual saturation was measured to nearly 0%.

The liquid residuals are not constant. As seen in the capillary pressure measurements; the liquid residuals are decreasing when gas is introduced to make it a three-phase system. Furthermore, zero oil isoperms were also measured, but only for a limited amount of gas saturations. It should be noticed that the relative permeability measurements were conducted at 21° Celsius and 7 bar, which does not resemble the reservoir conditions.

4.1.3 Experimental Procedure

Experiment 1 and 2 were conducted using a flooding apparatus in reservoir conditions. These conditions were 315 bar and 92° Celsius for Experiment 1 and 315 bar and 99° Celsius for Experiment 2.

As with the measurements, the cores used in the experiments was initially filled with only artificial formation water. Firstly, oil was injected until residual water saturation was reached. This exact process was followed to obtain the natural saturation history and wetting properties, which would have been seen in real reservoirs. This was followed by a water flooding from the bottom of the core, and production on top of the core. A process that continued until reaching the residual oil saturation with respect to water. Hence, there was 34.8% oil in the core after water flooding. The residual oil was slightly higher in Experiment 2, at 36.86%, most likely due to different pressure and temperature. This was followed by gas injection from the top of the core and production from the bottom of the core. The injection rate was kept rather low to obtain gravity stable displacement, and a high sweep efficiency. As stated earlier, equilibrium gas was injected in Experiment 1 and dry separator gas was injected in Experiment 2. All the fluids were collected, and produced phase volumes were measured at standard conditions. The produced fluids were also analyzed with respect to GOR, density, compositions and other PVT data. This data was used by the authors for the simulations, but is also used in the new simulations that will be presented later in this thesis. Furthermore, at the end of each experiment the cores were cooled down and depressurized. This allowed the cores to be cut in pieces and analysis of end-saturations throughout the core.

4.1.4 Results and Observations of Coreflooding Experiments

The experimental production data was recorded from the beginning of the gas injection, as this was the process of interest to the authors. The cumulative production data for the three phases may be seen in figure 4.3 and 4.4.

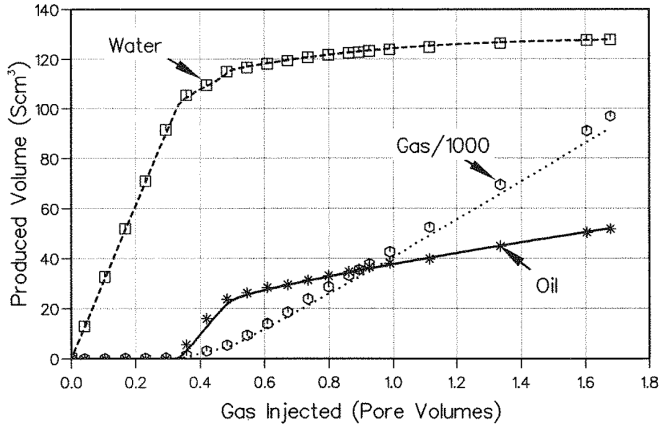

Figure 4.3: Cumulative production from Experiment 1. Includes both experimental and simulated results. (Hustad et al., 1992)

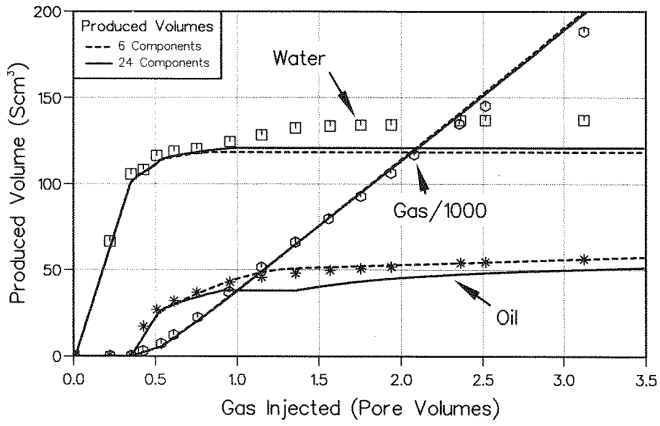

Figure 4.4: Cumulative production from Experiment 2. Includes both experimental and simulated results. (Hustad et al., 1992)

The experimental water data are represented by the square shaped data points, the gas are represented by the circles and oil by the astrix shapes. The production data shows that only water is produced at first, until gas and then oil breaks through. As the

core was filled with mobile water and immobile oil at the beginning of the gas flooding, this was an expected result. In Experiment 1, the oil had a breaktrough at 0.324 pore volumes of gas injected, and the gas at 0.469 pore volumes injected. For Experiment 2 the breakthrough came at 0.342 and 0.477 pore volumes injected, for oil and gas. The exact time of the breakthrough was caught on video recordings. After breakthrough of oil, quite large volumes of oil could be seen in both experiments, explained as an arrival of an oil bank. After the oil bank was produced, a decline in oil production could be seen. However, in both experiments oil was still produced, but by entirely different mechanisms. In Experiment 1 oil was still being produced due to condensate from the equilibrium gas. Hence, the oil after oil breaktrough is most likely not a product of convective flow of oil in the core, but rather condensate falling out from the equilibrium gas at separator conditions. Furthermore, in Experiment 2 only dry gas was injected, and all produced oil must be from original oil in place in the core. After the oil bank is produced, the following oil production is most likely a result of vaporization of the oil in the core. Hence, oil is still produced due to mass transfer effects. As the equilibrium oil and gas were recombined from known separator rates, the GOR are also known. These parameters and the production data, may be used to separate what parts of the oil that originated from the original oil in place, and what parts that is condensate from the equilibrium gas that was injected.

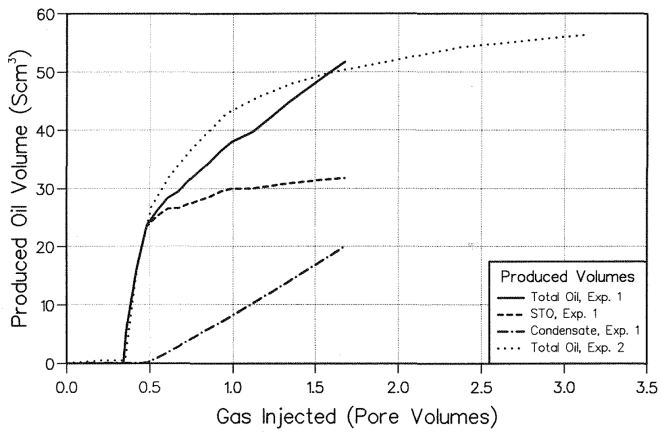

Figure 4.5: Oil production from Experiment 1 and 2 (Hustad et al., 1992)

While one could be easily fooled by the total oil production curves, figure 4.5 reveals

that after the oil bank is produced there was nearly no production of oil in Experiment 1. While in Experiment 2 the oil bank was far bigger, and that oil was being produced at late times as well. Hence, Hustad et al. (1992) was convinced that the effect of mass transfer was significant in these experiments.

Furthermore, when looking at the water production data, Experiement 1 and 2 are quite similar at early times. In both experiments, a period of water production is seen, before declining. The abrupt stop in water production around gas breakthrough is most likely a result of capillary end effects. This phenomenon will be discussed further as it applies to the recent simulations as well. After breakthrough there is a decline and the production flattens out. However, in Experiment 2 a small "bump", or increase, in the water production may be seen. It seems like the water production curves are flattening out, but at approximately 1.4 pore volumes injected, the production increases again.

The analysis of the saturation of cores at the end of the simulations revealed that strong capillary end effects indeed had taken place. The wetting phases, in this case water, showed large saturations near the outlet of the core. As the pressure over the outlet must be continuous, the saturation profiles cannot. This forces the water saturation to increase near the outlet of the core.

4.2 Previous Simulation Attempts

Hustad et al. (1992) performed simulations of the two displacement experiments using an IMPES type simulator with a compositional model. 30 gridblocks were used to represent the core, in a one-dimensional gridblock model. The first and last gridblock were used to represent the inlet and outlet to the vertical core. Straight lines were used to model the relative permeability and the capillary pressure was set to zero in these blocks, to model the end effects properly. The measured relative permeability from figure 4.2 was applied in the simualtions. IFT scaling was applied to the capillary pressure, to match the actual fluids used in the experiments. These rock curves were used to match Experiment 1. By matching Experiment 1 with these rock curves, the authors were ensured that these rock curves truly described the flow of the fluids in the core due to convective flow. Hence, the same rock curves that matched Experiment 1 were used in Experiment 2.

Furthermore, two pseudocompostional fluid models were made, one with 6 components and one with 24 components. Associated equation of state models of Soave-Redlich-Kwong type were also made to fit the experimental PVT-data, using the PVT data seen in table A.2. The EOS parameters may be seen in table A.1. A third fluid model was made especially for Experiment 1 with only three pseudocomponents and an explicit PVT model, using K-values.

To model the three phase flow properties in the three phase space neither Stones first nor second model proved to match the properties in an sufficient way. Also, simulations with Stones model 1 and 2 in earlier simulations attempts were never able to match neither oil nor the water production in an exact manner. Hence, Hustad et al. (1992) used, and developed, the Extended Stones model, shown in chapter 2. The coefficient in the Extended Stones model was chosen to be 4, as this made the oil relative permeability in the three phase space match the measured oil isoperms.

Hustad et al. (1992) also had to choose the most appropriate residual saturations. This was not straightforward, as different measures had given a range of different residuals. The residual water saturation exemplifies this. The residual water saturation found in the oil-water relative permeability measurements was found to be 17.7%, but when drained by air in the capillary pressure measurements, the residual water saturation was found to be 4.5%. Hence, appropriate residuals had to be chosen. This choice affected the maximum gas saturation in the core, as the maximum gas saturation in the core had to be one minus irreducible water saturation minus residual oil saturation. An effort Hustad et al. (1992) made to avoid the maximum gas saturation problem, was to develop a method to have different saturation endpoints in the gridblcoks than the rock curves. The method normalized the gridblock saturations to look up values from the rock curves and then apply the given value to the gridblock. This allowed the gridblocks to obtain higher gas saturation than would be possible by only using the rock curves directly to each gridblock.

Simulation Results

The produced production curves from Hustad et al. (1992) simulations may be seen in figure 4.3 and 4.4, along with the respective experimental data.

As seen in figure 4.3 the simulations of Experiment 1 proved to be very accurate with respect to all phases. Especially the water and oil production is on point, while the gas production had too small volumes at late times. The authors tried to vary the gas relative permeability and to use a model incorporating three-phase gas relative permeability. However, the gas production proved to be insensitive to changes in relative permeability. The small deviance in gas production is more likely a factor of experimental error and EOS modeling. The simulations were also able to include the end effects seen in the core, as rather high water saturations could be seen in the bottom gridblocks of the core.

Regarding Experiment 2, Hustad et al. (1992) experienced problems, which they could not solve with the models available at the time. They did manage to simulate the oil and gas in a desirable way, as seen in figure 4.4, but met problems with the water production. The history match of the gas phase was overall good, even though the simulated gas volumes was a little too large at late times of the injection process. The oil phase was properly matched with the 6 pseudocomponents model. Oddly, the 24 components model performed a worse history match of the oil phase. Oil production curves were expected to show optimistic oil recoveries due to constant interfacial tension in the reservoir simulator during the simulation. As the oil was vaporized by the gas the interfacial tension would increase, and then increase the capillary pressure as well. This phenomenon was not possible to model with the used model. The water production was matched until approximately 1.4 pore volume injected. At this point the experimental water production increased, while the simulated water production flattened out. Thus, the simulted water production did not manage to reproduce the so-called "bump" in water production.

Simulation Problems

Hustad et al. (1992) speculated that the increased water production in Experiment 2 was a result of vaporization of oil. As the oil was vaporized from the core, more space was made available for water flow.

The main issue with the simulations presented by Hustad et al. (1992) was the misfit of water production in Experiment 2. It may seem like a small issue, due to the small

deviation from the experimental data. However, Hustad et al. (1992) was not able to increase the water production. This implicates that there is something fundamental wrong with the model used to model the three phase saturation properties. This effect is the so-called capillary lock-in effect of water. As the gas saturation increases at late times during the injection process the water saturation decreases. The residual water saturation is highly dependent on the capillary pressure curve between oil and water. As seen from the capillary pressure curves in figure 4.1 the oil-water curve has an asymptote at approximately 11.5% water saturation. Hence, this curve would stop the decreasing water saturation at this limit, due to the capillary pressure being higher than the pressure gradient in the core. This is in line with traditional theory. However, as large amounts of gas is injected to the core one may reach a point where the oil film separating the gas and water in the pores is so thin that it may rupture, which would make contact between gas and water in the pores. Even if the oil film would not rupture, it could be so thin that the flow of water was not defined by the water-oil properties, but rather by the water-gas properties. Hustad et al. (1992) speculated that the flow of water is more affected by the gas-water properties than the oil-water at low oil saturation.

As seen in the capillary pressure measurements, the water-gas capillary pressure could be measured to a water saturation residual of 4.5%. Hence, as the gas saturation increased it would be natural that the relationship that governed the flow would be a transition from the water-oil rock curves into the gas-water rock curves. It would be advantageous to use the gas-water rock curves at high gas saturations. However, water-gas properties are, as mentioned in chapter 2, not used in any of Stones models. Most three-phase models assumes that oil at all times are separating the gas and water phases. Another issue arises from this chain of thought as well. Even if one chose to use the rock curves between gas and water at high gas saturations, it would be impossible to reach such high gas saturations with the current models. This relates back to the residual saturations. In the more traditional models the maximum gas saturation is described as unity minus irreducible water saturation minus residual oil saturation. As discussed in previously, this would provide a maximum gas saturation far lower than observed in gas flooding experiments. Hustad et al. (1992) also observed this phenomenon in their simulations. In figure 4.1 the measured capillary pressure between oil and gas is plotted, and a hard line shows the actual values that were used in the simulations by the

simulator. As one may see, the curve only goes on until around 40% oil saturation, implicating that the highest gas saturation that was used was about 60%. This value is far lower than expected from the long duration of the gas injection.

Henceforth, even though Hustad et al. (1992) simulations were overall a good match of most production curves, it did not truly describe the mechanisms in the tertiary gas flooding of the core. Hence, a more complex model is used in this thesis to describe the mechanisms in the core. This is done by utilizing all available data, and in this case, the water-gas rock curves. Furthermore, residual saturation has to be described with the true values between all phases, and not only estimates.

Chapter 5

Method and Procedure

This chapter presents the method and procedure to model the two experiments presented in the Background-chapter. The new simulations are based on, and inspired by, the previous simulation attempt by Hustad et al. (1992). However, as neither their reservoir simulator nor simulation model were available, a completely new model is presented here. The main difference is the use of the ODD3P three-phase model to model the three-phase relative permeability and capillary pressure appropriately. To simulate the experiments, the Eclipse E300 simulator is used. This is a compositional simulator, as elaborated in more detail in chapter 3. A new surface Equation of State is developed as well, and presented in the first subsection of this chapter, along with modelling of all PVT properties.

Throughout this chapter the method, procedure and implementation behind both experiments are presented. This includes the thinking and logic behind the models, the input data and methods. Along with this comes how certain keywords are used to implement inputs and models. Even though some ECLIPSE-keywords are shown, it is not the case for all the keywords. The keywords that are not mentioned are assumed simple and intuitive to understand.

The simulations begins at the moment of gas injection in the cores. Hence, the previous water flooding is not simulated, but the data from the experiments are used to obtain the initial conditions for the gas floodings.

5.1 PVT Modelling

The fluid description, and the PVT model that describes said fluids, are based on the PVT data measured at separator conditions, presented in Hustad et al. (1992). In both Experiment 1 and 2, the produced fluids were measured with respect to different fluid parameters right after production. The compositions were found using gas chromatography. Furthermore, several fluid parameters were also measured at reservoir conditions, such as density, viscosity, saturation pressure and temperature, formation volume factor, gas oil ratio and molar weight. All relevant data can be seen in table A.2 in the appendix.

The hydrocarbon fluids are modelled with six pseudocomponents. Using all original components, seen in table A.2 would be too computational intensive. The six pseudocomponents are seen in table 5.1 along with the components that are included in each pseudocomponent.

The pseudocomponent oil and gas compositions are made up by recombining the separator fluids. As the GOR, molar weight and densities are known for all fluids at separator conditions, this can be used to recombine the separator fluids together to obtain the reservoir compositions. This is done to find the equilibrium oil and gas in Experiment 1 and the initial oil in Experiment 2. The dry gas in Experiment 2 consists only of separator gas, therefore is not any recombination required.

To recombine the oil and gas, molar percentages of each component in each phase are used. As seen in table A.2, the gas is already listed in terms of molar fractions, y_i. The oil is listed in terms of weight fractions, m_i, and is converted to molar fractions with the use of the components molar weights, MW. The procedure is seen in equation 5.1.

$$x_i = m_i \frac{MW_i}{\sum_{i=1}^{n} MW_i} \tag{5.1}$$

Furthermore, to find the ratio of oil and gas in the recombined fluid, the separator GOR is used. However, as the GOR is measured in volumes, the densities and molar weights are used to find the gas-oil ratio in terms of moles, as described in equation 5.2.

$$R_n = GOR \frac{\rho_g MW_o}{\rho_o MW_g} \tag{5.2}$$

ρ is fluid density, MW is the molar weight of the fluid and GOR is the gas-oil ratio. The molar ratio is then used to find the total amount of moles of each component, as seen in equation 5.3.

$$z_i = R_n x_i + y_i \tag{5.3}$$

Lastly, the molar fractions of all components included in one pseudocomponent is summarized to find the molar fraction of the given pseudocomponent.

$$z_i\% = \frac{z_i}{\sum_{i=1}^{n} z_i} \tag{5.4}$$

Using the values seen in table A.2, and the use of equation 5.1 to 5.4, the oil and gas in Experiment 1 and oil in Experiment 2 is recombined, and the compositions may be seen in tables 5.1 and 5.2.

Table 5.1: Recombined pseudocomponent compositions for equilibrium gas and equilibrium oil. Experiment 1

Pseudocompnent	Components	Eq. Oil Zi (mole %)	Eq. Gas Zi (mole%)
HC1	N1+C1	0.51639	0.71659
HC2	C02+C2+C3	0.14067	0.19459
HCS	C4-C6	0.06116	0.06033
HC9	C7-C15	0.16916	0.01876
HC21	C16-C28	0.06848	0.00592
HC40	C29+	0.04414	0.00382

Table 5.2: Recombined pseudocomponent compositions for equilibrium gas and equilibrium oil. Experiment 2

Pseudocompnent	Components	Oil Zi (mole %)	Dry Gas Zi (mole%)
HC1	N1+C1	0.488001427	0.8198
HC2	C02+C2+C3	0.13596298	0.14712
HCS	C4-C6	0.080436444	0.02949
HC9	C7-C15	0.187865683	0.00359
HC21	C16-C28	0.070975213	0
HC40	C29+	0.036758252	0

However, early simulations indicated that the oil and gas were not in equilibrium during Experiment 1, as it should have been. Factors such as IFT and density varied more than expected, which is a sign that mass transfer occurs. Hence, efforts were made to ensure that the gas composition was in equilibrium with the oil in Experiment 1. A simple model was made in ECLIPSE E300 to find the gas that were in equilibrium with oil in Experiment 1. The oil from Experiment 1 was subjected to a small pressure drop, to let gas out of solution. The smallest pressure drop that gave any gas was approximately 0.4 bar. By analyzing the composition of this gas, a new composition was found, that was truly in equilibrium with the oil in Eclipse. The new composition, which are the final one and used in the simulation of Experiment 1, can be seen in table 5.3.

Table 5.3: Final oil and gas compositions for Experiment 1

Pseudocompnent	Components	Eq. Oil Zi (mole %)	Eq. Gas Zi (mole%)
HC1	N1+C1	0.51639	0.779171
HC2	C02+C2+C3	0.14067	0.13325
HCS	C4-C6	0.06116	0.037295
HC9	C7-C15	0.16916	0.047617
HC21	C16-C28	0.06848	0.002618
HC40	C29+	0.04414	0.000049

The new gas composition is not too far from the one based on measured values. Hustad et al. (1992) observed that there was some discrepancies in the measurements

of the molar weight of the pseudocompnents, thus the recombination may have included inaccuracies. This justifies the small changes in gas composition. It is of high importance that the gas and oil are in equilibrium during the simulation of the first experiment, as this experiment is used to calibrate the rock curves for both experiments. If mass transfer occurred, it would be very hard to differentiate which effects that could be tied back to mass transfer effects, and which are due to convective flow.

The PVT properties are described with the use of a SRK-type Equation of State. To model the PVT-behavior the same Equation of State that Hustad et al. (1992) used is taken use of here, as it describes the PVT properties in a sufficient manner in the core at reservoir conditions. The EOS-parameters can be seen in table 5.4.

Table 5.4: SRK EOS parameters

Pseudocompnent	$MW\left(\frac{g}{mole}\right)$	$p_c(bar)$	$V_c\left(\frac{cm^3}{mole}\right)$	$T_c(^\circ Celsius)$	Acentric factor
HC1	16.236	46	85.93	-82.98	0.0078
HC2	36.139	46.28	150.22	61.31	0.1349
HCS	68.592	34	278.24	181.97	0.238
HC9	134.992	25.56	460.17	292.72	0.5913
HC21	279.089	15.24	1045.56	493.45	1.0133
HC40	607.199	13.19	1648.19	709.28	1.2781

This EOS do model the PVT-behavior in the core at reservoir conditions, but simulations with E300 proved that the performance was not good enough for the flash-calculation to surface conditions. Neither the GOR nor the density that were seen from the simulation were in line with the measured values from Hustad et al. (1992). Henceforth, two surface EOS were made to model the flash-calculations. These two equation of states are based on the original SRK EOS, but were modified to fit the flash processes seen in the experiments. The objective of this modelling was to obtain the right surface volumes, which depends largely on the GOR of the fluids and the densities. To obtain these parameters an appropriate regression tool was used to alter critical parameters in the models to obtain the correct densities and GORs. Regression was applied to critical parameters of the former model. Hence, critical temperature, critical pressure and acentric factor for each of the six pseudocomponent were allowed to vary. The target of

the regression calculations was to obtain tabulated values of density and GOR from table A.2. Hence, a total of 18 variables was allowed to vary. Unfortunately, it was troublesome to obtain a match of both the GOR and density for both the oil and gas. Instead of making a compromise, where both the oil and gas were a little erroneous with respect to these parameters, it was decided to match only the oil properly. The surface-EOS parameters obtained from the regression for Experiment 1, may be seen in table 5.5. The same process was applied to the surface-EOS for Experiment 2, which had slightly different parameters. Also, Experiment 2 was performed at somewhat different temperature and pressure. This also impacts the flash calculation, and the surface-EOS as well.

Table 5.5: Surface-EOS critical parameters for Experiment 1

Pseudocompnent	$MW\left(\frac{g}{mole}\right)$	$p_c(bar)$	$V_c\left(\frac{cm^3}{mole}\right)$	$T_c(^\circ Celsius)$	Acentric factor
HC1	16.236	47.0594	85.93	-90.8365	0.00777
HC2	36.139	47.3458	150.22	47.4925	0.134386
HCS	68.592	34.7830	278.24	163.1677	0.237093
HC9	134.992	25.8126	460.17	298.1527	0.591657
HC21	279.089	15.3906	1045.56	500.8098	1.013912
HC40	607.199	13.3203	1648.19	718.7119	1.278872

Table 5.6: Surface-EOS critical parameters for Experiment 2

Pseudocompnent	$MW\left(\frac{g}{mole}\right)$	$p_c(bar)$	$V_c\left(\frac{cm^3}{mole}\right)$	$T_c(^\circ Celsius)$	Acentric factor
HC1	16.236	46.1083	85.93	-92.4884	0.00819
HC2	36.139	46.3889	150.22	44.58700	0.141645
HCS	68.592	34.0800	278.24	159.2140	0.2499
HC9	134.992	24.7179	460.17	267.2651	0.620865
HC21	279.089	14.7379	1045.56	458.9656	1.063965
HC40	607.199	12.7554	1648.19	665.0868	1.342005

Using these two surface-EOS models to model the flash-calculations provides the following fluid parameters, seen in table 5.7.

Table 5.7: Density and GOR from Hustad et al. (1992) and from surface-EOS.

	Experiment 1		Experiment 2	
	Table value	Sim. Value	Table value	Sim. Value
ρ_o	0.6468	0.658345	0.6532	0.645885
ρ_g	0.2644	0.292771	-	0.21656
GOR Oil	200.9	200.782	204.1	194.918
GOR Gas	4341.63	2620	-	-

Hence, the oil GOR and density are near perfect with respect to the measured values of Hustad et al. (1992). However, the surface-EOS that gave a perfect match of the oil, is somewhat inaccurate for the gas phase, especially with respect to the gas GOR. This is not an issue in Experiment 2, as the gas injected is a dry gas. Hence, the GOR is zero in any case. While in Experiment 1, it grants a bigger problem related to the condensate produced. As seen in table 5.7, the GOR seen in the Experiment 1 from Hustad et al. (1992) is 4341.63, while the new surface-EOS grants a GOR of 2620. This error leads to two things; a lot more condensate comes with gas and too little gas is produced. As the condensate production is not of any interest, the problem is not crucial. As seen in figure 4.5 the condensate may be removed anyway, to look at the actual production of oil from the core. This will be done in these simulations as well. Hence, that the GOR is too low only indicates that more condensate must be removed when calculating how much oil that actually came from the initial oil in place from the core. However, regarding history matching it is a problem. By having this much difference in the experimental condensate production and the simulated one, obtaining a proper history match will prove very difficult. To resolve this issue, a method for making up for the excess condensate is presented.

As the fluids GORs and cumulative production rates are known, one may calculate what parts of the produced oil volumes that are from the initial core and what are from condensate production from the injected equilibrium gas. The same may be done for the gas. The GORs are known, and defined as seen in equation 5.5 and 5.6.

$$GOR_o = \frac{G_o}{O_o} \tag{5.5}$$

$$GOR_g = \frac{G_g}{O_g} \tag{5.6}$$

Furthermore, the cumulative production must be made up by production from components of either the initial oil or the injected gas, described in equation 5.7 and 5.8.

$$N_o = O_o + O_g \tag{5.7}$$

$$N_g = G_o + G_g \tag{5.8}$$

N_o is the cumulative oil production, O_o is oil from the initial oil and O_g is oil from the injected gas, also referred to as the condensate from the gas. N_g is the cumulative gas production, G_g is gas from the injected gas and G_o is gas from the oil phase. All these values are surface values, measured at separator conditions. Equation 5.5 to 5.8 may be combined to find the values of interest, namely what parts of fluids that are from which phase. By using these equations the oil from the original oil in the core may be calculated with equation 5.9.

$$O_o = \frac{T_g - GOR_g T_o}{GOR_o - GOR_g} \tag{5.9}$$

Furthermore, this value may be used to find the oil from gas. The oil from gas is used to find the gas from the oil phase, and at last the gas from the gas phase. All this is seen in equation 5.10 to 5.12.

$$O_g = N_o - O_o \tag{5.10}$$

$$G_o = GOR_o O_o \tag{5.11}$$

$$G_g = N_g - G_o \tag{5.12}$$

By using this method, one may determine what parts of the oil that originates from the oil in the core in Experiment 1. This is not an issue in Experiment 2, since there is no condensate involved in the injected gas. This method will be used to compare oil production from the core between Experiment 1 and 2. However, it may also be applied to correct for the deviancies in the simulation-GOR. The method may be applied to both simulations data and experimental production data from Experiment 1. Hence, the difference in condensate production from the gas may be adjusted for, since both volumes are known values. The result of this adjustment can be seen in the results section.

As the objective is to look at oil production from the core, one could say that adjustment to the total oil production curves are not necessary, which is in part true. The GOR-correction does not affect the oil production from the core, but rather makes it possible to history match the oil production in a sufficient way. Furthermore, it should be noticed that there was initial errors in the fluid measurements, especially with respect to the distribution of molar weights to the pseudocomponents. As the densities as closely linked to the molar weights, errors are introduced. This justifies the changes to certain data, especially the gas data, as it is of more importance that the oil-behavior is correct than the gas properties.

The EOS and surface-EOS are implemented in Eclipse with the keywords EOS and EOSS. Furthermore, all relevant keyword that describes the input parameters may be seen in the datafiles in the appendix.

The viscosity of the oil was measured to be 0.43 cP, as seen in table A.2. To model the viscosity in the simulations, the Lohrenz-Bray-Clark correlation is used. This is an empirical correlation which requires five user-defined coefficients. These inputs are already tuned in Hustad et al. (1992) to fit the viscosity of 0.43 cP, hence, the same coefficients are used here. The coefficients are given in table 5.8. This correlation is implemented in the datafiles with the keyword LBCCOEF.

Table 5.8: LBC coefficients

Coefficient	Value
1	0.1023
2	0.023364
3	0.058533
4	-0.040758
5	0.0127642

5.2 Simulation Procedure of Experiment 1

5.2.1 Rock Geometry and Properties

Since the flooding experiments were conducted in a gravity stable procedure, a one-dimensional model is suitable to represent the displacement experiments. During gravity-stable injection it is assumed that the areal sweep efficiency is approximately a hundred percent. This implies that there is no flow in any areal direction, only from top to bottom, following the pressure gradient. It also includes an assumption that there is no, or very little, viscous fingering effects. As the Bentheimer sandstone is very homogeneous, this is a reasonable assumption.

To resemble the 122.6 cm long core, 74 cubic gridblocks are used. The first and last gridblock are used to represent the inlet and outlet to the core, while the rest represents the core in itself. While the gridblocks are all equal in the areal direction, the height of each gridblock vary. The gridblocks near the inlet and outlet are made smaller, while the gridblocks in the middle part are a little larger in height. As most effects and mechanisms are seen near the outlet, a higher resolution of gridblocks near the outlets would provide more details of interesting phenomena. The exact heights, Δz, of each gridblock may be seen in the Eclipse-datafile in the appendix under the DZ keyword. Furthermore, the cross section area of the core was circular with a diameter of 3.78 cm. As the shape of the area is of no concern in a one-dimensional model, it does not matter that cubes are used instead of cylinder like shapes, as long as the area between each gridblock remains the same. Hence, the equivalent length of the side of the blocks are calculated from the diameter, seen in equation 5.13 and 5.14. Using this Δx and Δy ensures that the cross section area is equal in the simulation to the cores cross section area.

$$\Delta x \Delta y = \pi \left(\frac{D}{2} \right)^2 \tag{5.13}$$

$$\Delta x = \Delta y = \sqrt{\pi} \frac{D}{2} \tag{5.14}$$

Furthermore, the absolute permeability remains the same as seen in the original simulations, seen in table 4.1. As mentioned, the core was homogeneous; hence, the absolute permeability is set to 2.566 Darcy in all spatial directions.

The porosity of the core was 22.7% for Experiment 1. This value is used for all the gridblocks that represent the core. In the inlet and outlet, a porosity of approximately 2.035% is used. This porosity originates from the total volume of pipes and other practical flooding apparatus that were filled with fluids after the water flood, but before the gas flooding had started.

5.2.2 Saturation Functions

As explained in chapter 3, the ODD3P model requires a vast amount of saturation functions input. Both primary and hysteresis data for both capillary pressure and relative permeability are required between all phases. The input curves are based on the measurements of Hustad et al. (1992). However, as this data is very limited, more data have been found using appropriate pore-scale models of flow in Bentheimer cores. This data have been found prior to this thesis, in relation to the RUTH program (Hinderaker et al., 1996). It includes hysteresis data and primary data, which are based on the curves from Hustad et al. (1992).

The relative permeability was not measured at reservoir conditions, also replacement fluids were used during these measurements. Hence, the original curves seen in Hustad et al. (1992) may not be the best representation of the actual relative permeabilities. Thus, the hysteresis and primary curves, developed from these curves, may also be inaccurate. Hence, Experiment 1 has been used to "tune" these curves to fit the production data and obtain a history match for Experiment 1. It should be noticed that the relative permeability curves were only slightly altered, and is close to the original curves seen in figure 4.2.

As no curves were measured between water and gas in the relative permeability measurements, these curves are represented by the oil-water curves. This is suggested practice in the ODD3P model (Hustad and Browning, 2010). The relative permeability input curves between oil and water may be seen in figure 5.1, (a) and (b). p, s and t indicate primary, secondary and tertiary curves.

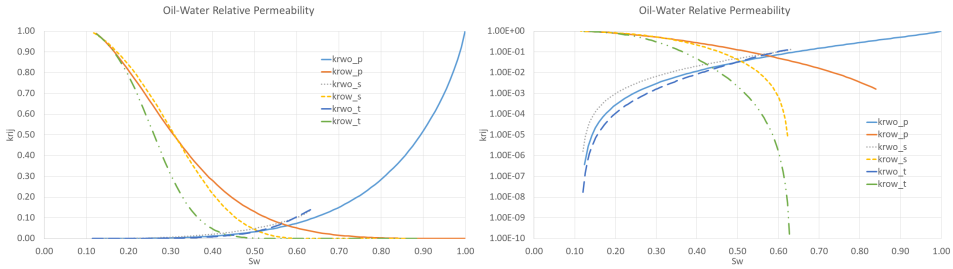

(a) Curves on a normal scale.

(b) Curves on a logarithmic scale.

Figure 5.1: Relative permeability input curves, with primary, secondary and tertiary curves.

The oil-gas relative permeability input curves may be seen in figure 5.2, (a) and (b).

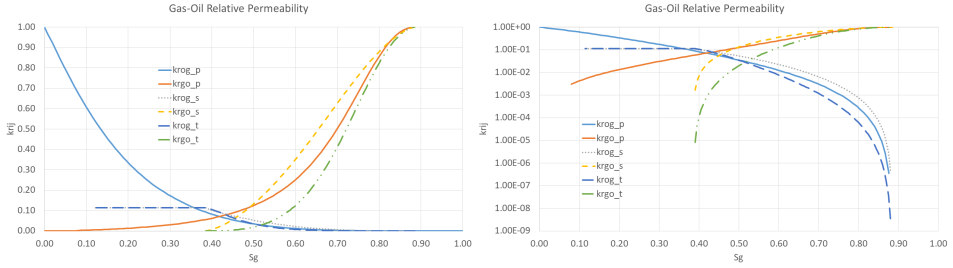

(a) Curves on a normal scale.

(b) Curves on a logarithmic scale.

Figure 5.2: Relative permeability input curves, with primary, secondary and tertiary curves.

The measured capillary pressure is more representative for the reality. As the shape of capillary pressure curves are a rock property more than a fluid property the curves seen in figure 4.1 from Hustad et al. (1992) are an accurate representation. The curves also includes gas-water measurements. As the measurement fluids are not representative for the reservoir fluids, these curves have to be scaled with respect to interfacial tension. The measured interfacial tension of the fluids used for measurements may be

seen in table 4.2, in chapter 4. These values are scaled with the actual interfacial tension between the reservoir fluids, which is 21.6 mN/m between oil and water and 1.2 mN/m between oil and gas. This scaling is done once, to obtain curves that actually represents the reservoir fluids, and should not be mixed with the live scaling that occurs during the simulation, presented in the ODD3P model.

Furthermore, pore-scale models have also been used to find the associated hysteresis and primary curves for capillary pressure, as this was not included in the original measurements (Hinderaker et al., 1996). As there is no option to input the capillary pressure between water and gas in the E300 simulator, this is not inputted, but represented by the water-oil data. This is partly a problem, however, the oil-water and gas-water curves may be scaled differently throughout the simulation and most important, one may have different endpoints for the two curves. Hence, even though the gas-water input is very much alike to the oil-water, it is treated very differently throughout the simulation. This is seen in more detail in Experiment 2, where the use of water-gas capillary data is of very high importance.

The primary and hysteresis input curves between the oil and gas phase can be seen in figure 5.3.

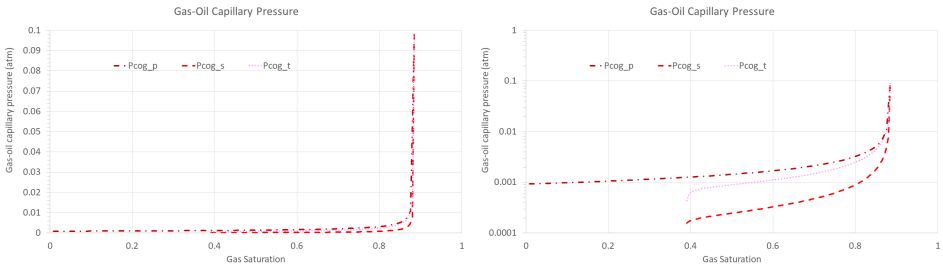

(a) Curves on a normal scale.

(b) Curves on a logarithmic scale.

Figure 5.3: Capillary pressure input curves, with primary, secondary and tertiary curves.

The primary and hysteresis input curves between the oil and gas phase can be seen in figure 5.4.

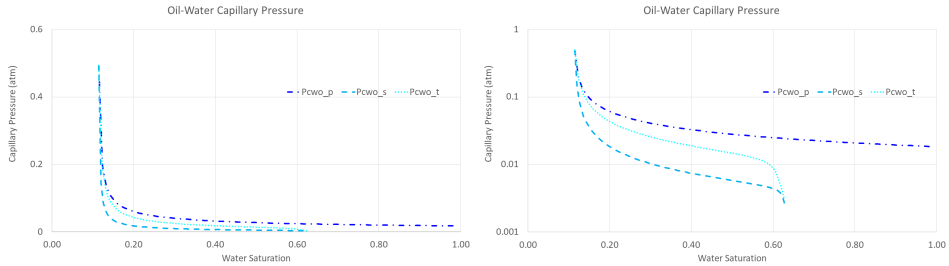

(a) Curves on a normal scale.

(b) Curves on a logarithmic scale.

Figure 5.4: Capillary pressure input curves, with primary, secondary and tertiary curves.

The capillary pressure curves are functions of the water and gas saturation. This is due to the system being water wet. This choice is elaborated more when the use of the ODD3P is explained.

As the flow properties are different in the inlet and outlet, a new set of saturation functions is defined for the two blocks that represents the inlet and outlet to the core. In these saturation functions, all the capillary pressure curves are zero and the relative permeability are modelled with straight lines. This applies to all curves, including hysteresis and primary functions. It is of high importance to include these properties to the inlet and outlet to model the capillary end-effects properly. As explained in chapter 4, there were significant end-effects in both experiments, and fluid saturation distribution would be wrongfully simulated if this effect was not included. The two different sets of saturation functions are allocated to the adequate blocks with the use of regions. Two regions are defined, one for the core blocks, and one for the inlet and outlet.

5.2.3 ODD3P Three-Phase Model

This subsection presents specific inputs that are needed in the ODD3P-model. Using the keyword ODD3P states that the ODD3P-model is used to model the three-phase properties.

All of the two-phase formulation inputs that are related to scaling are given under the keyword EPSODD3P. Land-scaling, seen in equation 3.7, is applied for the endpoint of all phases. Furthermore, capillary scaling is activated and the scaling-coefficient, l_{ij}, seen in equation 3.13 is set to unity. All the reference surface tensions are also given under this keyword. The reference IFT between oil and gas is 1.248 mN/m and 35.63201

mN/m between oil and water, and gas and water. These IFTs are based on the measured values from the reservoir fluids under reservoir conditions. However, the values are somewhat altered due to different parameters used in the pore-scale model (Hinderaker et al., 1996). In the simulation of Experiment 1, the IFT should not change, or at least change in a negligible magnitude. Hence, substantial scaling of capillary pressure should not happen in Experiment 1.

Furthermore, the coefficients in equation 3.42, that is used to determine the IFT between the hydrocarbon phases and the water are also given under the EPSODD3P keyword. Coefficient A is set to be 16.13811, B to be 14.45386 and C to be 3.3487. As seen in equation 3.42, this correlation is based on the densities of the hydrocarbon fluids. Hence, after the initial calculation of the IFT, it should not change a lot, as it is expected that no mass transfer occurs in Experiment 1. Thus, the densities will not change too much either.

The threshold IFTs are given in this keyword too. The threshold value should not be confused with the reference IFTs. While the reference IFT is used to scale the capillary pressure without any limitations, the threshold IFT is a limit for when scaling of endpoints and relative permeability applies. This threshold value is set to be 0.5 mN/m between all phases. It is not expected that the IFT between any phase will decrease below this value during the simulations. Hence, neither endpoint scaling nor relative permeability is expected to be scaled in the respective simulations.

The rate of endpoint change from primary curve to hysteresis curve, seen in equation 3.8, is given in the EPSODD3P keyword. As seen in the datafile, 0.01 is used for this maximum rate of change.

The last notable input that is given in the EPSODD3P keyword, is the detection of saturation change, which is set to be 0.001. Hence, the saturation change must higher than this value for the saturation direction to be detected. This should prevent excessive switching and calculations.

All the other inputs seen under the EPSODD3P keyword are related to using scaling coefficients different from unity or capillary numbers, which are not used in the simulation of neither Experiment 1 nor Experiment 2.

The capillary pressure formulation is controlled by the PCODD3P-keyword. The first capillary pressure approach is used. Thus, the capillary dependence on a given

phase is chosen, and a saturation weighting scheme is not used. This is done on the basis of that it is known that the system is water wet. Capillary dependence number six is used, as this best represents the water wet system. This includes making oil-water capillary pressure dependent on the water saturation, the oil-gas capillary pressure dependent on the gas saturation and the gas-water capillary pressure dependent on the water saturation. In this formulation, the residual, R, is calculated in the way seen in equation 5.15.

$$R = \hat{P}_{cgw}\left(\tilde{S}_g\right) - \hat{P}_{cgo}\left(\tilde{S}_g\right) - \hat{P}_{cow}\left(\tilde{S}_w\right) \tag{5.15}$$

In this capillary option the P_{cow} and P_{cgo} is calcualated as seen in equation 5.16 and 5.17.

$$P_{cow} = \hat{P}_{cow}\left(\tilde{S}_w\right) + HR \tag{5.16}$$

$$P_{cgo} = \hat{P}_{cgo}\left(\tilde{S}_g\right) + FR \tag{5.17}$$

However, from simulation experience it is not necessary to distribute the residual in Experiment 1, as the water saturation does not decreases to values so low that it would have been affected. This phenomenon will be discussed further in the next subchapter, as it is vital to the simulation of Experiment 2. Hence, δ_G and δ_W are set to be zero. This implies that F and H are zero at all times, and G is unity at all times.

5.2.4 Initial Saturations and Endpoint Saturations

Initial saturation of the core is set to be 38.4% oil and 61.6% water. This is in line with the residual oil saturation, obtained after the period of water flooding, seen from Hustad et al. (1992). The outlet is completely filled with water, as the water was injected from the bottom, while the inlet is saturated with injection gas. However, the total phase volumes in the inlet and outlet are very small compared to the volumes in the core, but not negligible.

In Experiment 1, the option to change the endpoint saturations is not used. Hence, the gridblocks endpoint saturations are found from the saturation functions, which are

provided in tabulated form. Thus, the gridblock endpoints are in-line with rock curves in Experiment 1.

5.2.5 Other Simulation Features

Compositions of the oil in the core and the injected equilibrium gas is implemented with the keywords ZI, NEI and INJCOMP. ZI includes the composition of the initial oil, INJCOMP includes the composition of the injection gas and NEI includes both. The compostions presented in the PVT-modelling chapter are used.

To simulate the injection and production processes, two wells are used. The injection well is inserted in the first block, which represents the inlet. This well is controlled by reservoir rate. The injection rate is set to 2.47 $\frac{cm^3}{hours}$.

The production well is inserted to the last block, representing the outlet. This well is pressure controlled, and a bottom hole pressure limit of 309.4 atm is used. This ensures that the pressure drop is at a minimum throughout the core.

The simulation runs just as long as Experiment 1 did, which is until 1.7 pore volumes are injected. With the given injection rate this equals 216.6704 hours. The time steps are assigned to have a maximum length of 0.0002 hours. However, the time steps are subject to discussion, as it may affect the simulation results. Hence, the time step length is subject to a sensitivity study, presented in the results section.

Different solvers may be used in the E300 simulator. In these simulations, the CPR solver is used, as indicated by the keyword CPR. Other solvers were considered as well, such as AIM, IMPES and FULLIMP. The impact of using different solvers are studied, and presented in the results section.

5.3 Simulation Procedure of Experiment 2

The simulation of Experiment 2 has many similarities to Experiment 1. However, there are some small differences and some larger differences. Hence, it is necessary to give a presentation of the input and essential keywords of Experiment 2 in the same manner as Experiment 1.

The main difference is of course that another gas is injected, a dry separator gas.

Experiment 2 was conducted under slightly different pressure and temperature. The temperature was 98.4° Celsius and pressure of 310.6834 atm. The different conditions are one of the reasons that some parameters differ from Experiment 1.

5.3.1 Rock Geometry and Properties

Similar Bentheimer sandstone as was used in the first experiment, was used for the second one as well. However, as two different cores were used, there was small differences in rock properties that must be accounted for in the simulation of Experiment 2. To model the geometry a similar model is used; a one-dimensional gridblock based model, with 74 gridblocks. The same distribution is also used, which is smaller gridblocks near the outlet and inlet, while larger gridblocks in the middle part. The height of the second core was slightly different from Experiment 1, 122.1 cm exactly. This influences the height of each gridblock, DZ, which can be seen in the datafile in the appendix. Furthermore, the diameter of this core was 3.77 cm. By using equation 5.14, Δx and Δy can be calculated to be approximately 3.3411 cm. The porosity of the core is set to be 23.3% and the inlet and outlet porosity are set to be 2.054%. The core also had slightly different absolute permeability, of 2.645 Darcy.

5.3.2 Saturation Functions

The same saturation functions that were used in Experiment 1 are used in Experiment 2. As the saturation functions were tuned and altered to model the convective flow in the core, it should represent the same convective flow in Experiment 2. Henceforth, the relative permeability and capillary pressure input curves are exactly the same as in Experiment 1, which can be seen in figure 5.1 to 5.4. As the fluids are slightly different in the two experiments one might ask whether the relative permeability is representable for both experiments. However, the capillary pressure is scaled with changing IFT, which provide more correct capillary pressure for both experiments. It is also expected that the flow is more dependent on the capillary pressure than the relative permeability. Zero capillary pressure and straight line relative permeability are applied in the inlet and outlet, with the use of regions.

5.3.3 ODD3P Three-Phase Model

The ODD3P keywords are to some degree equal to the ones used in the simulation of Experiment 1. However, the effects of the inputs are more significant in Experiment 2, as the interfacial tension is expected to vary a lot. Furthermore, endpoints are treated differently in Experiment 2 and the distribution of the residual, R, is becoming a key factor in the capillary pressure model.

The inputs to the scaling in the two-phase formulation, seen under the EPSODD3P, are exactly the same as in Experiment 1. Henceforth, the same reference interfacial tensions are used, the scaling exponents are still unity and the threshold interfacial tensions are still 0.5 mN/m for all phases. It is expected that the interfacial tension will not decrease below the threshold value in Experiment 2 either.

Saturation endpoints are different in Experiment 2. The keyword ENDSCALE is applied to signify that endpoints different from the endpoints of the rock curves are used. With this keyword, all saturation endpoints between all phases are required as input. These endpoints are the same that were discussed in equation 3.1 in the ODD3P theory. In Experiment 1 these were not used, and the rock curves endpoints were used as default.

Some of the endpoint saturations are easily determined, as the data is evident and all measurements points at a given value. An example of this is the oil endpoint with respect to water, S_{orw}, which is found from imbibition of the initial cores. This is data that is based on clear and precise measurements. Other endpoints are based on very limited, or none, experimental data. Data, such as the gas endpoint with respect to water, S_{grw}, is not measured in any experiments. Henceforth, some of the endpoints are from known values, other are estimated from a range of experimental values and some endpoints are estimated and tuned to make the simulation fit the experimental production data and obtain a history match. In the datafile all the endpoints are given under the keywords PSIRJ and HSIRJ, where P is for primary and H is for hysteresis, I is for the phase and J indicates the other phase present. Table 5.9 includes all endpoints, including whether it is based on data from Hustad et al. (1992) or found from tuning and adjustment.

Table 5.9: Endpoint saturations, including sources

Keyword	Endpoint Saturation		Source
PSGRO	$\bar{S}^{pr}_{gro}$	7.25%	Tuned
HSGRO	$\bar{S}^{hr}_{gro}$	38.54%	Rel. Perm. Measurements
PSGRW	$\bar{S}^{pr}_{grw}$	7.25%	Tuned
HSGRW	$\bar{S}^{hr}_{grw}$	38.54%	Tuned
PSORG	$\bar{S}^{pr}_{org}$	4.5%	Pc Measurements
HSORG	$\bar{S}^{hr}_{org}$	4.5%	Pc Measurements
PSORW	$\bar{S}^{pr}_{orw}$	15.82%	Measurements and tuning
HSORW	$\bar{S}^{hr}_{orw}$	36.86%	Rel. Perm. Measurements
PSWRG	$\bar{S}^{pr}_{wrg}$	7.75%	Pc Measurements and tuning
HSWRG	$\bar{S}^{hr}_{wrg}$	7.75%	Pc Measurements and tuning
PSWRO	$\bar{S}^{pr}_{wro}$	11.50%	Pc Measurements
HSWRO	$\bar{S}^{hr}_{wro}$	11.50%	Pc Measurements

Table 5.9 presents some essential endpoints that should be noticed. As mentioned earlier, the so-called bump in water production in Experiment 2 is related to these endpoints. It has been theorized that at high gas saturations the water production is controlled by the water-gas capillary pressure. It has also been pointed out that water-gas capillary pressure are reaching lower water saturation values than the oil-water capillary pressure curves. However, as the oil-water and gas-water has the same input curves, the endpoint values are of high importance to model the phenomenon correct. From the capillary pressure measurements of Hustad et al. (1992) it is evidential that the endpoint between water and oil stops at approximately 11.5% water saturation. This may be seen in figure 4.1. Furthermore, the water-gas capillary curve does not stop until approximately 4.5%. Thus, the water endpoint between water-gas and water-oil is essential to the modelling. As seen from table 5.9, the water endpoint with respect to oil has been set to 11.5% in accordance with the measured values. Furthermore, the water endpoint with respect to gas has been set to 7.75%. The deviance in this value compared to the measurements is due to adjustments done to obtain a history match. The endpoint saturation seen in the measurements do include some inaccuracies, hence,

some adjustment is acceptable. There is also a large variety of potential sources of error, which is discussed more comprehensively in the discussion chapter.

Table 5.9 also includes certain values that are purely chosen with respect to history matching the experiment. This includes the residual gas saturation with respect to the water phase. As mentioned there are no measured data on these parameters. The hysteresis gas endpoints are never reached, as the gas phase is increasing at almost all times. Hence, these values does not impact the results directly, but they do impact indirectly through the normalization of the saturation in the three-phase space. This can be seen in equation 3.19 and 3.20. Hence, this value is purely used for tuning the model to obtain a better history match.

Another notable value is the endpoint saturation of oil with respect to water, HSORW. This value is set to be 36.86%, which is also the initial oil saturation in the core. This value differ with approximately 2% from the same value in Experiment 1. This is most likely due to difference in pressure and temperature.

To model the treatment of the capillary pressure the first capillary pressure approach is used in Experiment 2, just as in the simulation of Experiment 1. Hence, the same dependency of saturation and residual is used, seen in equation 5.15. The simulation of Experiment 2 differs from Experiment 1, due to the treatment of the residual, R. The residual is distributed in such a way that the capillary pressure dependence has a smooth transition from being weighted towards the oil-water capillary pressure into the gas-water capillary pressure. This should happen at lower water saturation. To do this the F, H and G distribution functions must be modelled properly. As there is six different user defined input parameters, δ_W, α_W, β_W, δ_G, α_G and β_G, there is a wide range of possibilities to model the phenomenon. Furthermore, these six user-defined inputs do not have any physical foundation, but are rather functions of a range of different properties. Thus, much effort has been dedicated to tune these parameters to get the right distribution functions. The resulting user inputs may be seen in table 5.10.

Table 5.10: Best fit distributions parameters.

	$F(S_w)$	$H(S_g)$
δ	1	1
α	10	10
β	0.5	0.5

The values in table 5.10 are used to produce the F, H and G functions, and the resulting functions can be seen in figure 5.5.

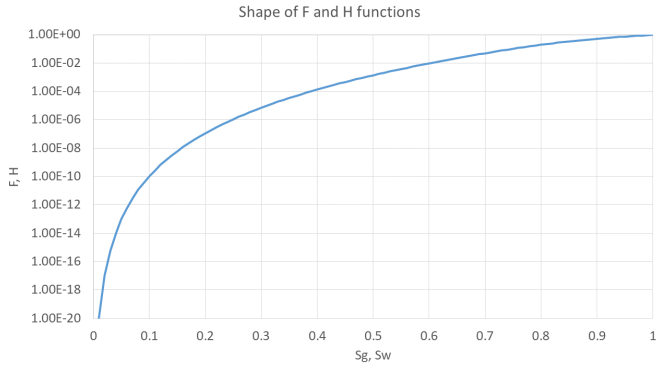

Figure 5.5: Distribution functions F and H.

The smooth transition from water-oil capillary pressure to water-gas capillary pressure should produce the so-called bump in water production.

5.3.4 Other Simulation Features

The composition of the oil and the dry injection gas are found in the PVT chapter and implemented in the same manner as in Experiment 1. The same goes for the injection and production wells. Injection rate controls the injection well. The rate is set to be $2.58 \frac{cm^3}{hour}$, which is slightly higher than Experiment 1. The bottom production well is pressure controlled, to maintain a low pressure drop through the core.

The length of the simulation timesteps is set to be 0.0002 hours, and the same solver used in Experiment 1 is used, namely the CPR solver.

Chapter 6

Results

This chapter presents the simulation results of the two experiments. This includes a comparison with former simulations attempts. The results are presented in chronological order, Experiment 1 first, then Experiment 2. Lastly, a sensitivity study is presented. This includes the results of varying different critical parameters. This chapter does only include results and observations, all discussion around observed phenomena is given in the Discussion chapter.

6.1 Experiment 1

The simulated cumulative production curves of water, oil and gas along with experimental data for Experiment 1 are shown in figure 6.1.

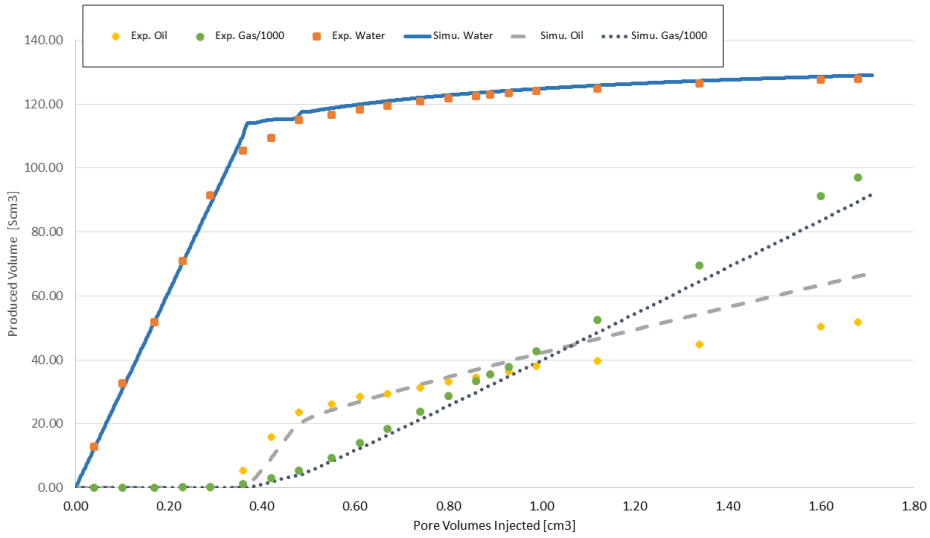

Figure 6.1: Simulated cumulative production and experimental data. Experiment 1.

All production curves are plotted in terms of produced volumes in standard conditions versus total pore volumes injected. One should notice that neither the gas nor the oil is properly matched, which is due to the error in the injection gas GOR. As explained in the Method-chapter, this may be adjusted for by adding the difference in condensate from simulated experimental data. By using equation 5.9 to 5.12 one can calculate the condensate production, which may be seen in figure 6.2.

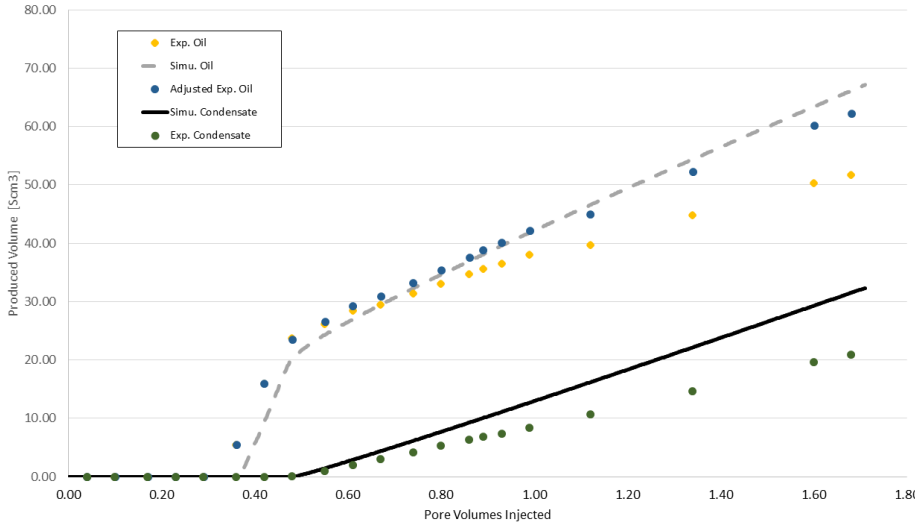

Figure 6.2: Simulated oil production and experimental oil production. Condensate production is included.

Figure 6.2 a) shows the total oil production and the production which is only caused by condensate. This includes both the simulated and experimental data. The difference in the experimental condensate and the simulated condensate is used to adjust the experimental data of total oil production. The experimental oil production data are represented by the yellow data points, while the adjusted values as represented by the blue data points in figure 6.2. The same procedure is used to adjust the total gas production, as this is also affected by the erroneous GOR. By using this correction on the experimental data, one obtains a new production curve history match, given in figure 6.3.

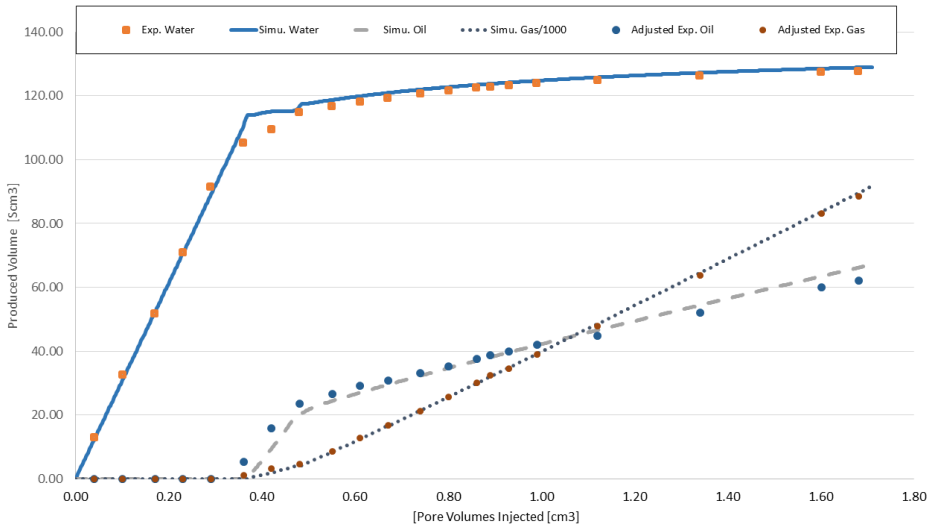

Figure 6.3: Simulated cumulative production curves and adjusted experimental data. Experiment 1.

Naturally, the production curves of oil and gas now has a better fit, seen in figure 6.3. This adjustment is not a problem for the simulation validity, as the problem is with the flash from reservoir to separator conditions and not with fluid flow in the core. Furthermore, the total oil production is not of high importance, as the real objective is investigate the oil produced that was originally in the core.

The simulated production curves shows that water production begins from the injection start. As the core is filled with mobile water, and immobile oil, this is natural and in line with experimental data. At oil breakthrough, approximately 0.36 PVI, the water production flattens out, before the production continues shortly after. Some deviancy from experimental data is experienced around the breakthrough of gas and oil; otherwise, the history match of water is very accurate.

The simulated oil production curve has a breakthrough time at approximately 0.37 PVI, which is a little later than seen in experimental production data. After the breakthrough, a period of high oil production is seen, most likely due to an arrival of an oil bank. The oil bank continues until approximately 0.49 PVI. After the oil bank is produced, the oil production continues, with a steady, but lower rate. However, the rate seen at late times is larger than the one seen in the experimental data. Overall, the his-

tory match of oil is accurate, with some small discrepancies.

The gas production history match is also very accurate. The breakthrough time of gas is at approximately 0.39 PVI, which is a little later than in the experimental data. After the breakthrough a steady production continues. Since the gas expands tremendously during the flash from reservoir to separator conditions, it is very sensitive to the flash calculation. This is reflected through the significant effect off adjusting the gas production due to the wrong GOR.

Compared to the simulations done by Hustad et al. (1992) the results are more or less reproduced. As Hustad et al. (1992) used an explicit fluid model, the problems with GOR did not occur in their simulations.

As the total oil production does not represent the oil production from the core, which is of high interest, the condensate is removed from both experimental data and simulation data. This can be seen in figure 6.4.

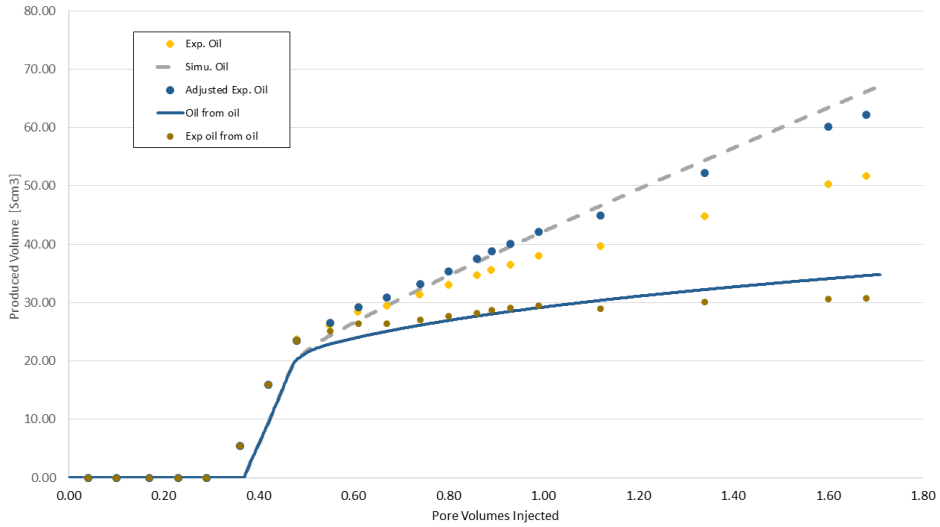

Figure 6.4: Simulated and experimental oil production, with and without condensate from equilibrium gas.

As seen in figure 6.4, the production curve of oil from the core is entirely different from the total oil production curve. The blue line represents simualtion of oil production of oil that originates from the core. The brown data points is the experimental oil that originates from the core. After the oil bank is produced, the experimental pro-

duction data flattens out. Hence, there is very little flow of oil from the core after the production of the oil bank. The large gradient of oil in the total oil production at late times, seems to be all condensate from the injection gas. The oil production without the condensate is unaffected of the GOR-adjustment, and truly shows the production from the core. The simulated oil from the core is a little bit off. From figure 6.4, one can see that the oil bank does not contain enough oil, and the oil rate after the oil bank is too high. This reveals that the saturations functions does not represent the fluid flow in the core perfectly.

Another interesting result is the saturation profile throughout the core at certain times during the injection. Figure 6.5 shows the saturation profile throughout the core at different times.

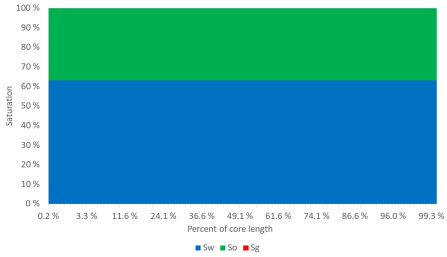

(a) Initial state

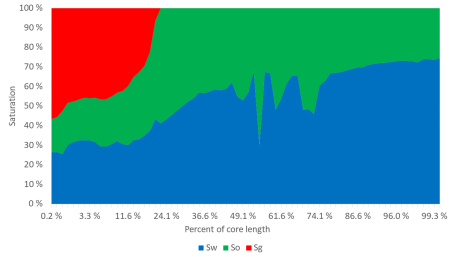

(b) 10 Hours, 0.079 PVI

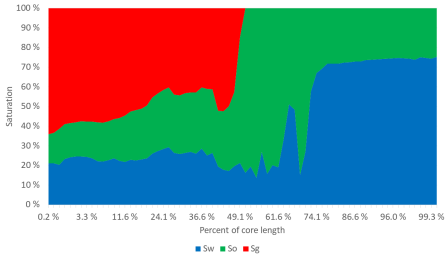

(c) 30 Hours, 0.237 PVI

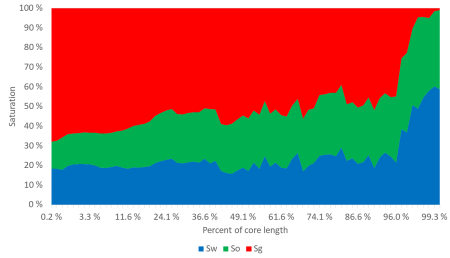

(d) 70 Hours, 0.553 PVI

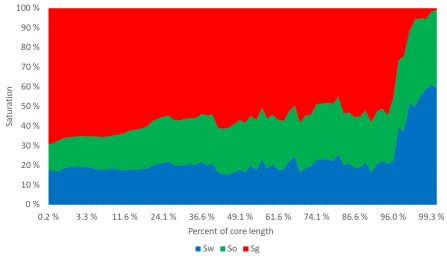

(e) 100 Hours, 0.790 PVI

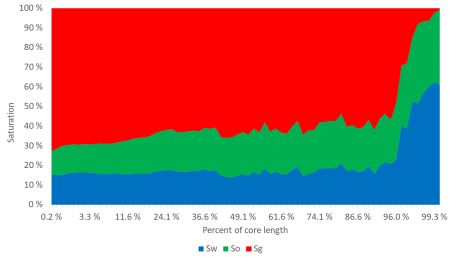

(f) 216 Hours, 1.706 PVI

Figure 6.5: Saturation profile of the core at different times during the gas injection.

Figure 6.5 shows the saturation profile of the core with respect to percentage of the total core length. From this series of plots, one may easily see the formation of an oil bank. Furthermore, the oil saturation throughout the core is not decreasing significantly after the oil bank has been produced. This was also seen in figure 6.4, and also indicates that there is very little oil production from the core after oil bank production.

Figure 6.5 also shows significant capillary end-effects. The wetting phase, water in this case, is increasing in saturation near the outlet. This is in-line with experimental observations. Figure 6.6 shows a more detailed series of the phenomenon.

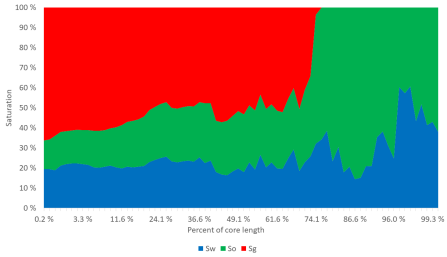

(a) 48 Hours, 0.379 PVI

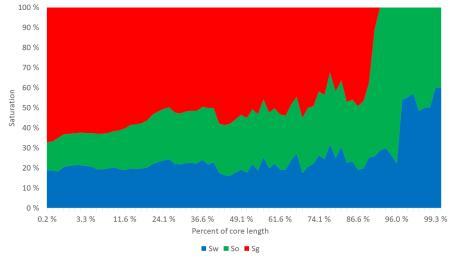

(b) 60 Hours, 0.474 PVI

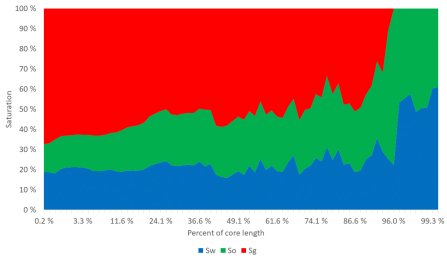

(c) 62 Hours, 0.490 PVI

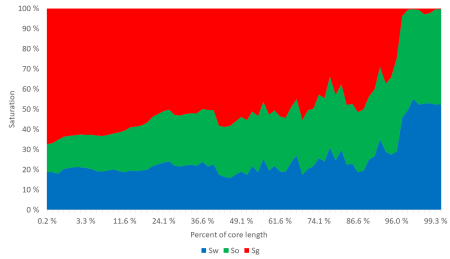

(d) 63 Hours, 0.497 PVI

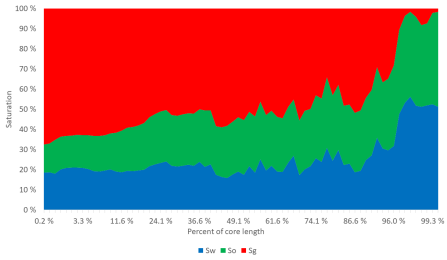

(e) 64 Hours, 0.505 PVI

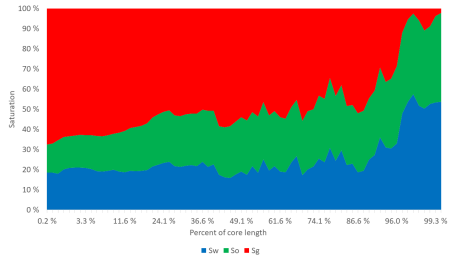

(f) 65 Hours, 0.513 PVI

Figure 6.6: Saturation profile of the core at different times around breakthrough time.

Figure 6.6 shows that the water phase is increasing in saturation near the outlet right before gas is about to break through. This explains the low water production rate around breakthrough of oil and gas that was seen in the production curves. This is due to capillary end-effects.

The experimental oil saturation average in the core was measured to be 22% in Hustad et al. (1992) at the end of the gas flooding. The simulation results is very close to this figure, with an average oil saturation of 21.3%. The average phase saturations in the core throughout the simulation can be seen in figure 6.7.

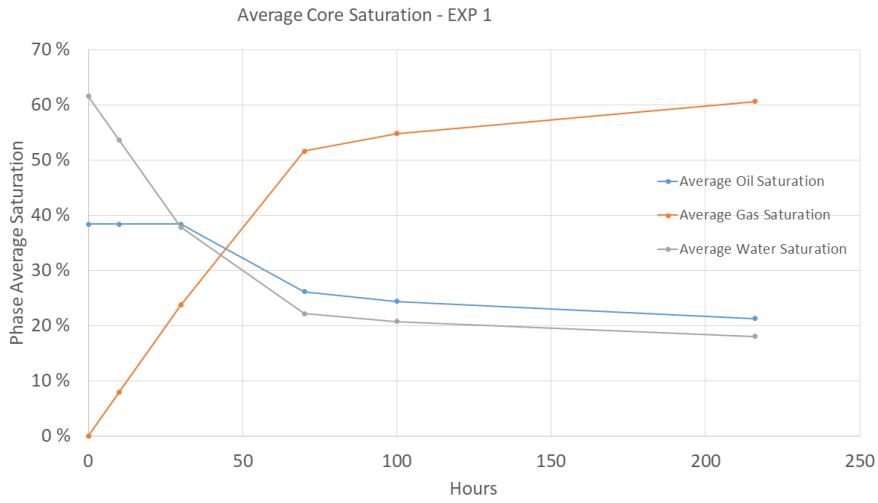

Figure 6.7: Average phase saturations in the core in Experiment 1.

6.2 Experiment 2

The production curves from the simulation of Experiment 2 can be seen in figure 6.8, along with experimental data.

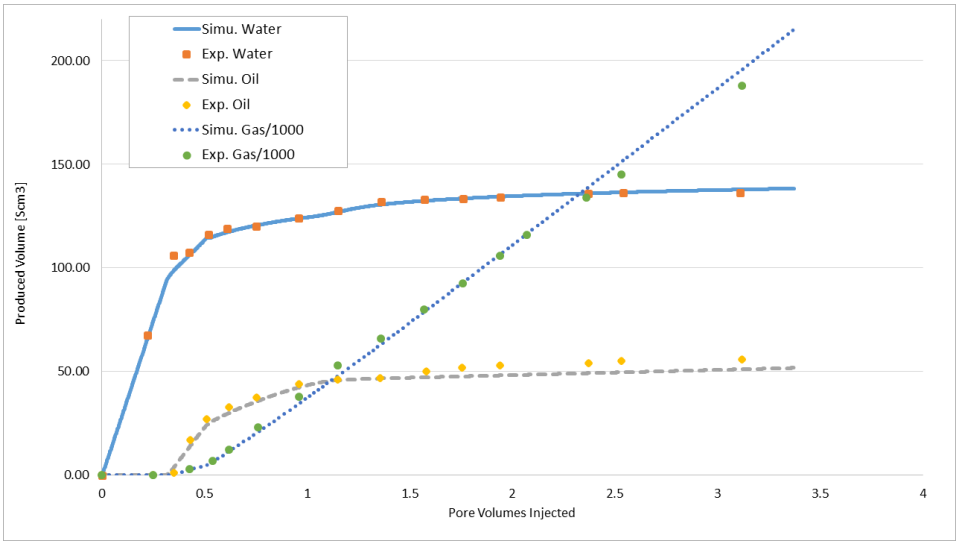

Figure 6.8: Simulated cumulative production curve with experimental data for Experiment 2.

Figure 6.8 shows cumulative production of the three phases in standard conditions versus total injected pore volumes. The water production looks similar as in Experiment 1, as water is produced from the beginning of the injection. At oil breakthrough, the water production rate declines, but not as significantly as in Experiment 1. After the oil breakthrough the water production decreases and the curve is flattening out. Furthermore, at approximately 1.4 PVI a small increase or so-called "bump" is seen in the water production. This is in-line with the experimental data. Henceforth, the water production history match in Experiment 2 is very accurate. The so-called water lock-in effect seen in earlier simulation attempts, is not seen here. More details around the increased water production and this phenomenon are discussed in the next chapter.

As mentioned earlier, there is no need for any correction for the GOR, as the injection gas is dry and contains no condensate. However, the surface EOS still calculates an error to the gas density, which may give errors in the surface volumes of gas. Figure 6.8 shows cumulative gas production along with experimental data. Gas breaks through at approximately 0.43 PVI, which is very close to the experimental breakthrough of 0.477 PVI. Furthermore, the gas production curve is a little bit too low in early times, but little too large at late times.

The oil has a breakthrough at 0.32 PVI, which is also very close to the experimental breakthrough of 0.342 PVI. Furthermore, the oil production rate is high and stable until approximately 1.2 PVI, where the rate declines. This high production right after the breakthrough is most likely a result of an oil bank arriving, just as in Experiment 1. After the oil bank is produced, the production of oil continues, but with a smaller rate. As there is no condensate from the injected gas, this must be oil from the core. Hence, this may be the result of vaporization of intermediate components in the core. At later times the simulation production curve is not reaching the experimental oil rates. There may be several reasons for this, for example that the mass transfer process is not modelled properly or that the flash of oil is inaccurate. This is discussed further in the next chapter.

When comparing this simulation result to the simulation attempt by Hustad et al. (1992), seen in figure 4.4, one can see that the oil and gas phase are reproduced, while the water production history match is improved. The simulation of gas production in Hustad et al. (1992) has the same features as this simulation, while the oil is a little bit

more accurate. The water production is improved, as the increased water production is successfully simulated.

As with Experiment 1, the results of the saturation profiles provides a lot of insight to the mechanisms throughout the gas flooding. Figure 6.9 shows a series of plots of the saturation profile of the whole core at a series of time steps.

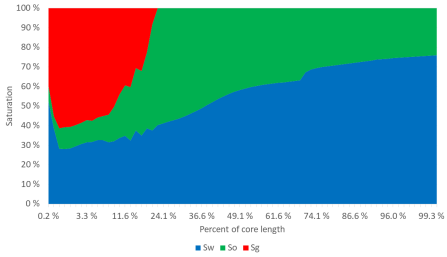

(a) 10 Hours, 0.081 PVI

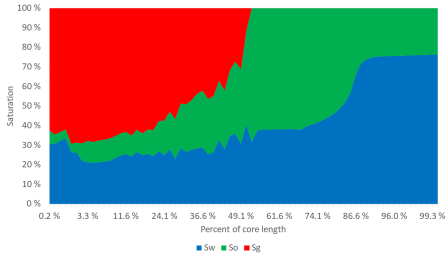

(b) 30 Hours, 0.244 PVI

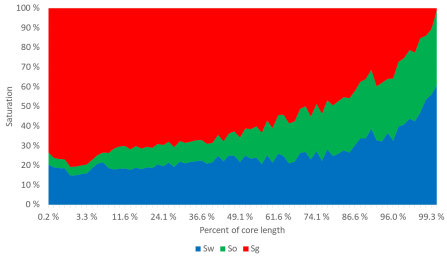

(c) 70 Hours, 0.569 PVI

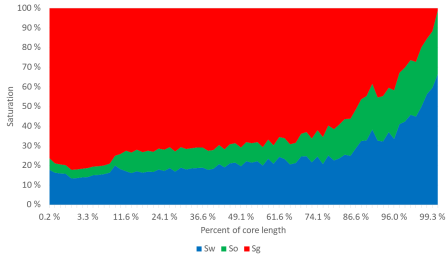

(d) 100 Hours, 0.813 PVI

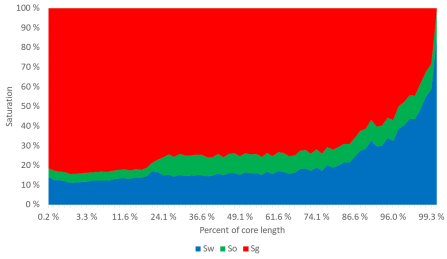

(e) 216 Hours, 1.757 PVI

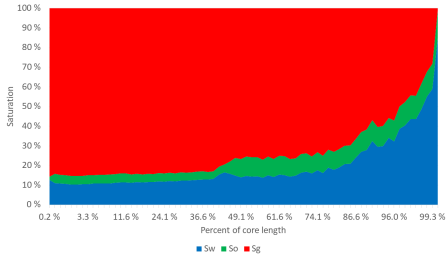

(f) 414 Hours, 3.367 PVI

Figure 6.9: Saturation profile of the core at a series of different timesteps. Experiment 2.

From figure 6.9, one can clearly see an oil bank building up. This was an expected result, which was also seen in the production curves, figure 6.8. After gas breaks through, the oil saturation continues to decrease. This was seen in a small degree in Experiment 1, while from figure 6.9 the effect is clearly a lot more extensive in Experiment 2. The oil

saturation decreases from the top of the core first, which may be due to the gas vaporizing the first oil that it is in contact with. Thus, it is likely that the oil in the top of the core is vaporized before the oil further down.

Some of the areas in the core obtains very small oil saturations, which also indicate that only a small oil film separates the gas and water phases. Large capillary end-effects are also seen after gas breakthrough. As soon as gas breaks through at the end of the core the water increases in the lower blocks. More saturation profiles are plotted in figure 6.10, which shows the phenomena at times around the breakthrough time.

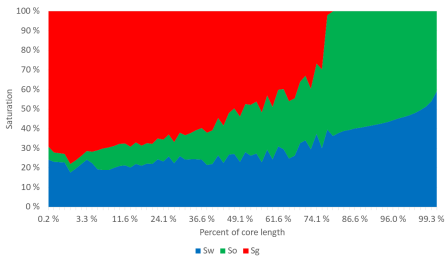

(a) 48 Hours, 0.390 PVI

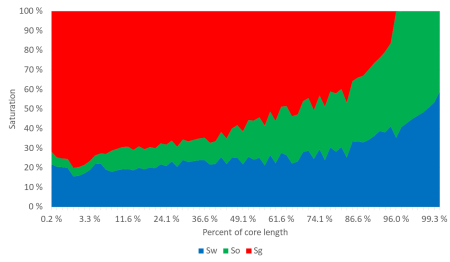

(b) 60 Hours, 0.488 PVI

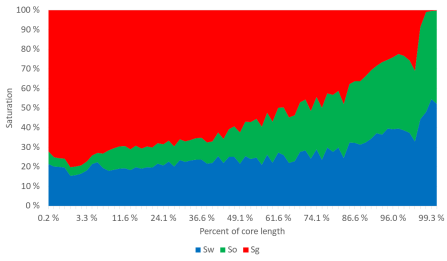

(c) 62 Hours, 0.504 PVI

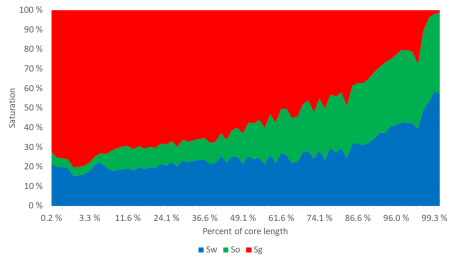

(d) 63 Hours, 0.512 PVI

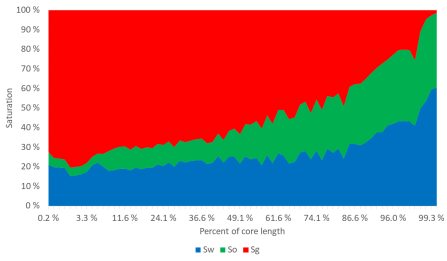

(e) 64 Hours, 0.521 PVI

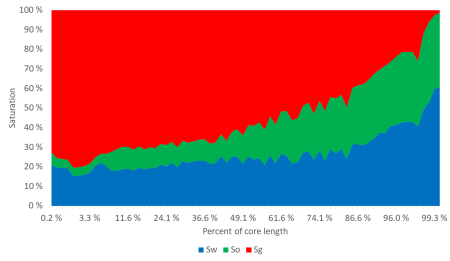

(f) 65 Hours, 0.529 PVI

Figure 6.10: Saturations profile of the core at times around the breakthrough time of oil and gas.

Figure 6.10 shows some of the same phenomena as in Experiment 1. As gas breaks

through the water saturation increases in the lower blocks, which indicates strong capillary end-effects. However, with time the oil saturation also decreases in the lower blocks, and the end-effects only affect the water phase.

The average oil saturation at the end of the gas injection is approximately 7%, compared to 9% from experimental data. This indicates that more oil is produced in the simulation than in the experiments, however, the production curves shows that too little oil is produced. This indicates that the flash calculation is inaccurate, and introduces an error to the production curve. The average saturation in the core versus the hours of production is given in figure 6.11.

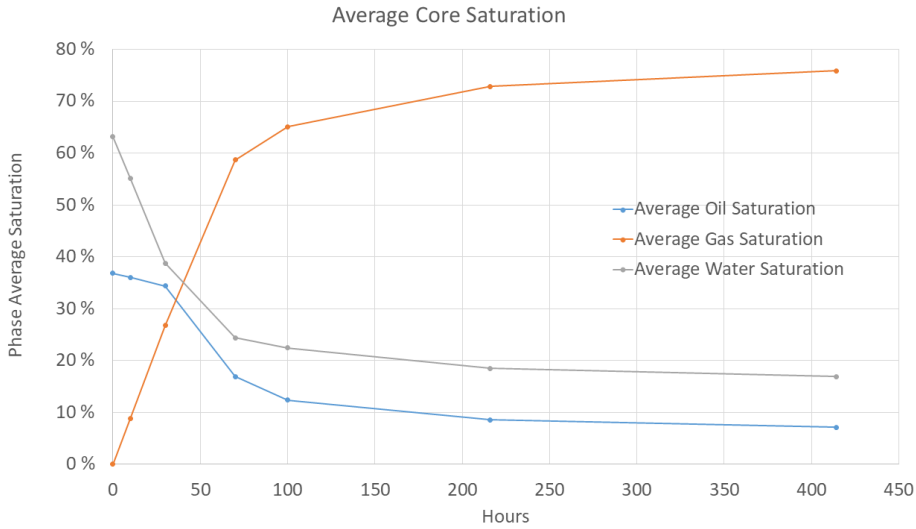

Figure 6.11: Average phase saturations during Experiment 2.

6.3 Sensitivity Studies

Three different parameters were subject to a sensitivity study. This includes the following parameters:

- Capillary Pressure Option
- Numerical Solution Solver
- Time Step

Exactly these three were chosen due indications that they had significant effect on the simulation results.

Capillary Pressure Option

To clearly see the effects of using capillary pressure, simulations without capillary pressure were conducted. The resulting production curves can be seen in figure 6.12.

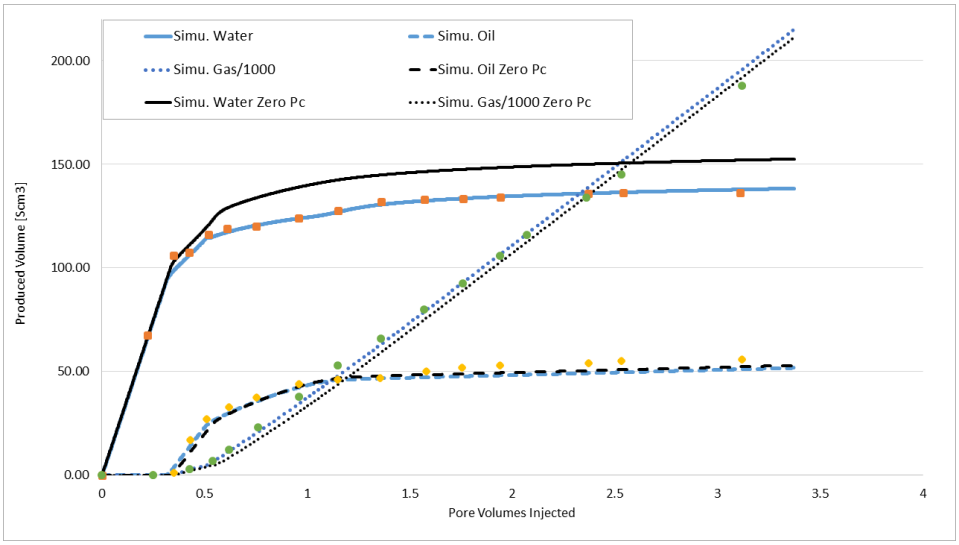

Figure 6.12: Sensitivity of applying capillary pressure in simualtions seen on production curves from Experiment 2.

Figure 6.12 shows the cumulative production curves of the three phases with and without capillary pressure applied in the simulations. All curves are from Experiment 2. Experiment 1 yielded similar results. The oil and gas production remains similar with and without the use of capillary pressure. However, neglecting the capillary pressure produces far more water. The large difference with and without capillary pressure on the water production is evident from figure 6.12, and proves the importance of capillary pressure modelling.

Numerical Solution Solver

Different numerical solution solvers other than the CPR solver were considered for simulating the experiments. Both AIM, IMPES and FULLIMP were considered, but early

simulations indicated that not all numerical solvers worked properly for the given problem. Thus, these three solvers were investigated in a sensitivity study.

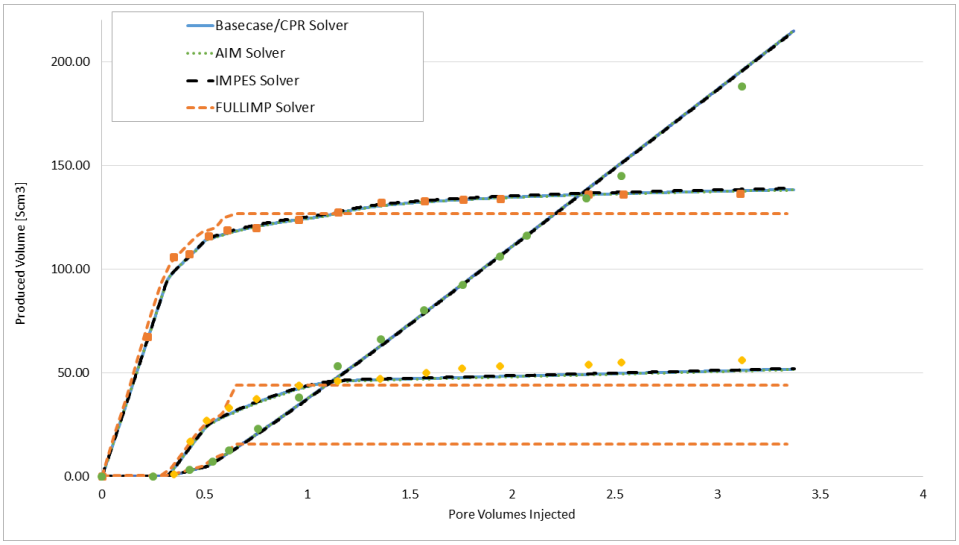

Figure 6.13: Sensitivity of using different numerical solvers seen on production curves from Experiment 2.

Figure 6.13 includes simulated production curves for Experiment 2, with the original simulations along with the three other solvers. It is evident that the some of the solvers handles this simulation better. The AIM and IMPES yields acceptable results compared to the CPR solver, while the FULLIMP solver produces curves far from acceptable range. The FULLIMP solver does not seem to handle either the ODD3P option or the the combination of gridblock sizes and time step length.

Time Steps

A range of different time step lengths were used for simulations, however the simulator reduced any time steps longer than approximately 2.8E-4 hours to said value. Thus, 2.8E-4 hours is the reference time step length, and the longest the simulator allowed to apply. To study if this time step length was sufficient to avoid numerical dispersion, and that the reference time step length yielded a stable solutions, a sensitivity study of the time steps are presented. Two other time steps were used in the simulation, 1E-4 hours and 5E-5 hours. 5E-5 was the smallest time step that was practically possible to

use, due to memory problems and data management.

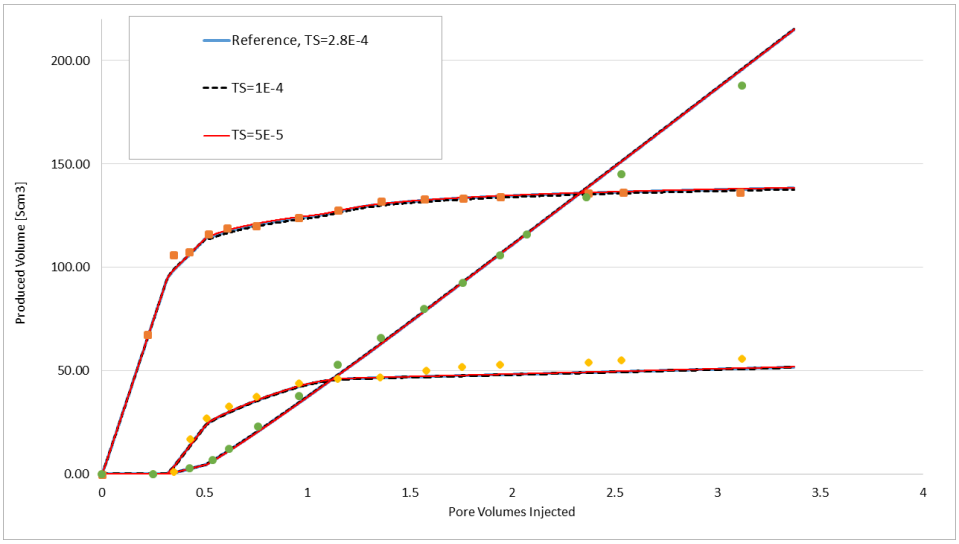

Figure 6.14: Simulated cumulative productions with different time steps for Experiment 2.

Figure 6.14 shows the simulated cumulative production curves with the three different time steps in Experiment 2. Experimental data are included too, for reference. There are very small deviations from the reference curves for all three fluid phases. Thus, the numerical solutions seem to have converged to stable values.

Chapter 7

Discussion

This chapter presents discussion around the results presented in the previous chapter. As the objective of the thesis is to history match Experiment 1 and 2, with emphasis on the water production, the results have proved to be very promising. However, even though the production curves have been history matched, there is no assurance that the physical phenomena seen in the core are modelled completely right. Henceforth, this chapter will discuss the recovery mechanisms seen in the simulations, three-phase modelling, explore formerly presented theories and look into uncertainties and sources of error. To investigate the magnitude of vaporization the two experiments are compared. This includes a comparison of recovery factor and water production.

7.1 Comparison of Experiment 1 and Experiment 2

To clearly see the effect of vaporization on the oil production, the production curve of oil from Experiment 1 and Experiment 2 are plotted together, seen in figure 7.1.

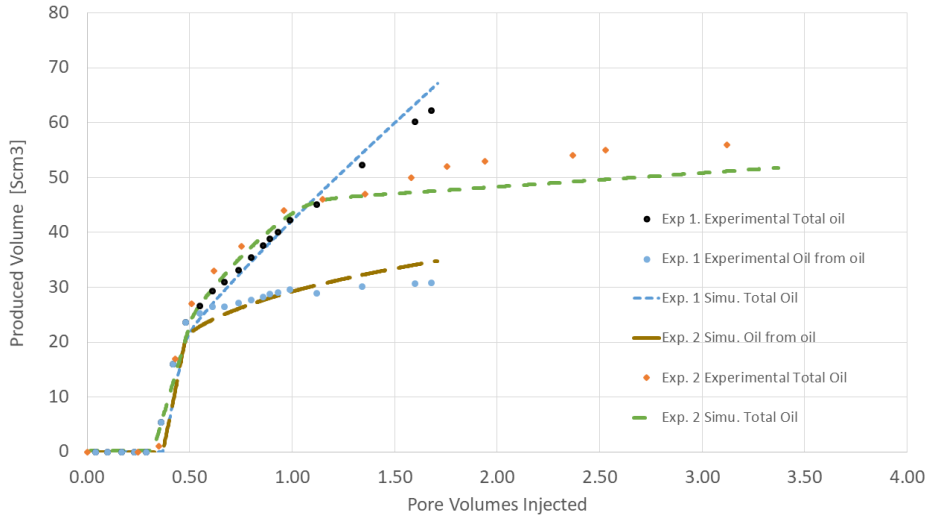

Figure 7.1: Oil production from Experiment 1 and 2. Including oil production without condensate for Experiment 1.

In figure 7.1 the oil production from Experiment 1 are plotted in terms of both total oil production and oil without condensate from the injection gas. Experimental data for each case is included as well. This plot shows that the total oil production from Experiment 1 exceeds the production from Experiment 2. However, large amounts of the oil in Experiment 1 are condensate. When only looking at oil that originates from the core, far more oil is produced in Experiment 2. This is a strong indication of the positive effects vaporization has on oil production. Figure 7.2 shows the saturation profiles of Experiment 1 and Experiment 2 at 1.7 PVI, which is at the end of gas injection in Experiment 1.

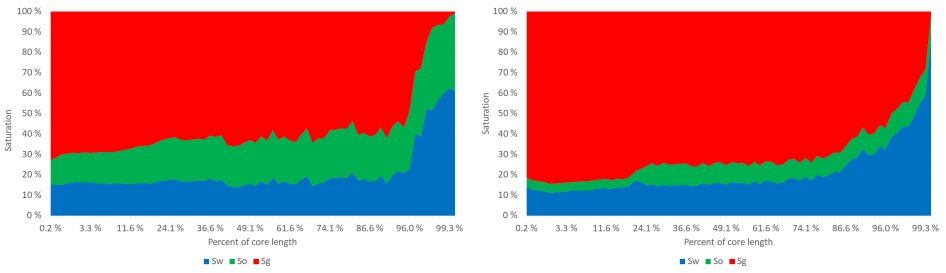

(a) Saturation profile of Experiment 1.

(b) Saturation profile of Experiment 2.

Figure 7.2: Saturation profiles of Experiment 1 and 2 at 216 hours of injection.

Figure 7.2 shows how vaporization of the oil affects the oil saturation throughout the whole core. When comparing the saturation profiles of the two experiments, it is evident how much the vaporization affects the oil saturation.

To understand the magnitude of the vaporization on the total oil production, the recovery factor of oil is calculated, and may be seen in figure 7.3.

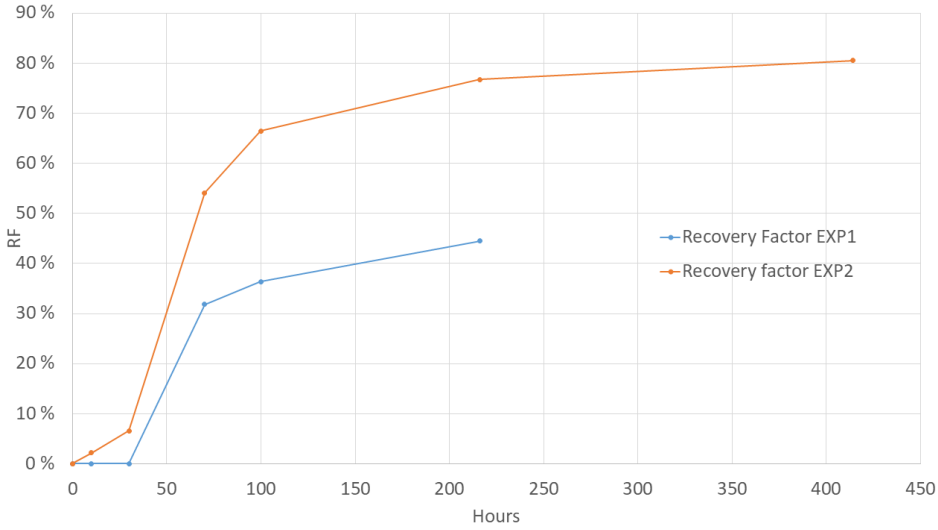

Figure 7.3: Recovery factors for Experiment 1 and Experiment 2.

The recovery factors seen in figure 7.3 are based on the original oil in place right before the gas injection began and not the original oil in place before water flooding. Gas injection in Experiment 1 recovers about 44.5% of the oil at 1.7 PVI, while the dry gas injection in Experiment 2 recovers 76.4% of the oil at 1.7 PVI and approximately 80% at 3.2 PVI. Henceforth, the difference in oil recovery is significant.

Similar to figure 7.1, simulated water production curves are shown in figure 7.4, along with experimental data.

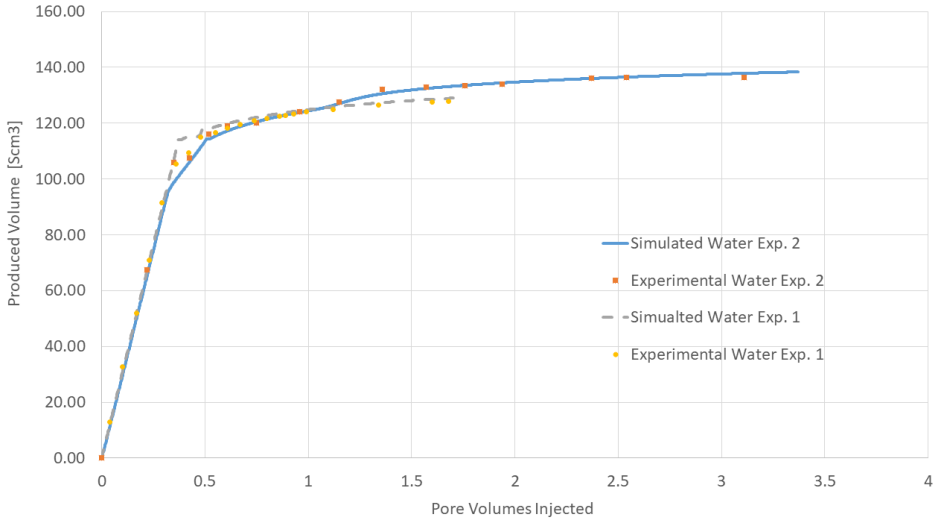

Figure 7.4: Cumulative water production comparison between Experiment 1 and 2.

The dashed line and yellow datapoints are representing simulated and experimental data from Experiment 1, while the blue line and red squares represent Experiment 2. The features of the two water production curves are quite similar in early times. Water is produced until gas and water breaks through. However, after approximately 1.4 PVI both curves seem to decline in water rate, but in Experiment 2 water production has a sudden increase in water production. Figure 7.4 clearly shows how vaporization of the oil affects the flow and production of water.

7.2 ODD3P Three-Phase Model Features

Due to the ODD3P models complex features, it is very interesting to look into the treatment of input data and especially how the rock curves are applied. Every gridblock may have different saturation endpoints, rock curve scaling and saturation at any timestep during the simulation. The capillary pressure in each gridblock is subject to scaling and changing residual distribution with changing saturation. This yields a huge amount of data at any given point, and it would be impossible to present all data for all blocks at all times. To examplify a typical treatment of capillary pressure, all the gridblocks oil-water capillary pressure values are plotted in figure 7.5. This is from the simulation of

Experiment 2.

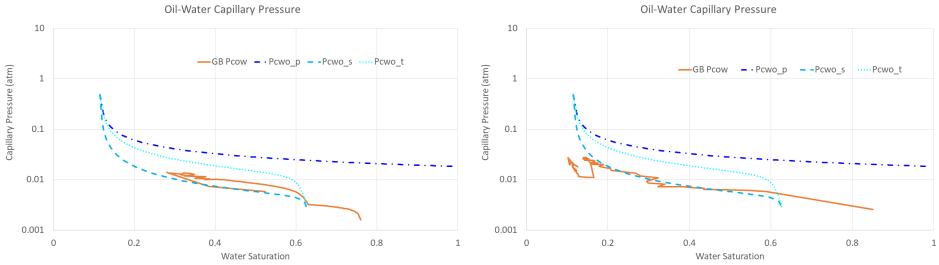

(a) 10 hours into the simulation.

(b) 414 hours into the simulation, at the end.

Figure 7.5: Water-oil capillary pressure input along with actual gridblock values

Figure 7.5 (a) is in beginning of the simulation, at 10 hours. Figure 7.5 (b) is at the end of the simulation. The capillary pressure is based on the blue input curves, but different mechanisms such as changing between hysteresis curves, IFT scaling and residual distribution are applied. At 10 hours of simulation the gridblock capillary pressures are still in the bounds of the input curves. However, at the end of the simulation, seen in figure (b), the water saturation is very low in some of the gridblocks, but due to treatment of capillary pressure the gridblock values are allowed to drift out of the range of the input curves. This proves how the ODD3P model is utilizing different methods to obtain a flexible capillary pressure modelling.

An interesting feature from the simulations is the high gas saturation at late times, which is especially high in the upper gridblocks of the core. The uppermost gridblock reaches gas saturation values of approximately 85%. The more traditional three-phase models would not allow this to happen, as the highest gas saturation would be unity minus irreducible water saturation minus residual oil saturation. By using the ODD3P-model, this is no longer an issue, due to the flexibility of inputting all endpoint saturations.

7.3 Water Production

As seen in figure 6.3, 6.8 and 7.4 the water production history match is very accurate, especially at late times, where the increased water production is seen in Experiment 2. In chapter 4 it was theorized that it is not the oil-water capillary pressure that controls

the residual water saturation, but the gas-water capillary pressure. The reasoning behind this theory was the so-called thin oil film theory, which states that at very high gas saturation the thin oil film that separates water and gas may rupture. Even if it does not rupture, it could be thin enough that the capillary pressure between gas and water is truly the factor that controls fluid flow. Saturation profiles of the core, seen in figure 6.5 and 6.9, indicates that this is likely to happen in Experiment 2, as the oil saturation is very low, especially in the upper gridblocks where most vaporization has occurred. Furthermore, in Experiment 1, the oil saturation seems to be overall much higher, and this phenomenon is more unlikely to take place.

As explained in the Method chapter, the effort to model the increased water production in Experiment 2 included the use of distribution functions of residual capillary pressure and input endpoint saturations. The physical significance of the distribution functions, F, H and G, is to obtain a smooth transition from a system where water-oil capillary pressure controls the water saturation, into a system where water-gas capillary pressure controls the system. As the water saturation decreases the F, H and G changes in such a way that weights $P_{cwo}(S_w)$ and $P_{cwg}(S_w)$ to let more water flow. The distribution functions resembles a series of different physical phenomena simultaneously. Parameters such as wettability, contact angle and IFT changes in gridblocks with little oil saturation. Hence, by tuning the distribution functions, all these effects are consolidated and tuned appropriately.

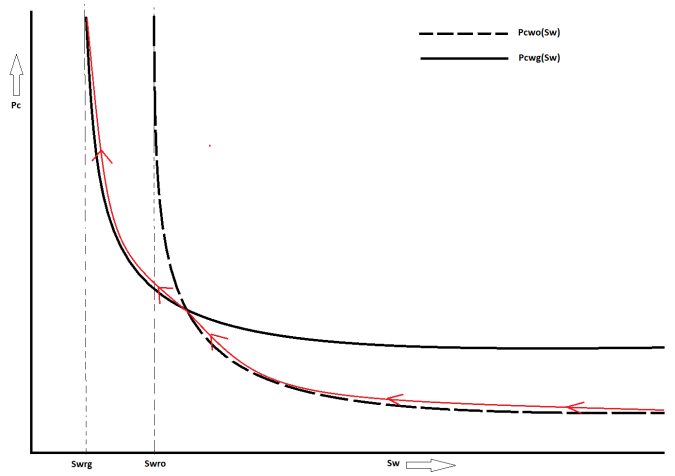

Figure 7.6: Schematic showing the transition from $P_{cwo}(S_w)$ to $P_{cwg}(S_w)$

A schematic of the transition from $P_{cwo}(S_w)$ to $P_{cwg}(S_w)$ are given in figure 7.6, the red line shows the capillary pressure that should control the water saturation. This schematic provides a conceptual idea of the thinking behind the shift of capillary pressure. However, the reality is more complicated, as there are hysteresis curves, the curves are continuously scaled and the distribution functions differ in each gridblock.

The measurements of capillary pressure in Hustad et al. (1992) revealed that the gas-water capillary pressure decreased down to lower water saturation than the oil-water capillary pressure did. This is the reason that more water is produced, as soon as the gas-water capillary pressure primarily controls the water saturation. However, as explained in the method-chapter, the input of the gas-water capillary pressure is identical to the oil-water capillary pressure. The difference in the curves are found in the IFT-scaling of the input curves, which are very different, and the endpoint saturations. The measured water endpoint saturation of oil-water capillary pressure was approximately 11.5%, while the water endpoint saturation of the water-gas capillary pressure curve was approximately 4.5%. However, this proved to produce too much water, and this had to be adjusted up to 7.75%, as seen in the Method chapter. The reason for this is still unknown, but there are several sources of error that may be the reason, which will be discussed later in this chapter. However, the simulations proved to be sensitive to these residual saturations. All of the residual saturations that was properly known from Hustad et al. (1992) were used. Some of the residuals were not measured at all, such as the residual gas saturation. This brought uncertainty to the simulations as these values had to be estimated. The endpoint gas saturation has an impact on the normalized gridblock saturations as it is used in the normalizations. Another feature of the primary gas saturation endpoint was how it impacted the so-called critical saturation. The critical saturations is where the phase has high enough saturation to flow. This may be a reason for the breakthrough of gas was seen at slightly later times in the simulations than in the experiments.

7.4 Surface EOS

Properly modelling fluids PVT-behavior proved to be very challenging. As the reservoir temperature and pressure was nearly constant throughout the simulation, the PVT be-

havior in the core was nearly constant. However, the challenging part was to obtain an accurate flash calculation from the surface EOS. As explained in chapter 5, the surface EOS that was used to calculate this flash, calculated a large error in the gas GOR. This was somewhat anticipated. The SRK EOS has a tendency to overestimate liquid volumes in a vapor-liquid equilibrium, VLE, which was exactly the problem in Experiment 1. The GOR was too low; hence, there was too much oil and/or too little gas. However, as both the experimental and simulated GOR were known values, this problem was solved, as the condensate was not of interest anyway. This would been a problem if the experimental GOR of the equilibrium gas was not known.

The surface EOS also calculated small errors in the hydrocarbon densities. This was also anticipated, as the molar weight distribution of the pseudocomponents had some discrepancies. This error in molar weight distribution has been a problem ever since the experiments were conducted, and is also presented in Hustad et al. (1992). The significance of this error is that density calculations becomes slightly wrong. Errors in reservoir and standard conditions densities provides the wrong volumes of the given phases during the flash calculations. Hence, the simulations provides slightly wrong surface volumes. This may be a reason for the gas production curve having a slightly too high gradient in Experiment 2. It may also affect the oil production in Experiment 2, which never reaches the experimental volumes. The effect the density error has on Experiment 1 is harder to detect, as the GOR problem in Experiment 1 completely disguise this error. The GOR adjustment may have included an adjustment of wrong volumes as well.

7.5 Oil Recovery Mechanisms

Experiment 1

The history match of the oil production curves may be the least accurate of the three phases. In Experiment 1, the total oil production curve fitted the experimental data very accurately after the GOR-adjustment. However, looking at only the oil from the core, seen in figure 6.4, the oil production proved to be more inaccurate. Conductivity, capillary forces and mass transfer govern this oil production. These three mechanisms

make up the transportation of oil out the core. Henceforth, analyzing these mechanisms further should provide an explanation to why the oil from the core does not have a better fit of the experimental oil from the core in Experiment 1.

The simulation of Experiment 1 was conducted in such a manner that the injection gas and oil was in equilibrium. The aim of this was to avoid all mass transfer effects. To investigate the magnitude of any mass transfer in Experiment 1, two properties that are highly dependent on phase compositions are looked into. Density is a direct function of the compositions and IFT is a direct functions of the density. Thus, to examplify what is happening through the core, IFT between oil and gas and oil density in three different gridblocks are plotted in figure 7.7 (a) and (b).

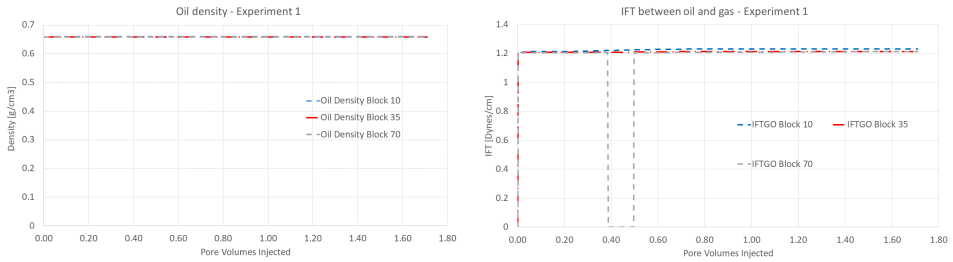

(a) Oil density in three different blocks.

(b) Gas-Oil IFT in three different blocks.

Figure 7.7: Oil density and IFT in three different blocks throughout simulation of Experiment 1.

Oil density, which is highly dependent on the composition of the oil phase, remains nearly constant. The interfacial tension between oil and gas remains nearly constant as well. There are small variations due to the small pressure gradient over the core. This change is negligible; hence, there is very little mass transfer in the simulation of Experiment 1, as expected. Thus, vaporization should not affect the oil production in any considerable degree in Experiment 1.

This implies that all oil production in Experiment 1 comes from convective flow due to capillary forces and conductivity. As the oil-water capillary pressure is a function of the water saturation, it would not restrict flow of oil at low oil saturations. The gas-oil capillary pressure curve might do, this curve is given in figure 7.8.

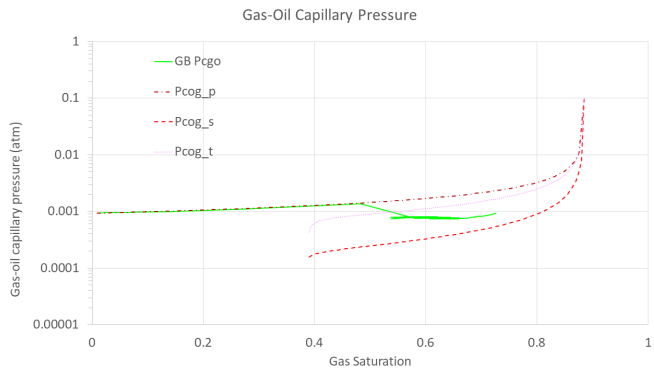

Figure 7.8: Gas-oil capillary pressure input along with gridblock values at the end of simulation.

Figure 7.8 shows the input gas-oil capillary pressure along with the actual data used for every gridblock at the end of the simulation. The gas-oil capillary pressure increases at high gas saturations, which implies low oil saturation. However, none of the gridblock values are near the limiting asymptote which increases to high capillary pressure values at around 85% gas saturation. Hence, it would be unreasonable to assume that the capillary forces in this simulation would limit the oil flow.

Regarding conductivity, the relative permeability is the key parameter. Figure 7.9 shows the relative permeability in block 10, 30 and 70 throughout the simulation.

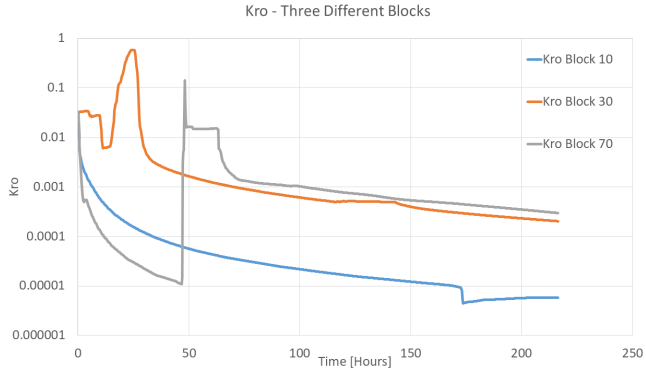

Figure 7.9: Relative permeability in three different blocks.

The blue line is the oil relative permeability in block 10. The relative permeability of oil decreases as the oil saturation decreases in the block. In block 30 and 70, one can

see how the oil bank passes, which increases the oil saturation and thus increasing the permeability. However, after the oil bank has passed, the relative permeability values does not decrease to zero, but decreases slowly and reaches rather small values. However, even though the permeability is low at late times, it is not zero, resulting in some flow of oil due to conductivity.

Thus, the simulated oil production in Experiment 1 is only a product of conductive flow, and not mass transfer. The oil production seems to mostly come through the oil bank, which is formed due the difference in oil residuals between water and gas. The injected gas mobilizes the oil as explained in chapter 2. However, after the oil bank has been produced, the conductive flow is too high compared to experimental data. This indicates that the relative permeability and capillary pressure are not measured or modelled perfectly.

Experiment 2

The simulated oil production curve is not a perfect history match in Experiment 2, either. Figure 6.8 shows the production curves, and one can easily see that the simulated oil production is too low in the time after the oil bank has been produced. The underlying mechanisms are the key to understanding this. As the injected gas is dry, one does not need to differentiate between oil from the core and condensate, since all produced oil must be from the core.

There is no doubt that some mass transfer is happening in Experiment 2. The magnitude of increased oil production can also be seen in figure 7.3. However, it is uncertain how and when the different mechanisms is governing the oil production.

The input capillary pressure between oil and gas, along with gridblock capillary pressure values in all gridblocks at the end of injection is shown in figure 7.10.

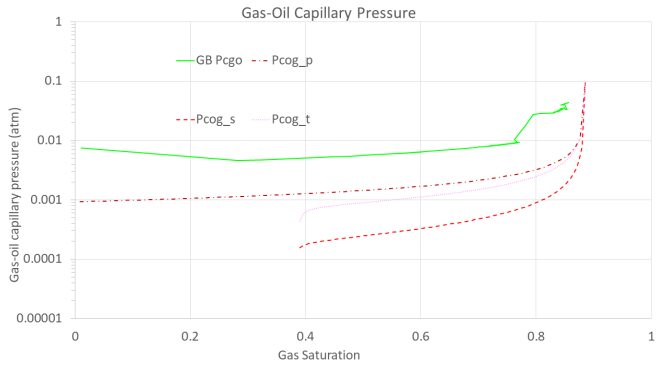

Figure 7.10: Gas-oil capillary pressure input along with gridblock values at the end of simulation.

The same tendency as in Experiment 1 is seen in figure 7.10. The oil-gas capillary pressure in the gridblocks are closer to the asymptote than in Experiment 1. Also, the gridblock capillary pressure has a tendency to have a larger value than the corresponding input curve. This is most likely due to IFT-scaling and residual distribution. However, it seems unlikely that the capillary pressure between oil and gas would lock the oil saturation completely.

Henceforth, it is more interesting to look at the relative permeability of oil. Figure 7.11 shows the relative permeability of block number 10, 30 and 70 throughout the simulation.

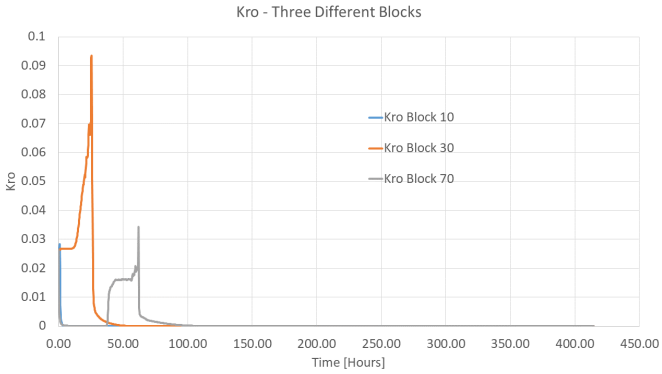

Figure 7.11: Oil relative permeability in three different gridblocks, Experiment 2.

The implications of figure 7.11 are very interesting. The arrival of the oil bank is easily seen in block number 30 and 70. Differently from Experiment 1, the oil relative

permeability rapidly decreases to zero after the oil bank has passed in the given gridblock. If the relative permeability is zero, there is no chance of oil flowing in the given gridblock. Thus, large oil volumes are produced with the oil bank, but shortly after the oil bank has been produced, there can not be any convective flow of oil. All the produced oil after approximately 100 hours, (0.813 PVI), must be from vaporization of intermediate components.

Figure 7.12 shows simulated IFT between gas-oil and oil density in block 10, 35 and 70.

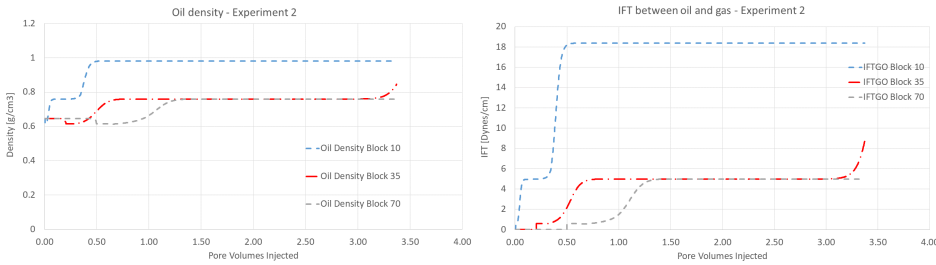

(a) Oil density in three different blocks.

(b) Gas-Oil IFT in three different blocks.

Figure 7.12: Oil density and IFT in three different blocks throughout simulation of Experiment 2.

These three blocks are picked to exemplify the change in properties that are dependent on in-situ compositions. As seen from figure 7.12, there are large variations in IFT and density in these three blocks throughout the simulation. This indicates vaporization of the oil. Notice the large increase in oil-gas IFT throughout the simulation. The increase in IFT is most likely the reason that the gridblock gas-oil capillary pressure values are so much higher than the input curves, seen in figure 7.10.

The vaporization of the oil involves transfer of intermediate components from the oil to the gas phase, which is produced as condensate when the gas is flash to standard conditions. This vaporization of oil might make the oil more viscous, hindering the flow.

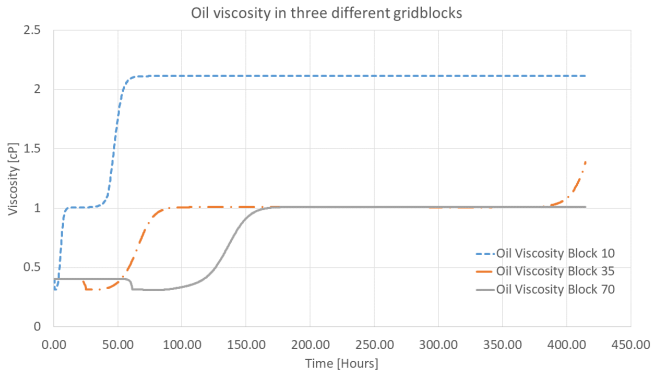

Figure 7.13: Oil viscosity in three different gridblocks throughout simulation of Experiment 2.

One may see from figure 7.13 that the oil viscosity is increasing throughout the simulation. As viscosity directly affects the flow of oil, this might reduce the magnitude of oil flow. However, after the oil bank has passed, the vaporization of oil keeps on until the oil saturation is less than the endpoint saturation, and relative permeability is zero. Hence, when the relative permeability reaches zero, the viscosity does not matter, as oil will not flow anyway.

Overall, the oil production seems to be governed by both convective flow and mass transfer at early times, and only mass transfer at late times. The vaporization of oil alters the interfacial tension and viscosity, which affects the convective flow, when convective flow still is a factor. This alteration happens through IFT-scaling of the rock curves and direct changes in oil viscosity. As the oil production cannot reach the experimental values at late times, there is a chance that the vaporization process is not modelled completely right.

7.6 Sources of Error

There are several uncertainties in the simulations of the two experiments. A chance exists that some parameters have been “overtuned”, to compensate for errors or uncertainties in other data. This is exemplified by the endpoint saturations and the distribution functions. As some of the endpoint saturations are not known properly, there is a chance that the distribution functions have been tuned nonphysically to compensate

for this.

Many of these sources of error are already discussed, such as the endpoint saturations, the surface EOS and molar weight distribution. However, some measurements and parameters introduces errors as well.

The rock curves are based on the measurements of Hustad et al. (1992). However, the curves have been altered since. The hysteresis curves were only based on the curves seen in Hustad et al. (1992), but truly found by the use of porescale simulations. Thus, they might be inaccurate, and not represent the reality.

The measurements of relative permeability includes uncertainties as well. Firstly, the fluids used for relative permeability measurements were different from the reservoir fluids. The temperature and pressure were different from reservoir conditions. As seen in the saturation profiles, in figure 6.5 and 6.9, large end effects were seen in both experiments. Since the core used for relative permeability measurements was half the length of the core used in the experiments, the end-effects would have a large impact. Hence, the saturation profile due to capillary end-effects could have altered the relative permeability measurements. A longer core could have been used instead, to avoid this effect. Overall, there are several potential sources of error in these measurements, and this may be the reason for the small misfit of oil production curves.

A source of error for the capillary pressure lies in the implementation of the ODD3P model in Eclipse E300. There is no option to directly input the water-gas capillary pressure, which would have been the optimal option. Instead, the gas-water capillary pressure is represented by the oil-water capillary pressure curve that is scaled with the water-gas IFT and appointed the gas-water endpoint. This ensures that the features of the gas-water capillary pressure curve is utilized, but it is still more inaccurate than using the water-gas curve directly.

Furthermore, the scaling coefficients to scale capillary pressure was set to be unity in both simulations. However, there are indications that this coefficient must be different from unity to resemble real physical conditions. Thus, the scaling of the capillary pressure throughout the simulation may include errors.

Chapter 8

Conclusion

Throughout this thesis two tertiary gas core flooding experiments have been presented. The main objective was to simulate an accurate history match of these two experiments, with emphasis on the water production. Another important aim was to investigate the role of mass transfer on the oil production in a tertiary gas flooding.

Other investigators proved that none of the more traditional three-phase models were able to reproduce the experimental results. The problem was mainly caused by poor treatment of capillary pressure. By using the ODD3P three-phase model along with saturation functions between all phases, including water and gas, the following simulation results were seen:

- In Experiment 1, the injection of equilibrium gas created an oil bank. Most of the oil production came from the production of this oil bank. Oil breakthrough came at 0.37 PVI compared to experimental breakthrough of 0.324 PVI. Analysis of the oil production revealed that only a small oil rate was seen after the oil bank was produced. This oil rate was driven by convective flow. The average oil saturation in the core was 21.3% at the end of the gas flooding. This provided a recovery of 44.5% of the oil in the core. This recovery factor is based on the oil in the core before the gas injection started. The saturation profile of the core revealed that the remaining oil was around 20% throughout the core. Large capillary end-effects were also observed for the water and oil saturation profiles.

- The flash calculations of oil and gas from reservoir to separator conditions proved to be cumbersome to model. A surface-EOS was developed, which unfortunately calculated errors in the density and GOR of the equilibrium injection gas. The error in equilibrium gas GOR yielded larger simulated condensate production than observed in experimental data. This error was adjusted for by modifying the oil recovery not accounted for by the flash process of equilibrium gas. By using this adjustment, it was possible to obtain an accurate history match of the oil and gas production curves for Experiment 1.

- The simulation of water production in Experiment 1 provided an accurate history match with experimental data. At breakthrough, the water production stopped for a while, and water saturation increased around the outlet of the core. This is a result of the extensive end-effects.

- A large oil bank was also seen in Experiment 2. After the oil bank was produced the oil rate declined, but was still larger than in Experiment 1. Analysis of the production mechanisms revealed that both convective flow and vaporization of oil was the basis of oil production at early times. After the oil bank had been produced, vaporized oil made up most of the oil production. The oil had a breakthrough at 0.342 PVI, while the experimental breakthrough came at 0.32 PVI. The average oil saturation at end of dry gas injection was 7%. This granted an oil recovery of 76.4% at 1.7 PVI and 80% at 3.2 PVI, which is substantially more than in Experiment 1. This indicates that the effect of vaporization of oil on the oil production is significant. Saturation profiles of the core exposed that large end-effects took place in the lower gridblocks of the core. The saturation profile also showed that the oil saturation was very low, especially in the upper gridblocks of the core. This indicates that water and gas may have been in contact, due to the small oil saturation that separates the water and gas.

- The simulation of the oil and gas production curves proved to be a very accurate history match of experimental data. The oil never reached the experimental volumes, which could be caused by a series of different errors. The largest error is probably erroneous flash calculation due to discrepancies in the molar weight distribution of the pseudocomponents.

- The simulated water production curves provided a precise history match of experimental data in Experiment 2. An increase in water production were seen at later times, when oil was vaporized. This phenomenon was accurately simulated with the use of a smooth transition from water-oil capillary pressure into water-gas capillary pressure. The capillary pressures were also scaled with respect to changing IFT throughout the simulation. Tuning the endpoint saturation of uncertain endpoints was also a key factor in the modelling of this phenomenon. This simulation indicates that the gas-water capillary pressure must be applied in combination with the oil-water capillary pressure to represent the recoveries and the physics of the fluid flow in the core.

- A sensitivity study proved that applying capillary pressure is vital to model the tertiary gas injection correctly. The study also proved the importance of choosing an appropriate numerical solver in the simulator. Lastly, the sensitivity study indicated that the the time step length that was used was sufficiently short to model the experiments properly.

Chapter 9

Further work

Throughout this thesis, it has been proven that it was in fact possible to model the two experiments by Hustad et al. (1992) with the use of proper three-phase modelling. The ODD3P model provided large flexibility, but required many user-defined inputs. As discussed, the user-defined inputs may have been tuned unphysically due to other data being inaccurate. Thus, further work should revolve around the inaccurate data that could be measured precisely. Thus, the following are recommended for further work:

Measure water-gas data properties

This thesis has proved that the interaction between the water and gas phase may play a more important role in tertiary gas injection, than traditional theory states. Still, the water-gas properties had to be based on water-oil properties due to lack of proper measurements. Better measurements of water-gas relative permeability and gas saturation endpoints would remove uncertainty, and provide more evidence for the theories related to gas-water controlled system.

Better implementation of the ODD3P model in a reservoir simulator

The E300 simulator has no option for water-gas capillary pressure inputs. Thus, efforts should be made to implement the option to directly input the gas-water capillary pressure to this simulator and other simulators.

Explore the scaling coefficients for IFT-scaling

During the simulations it was possible to use an exponent to the scaling factor of the capillary pressure. However, this was set to be unity, in lack of knowledge of this coefficients true physical value. There have been indications that it might differ from unity. Thus, the relationship between capillary pressure and changing IFT should be explored further.

Apply the ODD3P model to more experimental data

The ODD3P three-phase model should be applied to more experimental data, from experiments with changing IFT and untraditional saturation histories. Even though the model has proved to perform excellent, it should be applied to more data to validate the model and to prove that this type of flexibility and complexity may be needed for the more advanced three-phase problems.

Bibliography

Aziz, K. (1979). *Petroleum Reservoir Simulation*. Applied Science Publishers.

Baker, L. et al. (1988). Three-phase relative permeability correlations. In *SPE Enhanced Oil Recovery Symposium*. Society of Petroleum Engineers.

Bonnin, E., Levallois, B., and Joffroy, G. (2002). Full field tertiary gas injection: A case history offshore abu dhabi. In *Abu Dhabi International Petroleum Exhibition and Conference*. Society of Petroleum Engineers.

Burdine, N. (1953). Relative permeability calculations from pore size distribution data. *Journal of Petroleum Technology*, 5(03):71–78.

Burns, L., Richardson, G., and Kimber, R. (2002). Tertiary miscible gas injection in the alwyn north brent reservoirs. In *European Petroleum Conference*. Society of Petroleum Engineers.

Chen, Z. (2007). 10.1 design of study objectives.

Coats, K. H. et al. (1980). An equation of state compositional model. *Society of Petroleum Engineers Journal*, 20(05):363–376.

Fayers, F. (1989). Extension of stone&aposs method 1 and conditions for real characteristics in three-phase flow. *SPE Reservoir Engineering*, 4(04):437–445.

Graue, D. and Blevins, T. (1978). Sacroc tertiary CO2 pilot project. In *SPE Symposium on Improved Methods of Oil Recovery*. Society of Petroleum Engineers.

Hinderaker, L., Utseth, R. H., Hustad, O. S., Akervoll, I., Dalland, M., Kvanvik, B. A., Austad, T., Paulsen, J. E., et al. (1996). Ruth-a comprehensive norwegian r & d program on ior. In *European Petroleum Conference*. Society of Petroleum Engineers.

Hustad, O. S. (2015). New three-phase modeling capabilities in compositional eclipse. Powerpoint Presentation.

Hustad, O. S. and Browning, D. J. (2010). A fully coupled three-phase model for capillary pressure and relative permeability for implicit compositional reservoir simulation. In *SPE/EAGE Reservoir Characterization & Simulation Conference*.

Hustad, O. S., Holt, T., et al. (1992). Gravity stable displacement of oil by hydrocarbon gas after waterflooding. In *SPE/DOE Enhanced Oil Recovery Symposium*. Society of Petroleum Engineers.

Kantzas, A., Nikakhtar, B., and Pow, M. (1998). Principles of three phase capillary pressures. *Journal of Canadian Petroleum Technology*, 37(07).

Lake, L. (1989). *Enhanced oil recovery*. Prentice Hall.

Land, C. S. et al. (1968). Calculation of imbibition relative permeability for two- and three-phase flow from rock properties. *Society of Petroleum Engineers Journal*, 8(02):149–156.

Lawrence, J., Maer, N., Stern, D., Corwin, L., and Idol, W. (2002). Jay nitrogen tertiary recovery study: Managing a mature field. In *Abu Dhabi International Petroleum Exhibition and Conference*. Society of Petroleum Engineers.

Naar, J. and Wygal, R. (1961). Three-phase imbibition relative permeability. *Society of Petroleum Engineers Journal*, 1(04):254–258.

Parker, J. C., Lenhard, R. J., and Kuppusamy, T. (1987). A parametric model for constitutive properties governing multiphase flow in porous media. *Water Resources Research*, 23(4):618–624.

Ren, W., Bentsen, R., and Cunha, L. (2004). Pore-level observation of gravity-assisted tertiary gas-injection processes. *SPE Reservoir Evaluation & Engineering*, 7(03):194–201.

Ren, W., Cunha, L., and Bentsen, R. (2003). Numerical simulation and screening of oil reservoirs for gravity assisted tertiary gas-injection processes. In *SPE Latin American and Caribbean Petroleum Engineering Conference*. Society of Petroleum Engineers.

Shahverdi, H. and Sohrabi, M. (2013). Modelling of cyclic hysteresis of three-phase relative permeability during water-alternating-gas (WAG) injection. In *SPE Annual Technical Conference and Exhibition*. Society of Petroleum Engineers.

Simmons, C. T. (2008). Henry darcy (1803–1858): Immortalised by his scientific legacy. *Hydrogeology Journal*, 16(6):1023.

Skjæveland, S. and Kleppe, J. (1992). *SPOR Monograph—Recent Advances in Improved Oil Recovery Methods for North Sea Sandstone Reservoirs*.

Stone, H. (1973). Estimation of three-phase relative permeability and residual oil data. *J. Pet. Technol.;(United States)*, 12(4).

Stone, H. et al. (1970). Probability model for estimating three-phase relative permeability. *Journal of Petroleum Technology*, 22(02):214–218.

Whitson, C. H., Brulé, M. R., et al. (2000). *Phase behavior*. Henry L. Doherty Memorial Fund of AIME, Society of Petroleum Engineers Richardson, TX.

Nomenclature

Abbreviations

BSCF	Billion standard cubic feet
EOR	Enhanced Oil Recovery
EOS	Equation of State
GOR	Gas Oil Ratio
LBC	Lohrenz-Bray-Clark
MMSCFD	Million standard cubic feet
OOIP	Original Oil In Place
PVI	Pore Volumes Injected
PVT	Pressure Volume Temperature
SCAL	Special Core Analyses
SRK	Soave-Redlich-Kwong
STOIIP	Stock-Tank Oil Initially In Place
WAG	Water Alternating Gas

Subscripts

c	Critical parameter

fw Flowing water

G Gas

gc Connate gas

gro Gas residual in presence of oil

grw Gas residual in presence of water

imn Minimum three-phase saturation

imx Maximum three-phase saturation

iw Initial water

l liquid

lr Liquid residual

O Oil

of Flowing oil

om Residual oil

org Oil residual in presence of gas

orw Oil residual in presence of water

r Reference

W Water

wir Irreducible water

wrg Water residual in presence of gas

wro Water residual in presence of oil

Greek Letters

α User specified constant

β User specified constant

δ User specified constant

ϵ User defined constant

η IFT or Nc indicator

κ Primary or hysteresis indicator

λ Pore size distribution index

μ Viscosity

∇ Gradient

ν Shape factor

Ω SRK constant

ω Acentric factor

ρ Density

σ Interfacial tension

θ Contact angle

Symbols

$\bar{S}$ Gridblock saturation

$\check{S}$ Input saturation

$\dot{S}$ Rate of saturation change

$\hat{k_r}$ Scaled representative relative permeability

$\hat{P_c}$ Scaled representative capillary pressure

$\hat{S}$ Scaled gridblock endpoint saturation

$\tilde{k_r}$ Representative relative permeability

$\tilde{P_c}$ Representative capillary pressure

A Cross-sectional area

A IFT correlation constant

B IFT correlation constant

C IFT correlation constant

D Diameter

E_d Displacement efficiency

E_r Recovery efficiency

E_v Volumetric sweep efficiency

F Capillary pressure distribution function

f_{ij} Scaling factor

G Capillary pressure distribution function

G_g Gas from injection gas

G_o Gas from original oil in place

H Capillary pressure distribution function

k Permeability

k_a Absolute permeability

k_e Effective permeability

k_r Relative permeability

k_{rij} Relative permeability of phase i in presence of phase j

$k_{ro,dr}$ Relative permeability of oil in drainage process

$k_{ro,im}$ Relative permeability of oil in imbibition process

k_{rowc} Relative permeability of oil at connate water saturation

m Mass fraction

m User defined value

MW Molar weight

n User defined constant in Extended Stones model

N_g Cumulative gas production

N_o Cumulative oil production

N_c Capillary number

n_{ij} Scaling exponent

O_g Oil from injection gas

O_o Oil from original oil in place

p Pressure

P_c Capillary pressure

P_e Endpoint capillary pressure

q Flowrate

R Capillary pressure residual

R Ideal gas constant

r Radius

R_n Molar ratio

S Saturation

S^* Normalized saturation

S_t Sum of oil and water saturation

T Temperature

t Time

u Darcy velocity

v Volume

x Mole fraction in liquid

y Mole fraction in gas

z Mole fraction

Superscripts

d Decreasing

e Equivalent

h Hysteresis

hr Hysteresis process

i Increasing

l Scaling exponent for IFT

max Maximum saturation

pr Primary process

t Turning point

th Threshold

Appendix A

Tables

Comp. no.	Comp. ID.	Components	Eq. oil (Mole Frac.)	MW (g/mole)	p_c (Bar)	V_c (cm^3/mole)	T_c (°C)	Acentric Factor
1	HC1	N_2+C_1	0.51639	16.236	46.000	85.93	-82.98	0.0078
2	HC2	CO_2+C_2+C_3	0.14067	36.139	46.280	150.22	61.31	0.1349
3	HC5	C_4+C_5+C_6	0.06116	68.592	34.000	278.24	181.97	0.2380
4	HC9	C_7+...+C_{15}	0.16916	135.992	25.560	460.17	292.72	0.5913
5	HC21	C_{16}+...+C_{28}	0.06848	279.089	15.240	1045.56	493.45	1.0133
6	HC40	C_{29}+	0.04414	607.199	13.190	1548.19	709.28	1.2781

Figure A.1: EOS parameters. (Hustad et al., 1992)

		Experiment 1				Experiment 2		
		Equilibrium Oil		Equilibrium Gas		Oil		Inj. Gas
Comp.	Molecular Weight	Gas Mole %	Oil (STO) Weight %	Gas Mole %	Condensate Weight %	Gas Mole %	Oil (STO) Weight %	Gas Mole %
N_2	28.02	1.202	0.00	1.700	0.00	1.467	0.0	1.762
C_1	16.04	72.350	0.00	79.471	0.00	0.693	0.0	0.714
CO_2	44.01	0.737	0.00	0.651	0.00	71.461	0.0	80.218
C_2	30.07	11.359	0.00	8.582	0.00	10.793	0.03	9.053
C_3	44.09	7.873	0.03	4.971	0.03	8.244	0.21	4.945
$i-C_4$	58.12	1.014	0.03	0.611	0.04	1.129	0.12	0.544
$n-C_4$	58.12	2.848	0.18	1.655	0.19	3.203	0.53	1.406
$i-C_5$	72.15	0.693	0.22	0.444	0.25	0.793	0.45	0.309
$n-C_5$	72.15	0.880	0.43	0.605	0.52	1.016	0.81	0.396
C_6	86.17	0.590	1.23	0.573	2.05	0.711	1.90	0.294
C_7	91.62	0.418	2.96	0.598	6.09	0.446	4.04	0.359
C_8	104.53	0.0357	4.54	0.139	11.41	0.04351	5.05	
C_9	118.84		4.26		12.26		4.94	
C_{10}	134.0		3.76		11.14		4.54	
C_{11}	147.0		3.42		8.86		3.83	
C_{12}	161.0		3.18		7.46		3.45	
C_{13}	175.0		3.35		6.94		3.67	
C_{14}	190.0		3.25		5.82		3.37	
C_{15}	206.0		3.67		5.62		3.41	
C_{16}	222.0		3.16		4.14		3.20	
C_{17}	237.0		2.55		3.27		2.96	
C_{18}	251.0		3.07		3.18		3.23	
C_{19}	263.0		2.83		2.82		2.99	
C_{20}	275.0		2.50		2.06		2.44	
C_{21}	291.0		2.14		1.78		2.50	
C_{22}	300.0		2.14		1.53		2.05	
C_{23}	312.0		1.66		0.49		1.42	
C_{24}	324.0		1.55		0.39		1.33	
C_{25}	337.0		1.50		0.30		1.28	
C_{26}	349.0		1.46		0.24		1.25	
C_{27}	360.0		1.28		0.16		1.09	
C_{28}	372.0		1.42		0.15		1.21	
C_{29}	382.0		1.47		0.14		1.26	
C_{30}	394.0		1.52		0.11		1.30	
C_{31}	404.0		1.25		0.079		1.07	
C_{32}	415.0		1.05		0.052		0.90	
C_{33}	426.0		1.07		0.039		0.92	
C_{34}	437.0		0.98		0.036		0.84	
C_{35}	445.0		1.00		0.043		0.86	
C_{36}	456.0		0.88		0.049		0.75	
C_{37}	464.0		0.90		0.079		0.77	
C_{38}	475.0		0.72		0.059		0.62	
C_{39}	484.0		0.68		0.022		0.58	
C_{40}	495.0		0.61		0.016		0.52	
C_{41}	502.0		0.54		0.020		0.46	
C_{42}	512.0		0.50		0.020		0.43	
C_{43}	521.0		0.41		0.013		0.35	
C_{44}	531.0		0.35		0.007		0.30	
C_{45}	539.0		0.29		0.003		0.25	
C_{46}	548.0		0.24		0.002		0.21	
C_{47}	557.0		0.19		0.001		0.16	
C_{48+}	791.5		23.58		0.010		20.15	
MW (g/mole)		-	226	-	159	-	205	
Density (g/cm^3)		9.922E-4	0.8485	9.111E-4	0.8033	1.013E-4	0.845	
Formation Volume Factor (cm^3/Scm^3)		1.62		18.0		1.61		
Gas/Oil Ratio (Scm^3/Scm^3)		200.9		4341.63		204.1		
Saturation Temperature (°C)		91.9		91.9		98.4		
Saturation Pressure (bar)		313.5		313.5		275.1		
Saturation Density (g/cm^3)		0.6468		0.2644		0.6532		
Viscosity (cp)		0.43		-		-		
Interfacial tension (mN/m)		1.2						

Figure A.2: Experimental flash data and fluid properties. (Hustad et al., 1992)

Component	Concentration	
	(mg/dm^3)	($mmol/dm^3$)
$NaCl$	22 330	382.1
KCl	382	5.12
NH_4Cl	102	1.91
NaF	3	0.071
$NaHCO_3$	422	5.02
$CaCl_2$	837	7.54
$FeCl_2$	0.26	0.002
$MgCl_2$	207	2.17
$MnCl_2$	0.6	0.005
$SrCl_2$	82	0.516
$B(OH)_3$	301	4.87
$AlCl_3$	0.95	0.007
Total	24 667.81	409.331

Figure A.3: Composition of formation water. (Hustad et al., 1992)

Appendix B

Eclipse Data Files

```
-------
RUNSPEC
-------

TITLE
Equlibrium gas injection, experiment 1

NOECHO

START
 1 JAN 2007 /

LAB

OIL

WATER

GAS

COMPS
6 /

DIMENS
1 1 74 /

TABDIMS
--NTSFUN NTPVT NSSFUN NPPVT (Siste tallet angir K-verdi inputs)
6 2 400 / 100 / -- 1* 1* 1* 1* 1* 1* 1* 1* 1* 1* 1* 1* 1* 1* 1* 1* 1* 1* 1*
2 /

EQLDIMS
--1  / 20 /
 2  / -- osh

WELLDIMS
4 2 /

-- FMTIN

-- FMTOUT

-- FMTSAVE

UNIFOUT

UNIFOUTS

-- DISABLE PC RATE CHANGE CONTROL
NODPCDT

-- ENDSCALE optional with ODD3P but will usually be selected
--ENDSCALE

-- Hysteresis must be specified with ODD3P
SATOPTS
HYSTER
/

-- Select nomixing of Kro/Krg for ODD3P
-- This option is selected by default if ODD3P specified in PROPS Sect.
NOMIX

CPR
/


VECTABLE
```

```
13000  /

--IMPES
--FULLIMP
--AIM
-- IMPSAT

--NOSIM

----
GRID
----

-- Request output of init file
INIT

DX
74*3.34990536106928
/

DY
74*3.34990536106928
/

DZ
1*4.37857
8*0.54732125
4*1.0946425
48*2.189285
4*1.0946425
8*0.54732125
1*4.37857
--30*4.37857 -- = core lenght div by 28 in equlibrium gas injection,
experiement 1
/

NTG
74*1.0
/

TOPS
0.0
  4.37857      4.92589125  5.4732125    6.02053375 6.567855     7.11517625
  7.6624975    8.20981875  8.75714
  9.8517825   10.946425   12.0410625   13.13571
 15.324995    17.51428    19.703565    21.89285   24.082135    26.27142
 28.460705    30.64999    32.839275    35.02856   37.217845    39.40713
 41.596415    43.7857     45.974985    48.16427   50.353555    52.54284
 54.732125    56.92141    59.110695    61.29998   63.489265    65.67855
 67.867835    70.05712    72.246405    74.43569   76.624975    78.81426
 81.003545    83.19283    85.382115    87.5714    89.760685    91.94997
 94.139255    96.32854    98.517825   100.70711  102.896395   105.08568
107.274965   109.46425   111.653535   113.84282  116.032105   118.22139
119.3160325  120.410675  121.5053175  122.59996
123.14728125 123.6946025 124.24192375 124.789245 125.33656625 125.8838875
126.43120875 126.97853
/

PERMX
74*2566.0
/

PERMY
74*2566.0
/

PERMZ
74*2566.0
```

```
/

PORO
 1*0.0203517906754682 72*0.227 1*0.0203517906754682
/

RPTGRID
TOPS DX DX DZ NTG PERMX PERMY PERMZ PORO
/

-----
PROPS
-----


ZI
0.51639 0.14067 0.06116 0.16916 0.06848 0.04414
/

EOS
SRK
/

RTEMP
-- E300 Units are Celcius
91.9
/

CNAMES
HC1
HC2
HC5
HC9
HC21
HC40
/

MW
16.236
36.139
68.592
135.992
279.089
607.199
/

PCRIT
-- Atm        Bar
45.398     -- 46.0
45.675     -- 46.28
33.555     -- 34.0
25.226     -- 25.56
15.041     -- 15.24
13.017     -- 13.19
/

VCRIT
85.93
150.22
278.24
460.17
1045.56
1548.19
/

TCRIT
--  K            C
190.17 --       -82.98
```

```
334.46 --       61.31
455.12 --       181.97
565.87 --       292.72
766.6  --       493.45
982.43 --       709.28
/

ACF
0.0078
0.1349
0.2380
0.5913
1.0133
1.2781
/

BIC
0.0
0.0  0.0
0.0  0.0  0.0
0.0  0.0  0.0  0.0
0.0  0.0  0.0  0.0  0.0
/

---SURFACE EOS
EOSS
SRK
/

--RTEMP
-- E300 Units are Celcius
--91.9
--/

--CNAMES
--HC1
--HC2
--HC5
--HC9
--HC21
--HC40
--/

MWS
16.236
36.139
68.592
135.992
279.089
607.199
/

PCRITS
-- Atm        Bar
46.44406
46.72677
34.32822
25.47511
15.18938
13.14619
/

VCRITS
85.93
150.22
278.24
460.17
1045.56
```

```
1548.19
/

TCRITS
--  K            C
182.3135
320.6425
436.3177
571.3027
773.9598
991.8619
/

ACFS
0.00777
0.134386
0.237093
0.591657
1.013912
1.278872
/

BICS
0.0
0.0  0.0
0.0  0.0  0.0
0.0  0.0  0.0  0.0
0.0  0.0  0.0  0.0  0.0
/

PARACHOR
-- 57.4091 115.5259 210.2886 382.6816 711.8047 1466.4577 /
-- parachors three heaviest groups increased with 17% to obtain IFTGO=1.20
mN/m
57.4091 115.5259 210.2886 448 833 1715 / --IFTGO=1.20

LBCCOEF
4* 0.0127642 /

STCOND
--std. temp. std. pres.
   15.0       1.0 /

DENSITY
   1* 1.0 1* /
/

PVTW
-- Ref      Water    Water       Water   Water
-- Press     FVF     Comp        Visc  Viscob
-- 314.0    1.02187 4.351E-05    0.305      1*  -- Pressure and 1/pressure
in bar and 1/bar
   309.8928 1.02187 4.4087E-05   0.305      1* / -- Pressure and 1/pressure
   in atm and 1/atm
/

ROCK
--   Value for rock reference pressure
--   Ref      Rock
--   Press    Comp
-- rock type 1
-- 314.0      4.351E-05    -- Pressure and 1/pressure in bar and 1/bar
   309.8928   4.4087E-05   -- Pressure and 1/pressure in atm and 1/atm
/
-- rock type 2
-- 314.0      2.09E-04    -- Pressure and 1/pressure in bar and 1/bar
   309.8928   2.118E-04   -- Pressure and 1/pressure in atm and 1/atm
/
```

```
-- ========================
-- ODD3P SPECIFIC KEYWORDS
-- ========================

ODD3P

-- First table associated with primary, second and third not used.
EPSODD3P
-- when fitting, we used 22.594012 mN/m to match an experiment with
meassured 37.1.
-- For the input to this DATA file we used ift=21.7 in ecore, which by the
same factor would correspond to 35.63201
-- Land  Scaling        Pc Reference     Pc Exp     Water-Hydro        Kr
Threshold       Kr Thrsh  Satn  Satn  1st  Kr Exp
-- Proc  Control      Surface Tensions   Surf Tens  Corr Coeffs     Surf
Tens/Cap Num s   Cap Nums  EndP  Dirn  Con  Surf Tens
-- O G W Pc   Kr       GO     OW     GW  GO OW GW  A1    A2   A3       GO
OW     GW   OG WO WG  ds/dT Chnge Mis  GO OW GW
   1 1 1  1    1 1.248 35.63201 35.63201 1* 1* 1*  16.13811 14.45386 3.3487
   0.5 0.5 0.5  1* 1* 1*  0.01  0.001  0   1* 1* 1* -- reservoir condition
   ift
/
/
/
   1 1 1  1    1     1.2  21.7   28.2    1* 1* 1*  16.13811 14.45386 3.3487
   0.5 0.5 0.5   1* 1* 1*  0.01  0.001  0   1* 1* 1* -- reservoir condition
   ift
/
/
/

-- First table associated with primary, second and third not used.
PCODD3P
-- IPCFN DelG  AG   BG  DelW  AW  BW
--      6  0.0 1.0  1.0   0.0 1.0 1.0
       6  0.0 1.0  1.0   0.0 1.0 1.0
/
/
/
       6  0.0 1.0  1.0   0.0 1.0 1.0
/
/
/

RPTPROPS
PSORG PSGRO PSORW PSWRO PSGRW PSWRG
HSORG HSGRO HSORW HSWRO HSGRW HSWRG
SOF2
SGF3 SWF3 SOF3
/

INCLUDE
  flow_param_with_overlap_smoothed_right_gas_ow_endp.txt /

-------
REGIONS
-------

PVTNUM
1*2 72*1 1*2
/

FIPNUM
74*1
/

EQLNUM
```

```
  1  73*2  /

-- Primary saturation region numbers
PSTNUM
1*4 72*1 1*4
/

-- Increasing hysteresis saturation region numbers
ISTNUM
1*5 72*2 1*5
/

-- Decreasing hysteresis saturation region numbers
DSTNUM
1*6 72*3 1*6
/

SDROW
 74*4
/

SDRWO
 74*3
/

RPTREGS
PSTNUM ISTNUM DSTNUM
SDRGO SDROG SDROW SDRWO SDRGW SDRWG
/

--------
SOLUTION
--------

EQUIL
--   1           2            3        4       5       6   7  8   9  10
-- Datum      Pressure       WOC     Pcow    GOC     Pcgo
-- depth                    depth     WOC   depth    GOC
  2.37857    309.3994  / -- 126.4785458  0.0  4.37857   0.0   1* 1*  0   2
  /
126.97853    309.3994  / -- 126.4785458  0.0  4.37857   0.0   1* 1*  0   1
/

SWAT
-- 1*0.616 72*0.616 1*0.999 /
 0.0001  72*0.616  0.9999 /


SOIL
 0.0  72*0.384  0.0001 /


PRESSURE
74*309.3994 / --313.5 bar=309.3994 atm

NEI
0.779171 0.13325 0.037295 0.047617 0.002618 0.000049 /
0.51639  0.14067 0.06116  0.16916  0.06848  0.04414   /


RPTSOL
PRESSURE SWAT SOIL SGAS
/

RPTRST
 BASIC=2 KRO KRW KRG PCOW PCOG PCGW SOIL SWAT SGAS
 /
```

```
-------
SUMMARY
-------

--RUNSUM

INCLUDE
 summary_stuff.txt /

BDENO
--1 1 1 /
1 1 2 /
--1 1 5 /
--1 1 10 /
--1 1 15 /
--1 1 20 /
1 1 25 /
1 1 35 /
--1 1 45 /
--1 1 55 /
--1 1 65 /
--1 1 70 /
--1 1 72 /
1 1 73 /
--1 1 74 /
/
BDENG
--1 1 1 /
1 1 2 /
--1 1 5 /
--1 1 10 /
--1 1 15 /
--1 1 20 /
--1 1 25 /
1 1 35 /
--1 1 45 /
--1 1 55 /
--1 1 65 /
--1 1 70 /
--1 1 72 /
1 1 73 /
--1 1 74 /
/

--BSWAT
--1 1 1 /
--1 1 2 /
--1 1 5 /
--1 1 10 /
--1 1 15 /
--1 1 20 /
--1 1 25 /
--1 1 35 /
--1 1 45 /
--1 1 55 /
--1 1 65 /
--1 1 70 /
--1 1 72 /
--1 1 73 /
--1 1 74 /
--/
BVOIL
--1 1 1 /
1 1 2 /
--1 1 5 /
--1 1 10 /
--1 1 15 /
--1 1 20 /
```

```
--1 1 25 /
1 1 35 /
--1 1 45 /
--1 1 55 /
--1 1 65 /
1 1 70 /
--1 1 72 /
--1 1 73 /
--1 1 74 /
/

--BSGAS
--1 1 1 /
--1 1 2 /
--1 1 5 /
--1 1 10 /
--1 1 15 /
--1 1 20 /
--1 1 25 /
--1 1 35 /
--1 1 45 /
--1 1 55 /
--1 1 65 /
--1 1 70 /
--1 1 72 /
--1 1 73 /
--1 1 74 /
--/
--BSOIL
--1 1 1 /
--1 1 2 /
--1 1 5 /
--1 1 10 /
--1 1 15 /
--1 1 20 /
--1 1 25 /
--1 1 35 /
--1 1 45 /
--1 1 55 /
--1 1 65 /
--1 1 70 /
--1 1 72 /
--1 1 73 /
--1 1 74 /
--/
--BPCOWR
--1 1 1 /
--1 1 2 /
--1 1 5 /
--1 1 10 /
--1 1 15 /
--1 1 20 /
--1 1 25 /
--1 1 35 /
--1 1 45 /
--1 1 55 /
--1 1 65 /
--1 1 70 /
--1 1 72 /
--1 1 73 /
--1 1 74 /
--/
--BPCWOR
--1 1 1 /
--1 1 2 /
--1 1 5 /
--1 1 10 /
--1 1 15 /
```

```
--1 1 20 /
--1 1 25 /
--1 1 35 /
--1 1 45 /
--1 1 55 /
--1 1 65 /
--1 1 70 /
--1 1 72 /
--1 1 73 /
--1 1 74 /
--/
--BPCOGR
--1 1 1 /
--1 1 2 /
--1 1 5 /
--1 1 10 /
--1 1 15 /
--1 1 20 /
--1 1 25 /
--1 1 35 /
--1 1 45 /
--1 1 55 /
--1 1 65 /
--1 1 70 /
--1 1 72 /
--1 1 73 /
--1 1 74 /
--/
--BPCGOR
--1 1 1 /
--1 1 2 /
--1 1 5 /
--1 1 10 /
--1 1 15 /
--1 1 20 /
--1 1 25 /
--1 1 35 /
--1 1 45 /
--1 1 55 /
--1 1 65 /
--1 1 70 /
--1 1 72 /
--1 1 73 /
--1 1 74 /
--/
--BPCGWR
--1 1 1 /
--1 1 2 /
--1 1 5 /
--1 1 10 /
--1 1 15 /
--1 1 20 /
--1 1 25 /
--1 1 35 /
--1 1 45 /
--1 1 55 /
--1 1 65 /
--1 1 70 /
--1 1 72 /
--1 1 73 /
--1 1 74 /
--/
--BPCWGR
--1 1 1 /
--1 1 2 /
--1 1 5 /
--1 1 10 /
--1 1 15 /
```

```
--1 1 20 /
--1 1 25 /
--1 1 35 /
--1 1 45 /
--1 1 55 /
--1 1 65 /
--1 1 70 /
--1 1 72 /
--1 1 73 /
--1 1 74 /
--/

-------
SCHEDULE
--------

CVCRIT
-- DPMAX MAX-NLI LSR MAX-LI MAX-FUG MIN-LI DVMAX DSPE MIN-NLI
   0.01  50      1*  150    1*      1*     1*    1*
/

TSCRIT
-- TsIni MinTs   MaxTs MaxTsDf MasTsIf TgtTTE MaxTTE TgtTPR MaxTPR TgtSC
-- 0.01  0.1 1.0   1*     1*      1*     1*     0.05   0.01   0.0125
   0.0004  1.0E-10 0.0004   1*     1*      1*     1*     0.0005   0.005
   0.0250
/

WELLSTRE
'INJCOMP'
0.779171 0.13325 0.037295 0.047617 0.002618 0.000049 /
--5.01E-05
/

GRUPTREE
'WFILL' 'FIELD' /
'GINJ'  'FIELD' /
 /

-- Define the E300 wells
WELSPECS
--
--  1    2       3 4  5    6     7     8     9      10    11    12
16
--                  BHP                   Inst          Pres  Dens
Well
-- Wll  Group        Ref Pref   Drng Infl  Auto   Xflow  Tab   Calc
Model
-- Nme  Name     I J Dep Phase  Rad  Eqtn  Shut   Enabl  Num   Type
Type
'TOP'    'GINJ'  1 1 0.54732125    'GAS'   1*  'STD' 'SHUT' 'NO'   1*
'SEG'  3*  'STD' /
'WINJ'   'WFILL' 1 1 130.81  'WATER' 1*  'STD' 'SHUT' 'NO'   1*    'SEG'
3*  'STD' /
'BOTTOM' 'GINJ'  1 1 130.81  'OIL'   1*  'STD' 'SHUT' 'NO'   1*    'SEG'
3*  'STD' /
'TOPP'   'WFILL' 1 1 0.54732125    'OIL'   1*  'STD' 'SHUT' 'NO'   1*
'SEG'  3*  'STD' /
/

COMPDAT
-- 1     2 3 4 5   6     7    8     9    10   11    12    13    14
--                       Sat  Con                                Pres
-- Wl    I J K1         Tab  Trans Bore  Eff  Skin  D          Equiv
-- Nm         K2 Status Num  Fact  Diam  Kh   Fact  Fact  Dir  Rad
'TOP'    1 1 1 1   'OPEN'  1*   1*   0.008594   1*   1*   1*    'Z'   1* /
'WINJ'   1 1 74 74 'OPEN'  1*   1*   0.008594   1*   1*   1*    'Z'   1* /
'BOTTOM' 1 1 74 74 'OPEN'  1*   1*   0.008594   1*   1*   1*    'Z'   1* /
```

```
'TOPP'   1 1 1 1   'OPEN'  1*   1*   0.008594   1*   1*   1*    'Z'   1* /
/

WCONINJE
--    1     2       3      4      5    6     7
--        Inj             Cntl  Surf  Res   BHP
--        Type    Status  Mode  Rate  Rate  Lim
   'TOP'  'GAS'   'OPEN' 'RESV' 1*    2.47  800 / -- BHP atm
   'WINJ' 'WATER' 'SHUT' 'RESV' 1*    4.0  310.8798 / -- BHP atm
/

-- Define injected composition
WINJGAS
'TOP' 'STREAM' 'INJCOMP'  /
/

WCONPROD
--    1     2      3     4     5    6    7    8     9
--                                      Res
--                Cntl  Oil   Wat   Gas  Liq  Vol  BHP
--         Status  Mode  Rate  Rate  Rate Rate Rate Lim
-- 'BOTTOM' 'OPEN'  'BHP'  50.0  1*    1*   1*   1*   313.5 /  -- BHP bar
   'BOTTOM' 'OPEN'  'BHP'  1*  1*    1*   1*   1*   309.3994 /  -- removed
   oil rate
   'TOPP'   'SHUT'  'BHP'  1*  1*    1*   1*   1*   309.365 /
/

SEPCOND
 'SEPARGAS' 'FIELD' 1  15.0  1.0 2* / 1 /
 /

WSEPCOND
 'TOPP' 'SEPARGAS' /
 'BOTTOM' 'SEPARGAS' /
/

TIME
0.0001
/

RPTSCHED
PRESSURE SOIL SWAT SGAS KRO KRW KRG PCOG PCOW PCGW /

TIME
0.42743
--87.0
/

TIME
10.0
/

RPTSCHED
PRESSURE SOIL SWAT SGAS KRO KRW KRG PCOG PCOW PCGW SDROW SDROG SDRWO SDRWG
SDRGO SDRGW /

TIME
25
/

RPTSCHED
PRESSURE SOIL SWAT SGAS KRO KRW KRG PCOG PCOW PCGW SDROW SDROG SDRWO SDRWG
SDRGO SDRGW /

TIME
30.0
/
```

```
RPTSCHED
PRESSURE SOIL SWAT SGAS KRO KRW KRG PCOG PCOW PCGW SDROW SDROG SDRWO SDRWG
SDRGO SDRGW /



TIME
48.0
/

RPTSCHED
PRESSURE SOIL SWAT SGAS KRO KRW KRG PCOG PCOW PCGW SDROW SDROG SDRWO SDRWG
SDRGO SDRGW /

TIME
49.0
/

RPTSCHED
PRESSURE SOIL SWAT SGAS KRO KRW KRG PCOG PCOW PCGW SDROW SDROG SDRWO SDRWG
SDRGO SDRGW /

TIME
50.0
/

RPTSCHED
PRESSURE SOIL SWAT SGAS KRO KRW KRG PCOG PCOW PCGW SDROW SDROG SDRWO SDRWG
SDRGO SDRGW /

TIME
51.0
/

RPTSCHED
PRESSURE SOIL SWAT SGAS KRO KRW KRG PCOG PCOW PCGW SDROW SDROG SDRWO SDRWG
SDRGO SDRGW /


TIME
52.0
/

RPTSCHED
PRESSURE SOIL SWAT SGAS KRO KRW KRG PCOG PCOW PCGW SDROW SDROG SDRWO SDRWG
SDRGO SDRGW /

TIME
53.0
/

RPTSCHED
PRESSURE SOIL SWAT SGAS KRO KRW KRG PCOG PCOW PCGW SDROW SDROG SDRWO SDRWG
SDRGO SDRGW /

TIME
54.0
/

RPTSCHED
PRESSURE SOIL SWAT SGAS KRO KRW KRG PCOG PCOW PCGW SDROW SDROG SDRWO SDRWG
SDRGO SDRGW /

TIME
55.0
/

RPTSCHED
```

```
PRESSURE SOIL SWAT SGAS KRO KRW KRG PCOG PCOW PCGW SDROW SDROG SDRWO SDRWG
SDRGO SDRGW /

TIME
56.0
/

RPTSCHED
PRESSURE SOIL SWAT SGAS KRO KRW KRG PCOG PCOW PCGW SDROW SDROG SDRWO SDRWG
SDRGO SDRGW /

TIME
57.0
/

RPTSCHED
PRESSURE SOIL SWAT SGAS KRO KRW KRG PCOG PCOW PCGW SDROW SDROG SDRWO SDRWG
SDRGO SDRGW /


TIME
58.0
/

RPTSCHED
PRESSURE SOIL SWAT SGAS KRO KRW KRG PCOG PCOW PCGW SDROW SDROG SDRWO SDRWG
SDRGO SDRGW /


TIME
59.0
/

RPTSCHED
PRESSURE SOIL SWAT SGAS KRO KRW KRG PCOG PCOW PCGW SDROW SDROG SDRWO SDRWG
SDRGO SDRGW /




TIME
60
/

RPTSCHED
PRESSURE SOIL SWAT SGAS KRO KRW KRG PCOG PCOW PCGW SDROW SDROG SDRWO SDRWG
SDRGO SDRGW /


TIME
61
/

RPTSCHED
PRESSURE SOIL SWAT SGAS KRO KRW KRG PCOG PCOW PCGW SDROW SDROG SDRWO SDRWG
SDRGO SDRGW /

TIME
62
/

RPTSCHED
PRESSURE SOIL SWAT SGAS KRO KRW KRG PCOG PCOW PCGW SDROW SDROG SDRWO SDRWG
SDRGO SDRGW /


TIME
63
```

```
/

RPTSCHED
PRESSURE SOIL SWAT SGAS KRO KRW KRG PCOG PCOW PCGW SDROW SDROG SDRWO SDRWG
SDRGO SDRGW /

TIME
64
/

RPTSCHED
PRESSURE SOIL SWAT SGAS KRO KRW KRG PCOG PCOW PCGW SDROW SDROG SDRWO SDRWG
SDRGO SDRGW /


TIME
65
/

RPTSCHED
PRESSURE SOIL SWAT SGAS KRO KRW KRG PCOG PCOW PCGW SDROW SDROG SDRWO SDRWG
SDRGO SDRGW /



TIME
65.5
--154.0
/

TIME
65.6
--154.00001
/

RPTSCHED
PRESSURE SOIL SWAT SGAS KRO KRW KRG PCOG PCOW PCGW SDROW SDROG SDRWO SDRWG
SDRGO SDRGW /

TIME
70.0
/

RPTSCHED
PRESSURE SOIL SWAT SGAS KRO KRW KRG PCOG PCOW PCGW SDROW SDROG SDRWO SDRWG
SDRGO SDRGW /

TIME
80.0
/

RPTSCHED
PRESSURE SOIL SWAT SGAS KRO KRW KRG PCOG PCOW PCGW SDROW SDROG SDRWO SDRWG
SDRGO SDRGW /

TIME
100.0
/

RPTSCHED
PRESSURE SOIL SWAT SGAS KRO KRW KRG PCOG PCOW PCGW SDROW SDROG SDRWO SDRWG
SDRGO SDRGW /

TIME
120.0
/

RPTSCHED
```

```
PRESSURE SOIL SWAT SGAS KRO KRW KRG PCOG PCOW PCGW SDROW SDROG SDRWO SDRWG
SDRGO SDRGW /

TIME
140.0
/

RPTSCHED
PRESSURE SOIL SWAT SGAS KRO KRW KRG PCOG PCOW PCGW SDROW SDROG SDRWO SDRWG
SDRGO SDRGW /

TIME
160.0
/

RPTSCHED
PRESSURE SOIL SWAT SGAS KRO KRW KRG PCOG PCOW PCGW SDROW SDROG SDRWO SDRWG
SDRGO SDRGW /

TIME
180.0
/

RPTSCHED
PRESSURE SOIL SWAT SGAS KRO KRW KRG PCOG PCOW PCGW SDROW SDROG SDRWO SDRWG
SDRGO SDRGW /

TIME
200.0
/

RPTSCHED
PRESSURE SOIL SWAT SGAS KRO KRW KRG PCOG PCOW PCGW SDROW SDROG SDRWO SDRWG
SDRGO SDRGW /

TIME
216.6704
--303.243
/

END
```

```
-------
RUNSPEC
-------

TITLE
Equlibrium gas injection, experiment 1

NOECHO

START
 1 JAN 2007 /

LAB

OIL

WATER

GAS

COMPS
6 /

DIMENS
1 1 74 /

TABDIMS
--NTSFUN NTPVT NSSFUN NPPVT
6 2 400 / 100 / -- 1* 1* 1* 1* 1* 1* 1* 1* 1* 1* 1* 1* 1* 1* 1* 1* 1* 1* 1*
/        2 /

EQLDIMS
--1 20 /
2 / 200 /

WELLDIMS
4 2 /

-- FMTIN

-- FMTOUT

-- FMTSAVE

UNIFOUT

UNIFOUTS

-- DISABLE PC RATE CHANGE CONTROL
NODPCDT

-- ENDSCALE optional with ODD3P but will usually be selected
ENDSCALE

-- Hysteresis must be specified with ODD3P
SATOPTS
HYSTER
/

-- Select nomixing of Kro/Krg for ODD3P
-- This option is selected by default if ODD3P specified in PROPS Sect.
NOMIX

CPR
/

VECTABLE
13000  /
```

```
-- IMPES
--FULLIMP
--AIM
-- IMPSAT

--NOSIM

----
GRID
----

-- Request output of init file
INIT

DX
74*3.34106630783996
/

DY
74*3.34106630783996
/

DZ
1*4.36071429
8*0.54508929
4*1.09017857
48*2.18035714
4*1.09017857
8*0.54508929
1*4.36071429
--30*4.37857 -- = core lenght div by 28 in equlibrium gas injection,
experiement 1
/

NTG
74*1.0
/

TOPS
0       4.36071429      4.90580358      5.45089287      5.99598216
6.54107145
7.08616074      7.63125003      8.17633932      8.72142861      9.81160718
10.90178575
11.99196432     13.08214289     15.26250003     17.44285717     19.62321431
21.80357145
23.98392859     26.16428573     28.34464287     30.52500001     32.70535715
34.88571429
37.06607143     39.24642857     41.42678571     43.60714285     45.78749999
47.96785713
50.14821427     52.32857141     54.50892855     56.68928569     58.86964283
61.04999997
63.23035711     65.41071425     67.59107139     69.77142853     71.95178567
74.13214281
76.31249995     78.49285709     80.67321423     82.85357137     85.03392851
87.21428565
89.39464279     91.57499993     93.75535707     95.93571421     98.11607135
100.2964285
102.4767856     104.6571428     106.8374999     109.0178571     111.1982142
113.3785713
115.5589285     117.7392856     118.8294642     119.9196428     121.0098213
122.0999999
122.6450892     123.1901785     123.7352678     124.2803571     124.8254463
125.3705356
125.9156249     126.4607142
/
```

```
PERMX
74*2645.0
/

PERMY
74*2645.0
/

PERMZ
74*2645.0
/

PORO
0.0205432799844714    72*0.223    0.0205432799844714
/

RPTGRID
TOPS DX DX DZ NTG PERMX PERMY PERMZ PORO
/

-----
PROPS
-----


ZI
0.488001427 0.13596298 0.080436444 0.187865683 0.070975213 0.036758252
/

EOS
SRK
/

RTEMP
-- E300 Units are Celcius
98.4
/

CNAMES
HC1
HC2
HC5
HC9
HC21
HC40
/







MW
16.236
36.139
68.592
135.992
279.089
607.199
/

PCRIT
-- Atm        Bar
45.398     -- 46.0
45.675     -- 46.28
33.555     -- 34.0
```

```
25.226     -- 25.56
15.041     -- 15.24
13.017     -- 13.19
/

VCRIT
85.93
150.22
278.24
460.17
1045.56
1548.19
/

TCRIT
--  K            C
190.17 --       -82.98
334.46 --       61.31
455.12 --       181.97
565.87 --       292.72
766.6  --       493.45
982.43 --       709.28
/

ACF
0.0078
0.1349
0.2380
0.5913
1.0133
1.2781
/

BIC
0.0
0.0  0.0
0.0  0.0  0.0
0.0  0.0  0.0  0.0
0.0  0.0  0.0  0.0  0.0
/
---SURFACE EOS
EOSS
SRK
/

--RTEMP
-- E300 Units are Celcius
--91.9
--/

--CNAMES
--HC1
--HC2
--HC5
--HC9
--HC21
--HC40
--/



MWS
16.236
36.139
68.592
135.992
279.089
607.199
```

```
/

PCRITS
-- Atm        Bar
45.50536524
45.78235591
33.63439952
24.39472622
14.54521103
12.58867271
/

VCRITS
85.93
150.22
278.24
460.17
1045.56
1548.19
/

TCRITS
--  K            C
180.661501
317.7370017
432.3640023
540.4151982
732.1156642
938.2368797
/

ACFS
0.00819
0.141645
0.2499
0.620865
1.063965
1.342005
/

BICS
0.0
0.0  0.0
0.0  0.0  0.0
0.0  0.0  0.0  0.0
0.0  0.0  0.0  0.0  0.0
/



PARACHOR
-- 57.4091 115.5259 210.2886 382.6816 711.8047 1466.4577 /
-- parachors three heaviest groups increased with 17% to obtain IFTGO=1.20
mN/m
57.4091 115.5259 210.2886 448 833 1715 / --IFTGO=1.20



LBCCOEF
 0.1023 0.023364 0.058533 -0.040758 0.0127642  /


STCOND
--std. temp. std. pres.
   15.0       1.0 /


DENSITY
```

```
   1* 1.0 1* /
/

PVTW
-- Ref      Water    Water       Water   Water
-- Press     FVF     Comp        Visc  Viscob
-- 314.0    1.02187 4.351E-05    0.305      1*  -- Pressure and 1/pressure
in bar and 1/bar
   309.8928 1.02187 4.4087E-05   0.305      1* / -- Pressure and 1/pressure
   in atm and 1/atm
/


ROCK
--   Value for rock reference pressure
--   Ref      Rock
--   Press    Comp
-- rock type 1
-- 314.0      4.351E-05    -- Pressure and 1/pressure in bar and 1/bar
   309.8928   4.4087E-05   -- Pressure and 1/pressure in atm and 1/atm
/
-- rock type 2
-- 314.0      2.09E-04    -- Pressure and 1/pressure in bar and 1/bar
   309.8928   2.118E-04   -- Pressure and 1/pressure in atm and 1/atm
/

-- ========================
-- ODD3P SPECIFIC KEYWORDS
-- ========================

ODD3P

PSGRO
 0.0001  72*0.0725     0.0001 -- 1*0.0 72*0.0725 1*0.0
/
HSGRO
 0.0001  72*0.3854  0.0001 -- 1*0.01 72*0.3854 1*0.01
/


PSGRW
 0.0001  72*0.0725     0.0001 --  1*0.0 72*0.0725 1*0.0
/
HSGRW
 0.0001  72*0.3854  0.0001 --  1*0.01 72*0.3854 1*0.01
/



PSORG
 0.0001  72*0.045   0.0001 --  1*0.0 72*0.1150 1*0.0
/
HSORG
 0.0001  72*0.045   0.0001 --  1*0.00 72*0.1150 1*0.00
/



PSORW
 0.0001  72*0.1582  0.0001 -- 1*0.0 72*0.1582 1*0.0
/
HSORW
 0.0001  72*0.3686   0.0001 --  1*0.0 72*0.3686 1*0.0
/
```

```
PSWRG
 0.0001  72*0.0775   0.0001 --  1*0.00 72*0.1150 1*0.00
/
HSWRG
 0.0001  72*0.0775   0.0001 --  1*0.00 72*0.1150 1*0.00
/



PSWRO
 0.0001  72*0.1150   0.0001 --  1*0.00 72*0.1150 1*0.00
/
HSWRO
 0.0001  72*0.1150   0.0001 --  1*0.00 72*0.1150 1*0.00
/



-- First table associated with primary, second and third not used.
EPSODD3P
-- when fitting, we used 22.594012mN/m to match an experiment with
meassured 37.1. For the input to this DATA file we used ift=21.7 in ecore,
which by the same factor would correspond to 35.63201
-- Land  Scaling        Pc Reference     Pc Exp     Water-Hydro        Kr
Threshold       Kr Thrsh  Satn  Satn  1st  Kr Exp
-- Proc  Control      Surface Tensions   Surf Tens  Corr Coeffs     Surf
Tens/Cap Num s   Cap Nums  EndP  Dirn  Con  Surf Tens
-- O G W Pc   Kr       GO     OW     GW  GO OW GW  A1    A2   A3       GO
OW     GW   OG WO WG  ds/dT Chnge Mis  GO OW GW
   1 1 1  1    1 1.248 35.63201 35.63201 1* 1* 1*  16.13811 14.45386 3.3487
   0.5 0.5 0.5  1* 1* 1*  0.01  0.001  0   1* 1* 1* -- reservoir condition
   ift
/
/
/
   1 1 1  1    1     1.2  21.7   28.2    1* 1* 1*  16.13811 14.45386 3.3487
   0.5 0.5 0.5   1* 1* 1*  0.01  0.001  0   1* 1* 1* -- reservoir condition
   ift
/
/
/


-- First table associated with primary, second and third not used.
PCODD3P
-- IPCFN DelG  AG   BG  DelW  AW  BW
       6  1 10  0.5  1 10  0.5
/
/
/
      0  1 10  0.5  1 10  0.5
/
/
/

RPTPROPS
PSORG PSGRO PSORW PSWRO PSGRW PSWRG
HSORG HSGRO HSORW HSWRO HSGRW HSWRG
SOF2
SGF3 SWF3 SOF3
/


INCLUDE
  flow_param_with_overlap_smoothed_right_gas_ow_endp.txt /

-------
REGIONS
```

```
-------

PVTNUM
1*2 72*1 1*2
/

FIPNUM
74*1
/

EQLNUM
1  73*2  /


-- Primary saturation region numbers
PSTNUM
1*4 72*1 1*4
/

-- Increasing hysteresis saturation region numbers
ISTNUM
1*5 72*2 1*5
/

-- Decreasing hysteresis saturation region numbers
DSTNUM
1*6 72*3 1*6
/

SDROW
 74*4
/

SDRWO
 74*3
/



RPTREGS
PSTNUM ISTNUM DSTNUM
SDRGO SDROG SDROW SDRWO SDRGW SDRWG
/

--------
SOLUTION
--------

EQUIL
--   1           2            3        4       5       6   7  8   9  10
-- Datum      Pressure       WOC      Pcow    GOC     Pcgo
-- depth                    depth     WOC   depth    GOC
  2.37857    310.880829 /--126.46071421  0.0  4.37857   0.0   1* 1*  0   2
  /
126.4785458  310.880829 /--126.46071421  0.0  4.37857   0.0   1* 1*  0   1
/



SWAT
  0.0001 72*0.6314  0.9999 /


SOIL
--  0.99  72*0.3686  0.001 /
  0.0001  72*0.3686  0.0001 /

PRESSURE
```

```
74*310.6834 /

NEI
0.8198      0.14712    0.02949     0.00359     0.0         0.0         /
0.488001427 0.13596298 0.080436444 0.187865683 0.070975213 0.036758252 /


RPTSOL
PRESSURE SWAT SOIL SGAS
/

RPTRST
 BASIC=2 KRO KRW KRG PCOW PCOG PCGW SOIL SWAT SGAS
 /


-------
SUMMARY
-------

--RUNSUM



INCLUDE
 summary_stuff.txt /

BDENO
1 1 10 /
1 1 20 /
1 1 40 /
/
BDENG
1 1 10 /
1 1 20 /
1 1 40 /
/


BVOIL

1 1 2 /
1 1 5 /
1 1 10 /
1 1 35 /
1 1 70 /
/

BSWAT
1 1 10 /
1 1 35 /
1 1 70 /
/



BSGAS
1 1 10 /
1 1 35 /
1 1 70 /
/

BSOIL
1 1 10 /
1 1 35 /
1 1 70 /
/
```

```
BPCOWR
1 1 10 /
1 1 35 /
1 1 70 /
/
BPCWOR
1 1 10 /
1 1 35 /
1 1 70 /
/
BPCOGR
1 1 10 /
1 1 35 /
1 1 70 /
/
BPCGOR
1 1 10 /
1 1 35 /
1 1 70 /
/
BPCGWR
1 1 10 /
1 1 35 /
1 1 70 /
/
BPCWGR
1 1 10 /
1 1 35 /
1 1 70 /
/



--------
SCHEDULE
--------


CVCRIT
-- DPMAX MAX-NLI LSR MAX-LI MAX-FUG MIN-LI DVMAX DSPE MIN-NLI
   0.01  50      1*  150    1*      1*     1*    1*
/

TSCRIT
-- TsIni MinTs   MaxTs MaxTsDf MasTsIf TgtTTE MaxTTE TgtTPR MaxTPR TgtSC
-- 0.01  1.0E-10 1.0   1*     1*      1*     1*     0.05   0.01   0.0125
   0.0004  1.0E-10 0.01   1*     1*      1*     1*     0.0005   0.005
   0.0250
/

WELLSTRE
'INJCOMP'
0.82 0.147 0.0295 0.0035 0 0   /
/


GRUPTREE
'WFILL' 'FIELD' /
'GINJ'  'FIELD' /
 /

-- Define the E300 wells
WELSPECS
--
--  1    2       3 4  5    6     7     8     9      10    11    12
16
--                  BHP                   Inst          Pres  Dens
```

```
Well
-- Wll  Group        Ref Pref   Drng Infl  Auto   Xflow  Tab   Calc
Model
-- Nme  Name     I J Dep Phase  Rad  Eqtn  Shut   Enabl  Num   Type
Type
'TOP'    'GINJ'  1 1 0.54732125    'GAS'   1*  'STD' 'SHUT' 'NO'   1*
'SEG'  3*  'STD' /
'WINJ'   'WFILL' 1 1 130.81  'WATER' 1*  'STD' 'SHUT' 'NO'   1*    'SEG'
3*  'STD' /
'BOTTOM' 'GINJ'  1 1 130.81  'OIL'   1*  'STD' 'SHUT' 'NO'   1*    'SEG'
3*  'STD' /
'TOPP'   'WFILL' 1 1 0.54732125    'OIL'   1*  'STD' 'SHUT' 'NO'   1*
'SEG'  3*  'STD' /
/

COMPDAT
-- 1     2 3 4 5   6     7    8     9    10   11    12    13    14
--                       Sat  Con                              Pres
-- Wl    I J K1         Tab  Trans Bore  Eff  Skin  D          Equiv
-- Nm         K2 Status Num  Fact  Diam  Kh   Fact  Fact  Dir  Rad
'TOP'    1 1 1 1   'OPEN'  1*   1*   0.008594   1*   1*   1*    'Z'   1* /
'WINJ'   1 1 74 74 'OPEN'  1*   1*   0.008594   1*   1*   1*    'Z'   1* /
'BOTTOM' 1 1 74 74 'OPEN'  1*   1*   0.008594   1*   1*   1*    'Z'   1* /
'TOPP'   1 1 1 1   'OPEN'  1*   1*   0.008594   1*   1*   1*    'Z'   1* /
/




WCONINJE
--    1     2       3      4      5    6     7
--        Inj             Cntl  Surf  Res   BHP
--        Type    Status  Mode  Rate  Rate  Lim
   'TOP'  'GAS'   'OPEN' 'RESV' 1*    2.58  800 / -- BHP atm
   'WINJ' 'WATER' 'SHUT' 'RESV' 1*    4.0  310.8798 / -- BHP atm
/



-- Define injected composition
WINJGAS
'TOP' 'STREAM' 'INJCOMP'  /
/


WCONPROD
--    1     2      3     4     5    6    7    8     9
--                                      Res
--                Cntl  Oil   Wat   Gas  Liq  Vol  BHP
--         Status  Mode  Rate  Rate  Rate Rate Rate Lim
-- 'BOTTOM' 'OPEN'  'BHP'  50.0  1*    1*   1*   1*   313.5 /  -- BHP bar
   'BOTTOM' 'OPEN'  'BHP'  1*  1*    1*   1*   1*   309.3994/  -- removed
   oil rate
   'TOPP'   'SHUT'  'BHP'  1*  1*    1*   1*   1*   309.365 /
/




SEPCOND
 'SEPARGAS' 'FIELD' 1  15.0  1.0 2* / 1 /
 /

WSEPCOND
 'TOPP' 'SEPARGAS' /
```

```
 'BOTTOM' 'SEPARGAS' /
/


TIME
0.0001
/


RPTSCHED
PRESSURE SOIL SWAT SGAS KRO KRW KRG PCOG PCOW PCGW /

TIME
0.42743
--87.0
/

TIME
10.0
/

RPTSCHED
PRESSURE SOIL SWAT SGAS KRO KRW KRG PCOG PCOW PCGW SDROW SDROG SDRWO SDRWG
SDRGO SDRGW /


TIME
25
/

RPTSCHED
PRESSURE SOIL SWAT SGAS KRO KRW KRG PCOG PCOW PCGW SDROW SDROG SDRWO SDRWG
SDRGO SDRGW /

TIME
30.0
/

RPTSCHED
PRESSURE SOIL SWAT SGAS KRO KRW KRG PCOG PCOW PCGW SDROW SDROG SDRWO SDRWG
SDRGO SDRGW /

TIME
48.0
/

RPTSCHED
PRESSURE SOIL SWAT SGAS KRO KRW KRG PCOG PCOW PCGW SDROW SDROG SDRWO SDRWG
SDRGO SDRGW /

TIME
49.0
/

RPTSCHED
PRESSURE SOIL SWAT SGAS KRO KRW KRG PCOG PCOW PCGW SDROW SDROG SDRWO SDRWG
SDRGO SDRGW /

TIME
50.0
/

RPTSCHED
PRESSURE SOIL SWAT SGAS KRO KRW KRG PCOG PCOW PCGW SDROW SDROG SDRWO SDRWG
SDRGO SDRGW /

TIME
51.0
```

```
/

RPTSCHED
PRESSURE SOIL SWAT SGAS KRO KRW KRG PCOG PCOW PCGW SDROW SDROG SDRWO SDRWG
SDRGO SDRGW /


TIME
52.0
/

RPTSCHED
PRESSURE SOIL SWAT SGAS KRO KRW KRG PCOG PCOW PCGW SDROW SDROG SDRWO SDRWG
SDRGO SDRGW /

TIME
53.0
/

RPTSCHED
PRESSURE SOIL SWAT SGAS KRO KRW KRG PCOG PCOW PCGW SDROW SDROG SDRWO SDRWG
SDRGO SDRGW /

TIME
54.0
/

RPTSCHED
PRESSURE SOIL SWAT SGAS KRO KRW KRG PCOG PCOW PCGW SDROW SDROG SDRWO SDRWG
SDRGO SDRGW /

TIME
55.0
/

RPTSCHED
PRESSURE SOIL SWAT SGAS KRO KRW KRG PCOG PCOW PCGW SDROW SDROG SDRWO SDRWG
SDRGO SDRGW /

TIME
56.0
/

RPTSCHED
PRESSURE SOIL SWAT SGAS KRO KRW KRG PCOG PCOW PCGW SDROW SDROG SDRWO SDRWG
SDRGO SDRGW /

TIME
57.0
/

RPTSCHED
PRESSURE SOIL SWAT SGAS KRO KRW KRG PCOG PCOW PCGW SDROW SDROG SDRWO SDRWG
SDRGO SDRGW /


TIME
58.0
/

RPTSCHED
PRESSURE SOIL SWAT SGAS KRO KRW KRG PCOG PCOW PCGW SDROW SDROG SDRWO SDRWG
SDRGO SDRGW /


TIME
59.0
/
```

```
RPTSCHED
PRESSURE SOIL SWAT SGAS KRO KRW KRG PCOG PCOW PCGW SDROW SDROG SDRWO SDRWG
SDRGO SDRGW /

TIME
60
/

RPTSCHED
PRESSURE SOIL SWAT SGAS KRO KRW KRG PCOG PCOW PCGW SDROW SDROG SDRWO SDRWG
SDRGO SDRGW /

TIME
61
/

RPTSCHED
PRESSURE SOIL SWAT SGAS KRO KRW KRG PCOG PCOW PCGW SDROW SDROG SDRWO SDRWG
SDRGO SDRGW /

TIME
62
/

RPTSCHED
PRESSURE SOIL SWAT SGAS KRO KRW KRG PCOG PCOW PCGW SDROW SDROG SDRWO SDRWG
SDRGO SDRGW /

TIME
63
/

RPTSCHED
PRESSURE SOIL SWAT SGAS KRO KRW KRG PCOG PCOW PCGW SDROW SDROG SDRWO SDRWG
SDRGO SDRGW /

TIME
64
/

RPTSCHED
PRESSURE SOIL SWAT SGAS KRO KRW KRG PCOG PCOW PCGW SDROW SDROG SDRWO SDRWG
SDRGO SDRGW /

TIME
65
/

RPTSCHED
PRESSURE SOIL SWAT SGAS KRO KRW KRG PCOG PCOW PCGW SDROW SDROG SDRWO SDRWG
SDRGO SDRGW /

TIME
65.5
--154.0
/

RPTSCHED
PRESSURE SOIL SWAT SGAS KRO KRW KRG PCOG PCOW PCGW SDROW SDROG SDRWO SDRWG
SDRGO SDRGW /

TIME
65.6
--154.00001
/

RPTSCHED
```

```
PRESSURE SOIL SWAT SGAS KRO KRW KRG PCOG PCOW PCGW SDROW SDROG SDRWO SDRWG
SDRGO SDRGW /



TIME
70.0
/

RPTSCHED
PRESSURE SOIL SWAT SGAS KRO KRW KRG PCOG PCOW PCGW SDROW SDROG SDRWO SDRWG
SDRGO SDRGW /

TIME
80.0
/

RPTSCHED
PRESSURE SOIL SWAT SGAS KRO KRW KRG PCOG PCOW PCGW SDROW SDROG SDRWO SDRWG
SDRGO SDRGW /

TIME
100.0
/

RPTSCHED
PRESSURE SOIL SWAT SGAS KRO KRW KRG PCOG PCOW PCGW SDROW SDROG SDRWO SDRWG
SDRGO SDRGW /

TIME
120.0
/

RPTSCHED
PRESSURE SOIL SWAT SGAS KRO KRW KRG PCOG PCOW PCGW SDROW SDROG SDRWO SDRWG
SDRGO SDRGW /

TIME
140.0
/

RPTSCHED
PRESSURE SOIL SWAT SGAS KRO KRW KRG PCOG PCOW PCGW SDROW SDROG SDRWO SDRWG
SDRGO SDRGW /

TIME
160.0
/

RPTSCHED
PRESSURE SOIL SWAT SGAS KRO KRW KRG PCOG PCOW PCGW SDROW SDROG SDRWO SDRWG
SDRGO SDRGW /

TIME
180.0
/

RPTSCHED
PRESSURE SOIL SWAT SGAS KRO KRW KRG PCOG PCOW PCGW SDROW SDROG SDRWO SDRWG
SDRGO SDRGW /

TIME
200.0
/

RPTSCHED
PRESSURE SOIL SWAT SGAS KRO KRW KRG PCOG PCOW PCGW SDROW SDROG SDRWO SDRWG
SDRGO SDRGW /
```

```
TIME
216.6704
--303.243
/


RPTSCHED
PRESSURE SOIL SWAT SGAS KRO KRW KRG PCOG PCOW PCGW SDROW SDROG SDRWO SDRWG
SDRGO SDRGW /


TIME
414.86
/

END
```